

AD\_\_\_\_\_

Award Number: W81XWH-13-1-0129

TITLE: "Maximizing PTH Anabolic Osteoporosis Therapy"

PRINCIPAL INVESTIGATOR: Joseph Bidwell

CONTRACTING ORGANIZATION: INDIANA UNIVERSITY  
INDIANAPOLIS IN 46202-5130

REPORT DATE: September 2015

TYPE OF REPORT: Annual

PREPARED FOR: U.S. Army Medical Research and Materiel Command  
Fort Detrick, Maryland 21702-5012

DISTRIBUTION STATEMENT: Approved for Public Release;  
Distribution Unlimited

The views, opinions and/or findings contained in this report are those of the author(s) and should not be construed as an official Department of the Army position, policy or decision unless so designated by other documentation.

REPORT DOCUMENTATION PAGE			Form Approved OMB No. 0704-0188		
Public reporting burden for this collection of information is estimated to average 1 hour per response, including the time for reviewing instructions, searching existing data sources, gathering and maintaining the data needed, and completing and reviewing this collection of information. Send comments regarding this burden estimate or any other aspect of this collection of information, including suggestions for reducing this burden to Department of Defense, Washington Headquarters Services, Directorate for Information Operations and Reports (0704-0188), 1215 Jefferson Davis Highway, Suite 1204, Arlington, VA 22202-4302. Respondents should be aware that notwithstanding any other provision of law, no person shall be subject to any penalty for failing to comply with a collection of information if it does not display a currently valid OMB control number. <b>PLEASE DO NOT RETURN YOUR FORM TO THE ABOVE ADDRESS.</b>					
1. REPORT DATE September 2015		2. REPORT TYPE Annual		3. DATES COVERED 15 Aug 2014 - 14 Aug 2015	
4. TITLE AND SUBTITLE  "Maximizing PTH Anabolic Osteoporosis Therapy"			5a. CONTRACT NUMBER W81XWH-13-1-0129		
			5b. GRANT NUMBER		
			5c. PROGRAM ELEMENT NUMBER		
6. AUTHOR(S)  Joseph Bidwell  email: jbidwell@iupui.edu			5d. PROJECT NUMBER		
			5e. TASK NUMBER		
			5f. WORK UNIT NUMBER		
7. PERFORMING ORGANIZATION NAME(S) AND ADDRESS(ES)  INDIANA UNIVERSITY 980 INDIANA AVE RM 2232 INDIANAPOLIS IN 46202-5130			8. PERFORMING ORGANIZATION REPORT NUMBER		
9. SPONSORING / MONITORING AGENCY NAME(S) AND ADDRESS(ES) U.S. Army Medical Research and Materiel Command Fort Detrick, Maryland 21702-5012			10. SPONSOR/MONITOR'S ACRONYM(S)		
			11. SPONSOR/MONITOR'S REPORT NUMBER(S)		
12. DISTRIBUTION / AVAILABILITY STATEMENT Approved for Public Release; Distribution Unlimited					
13. SUPPLEMENTARY NOTES					
14. ABSTRACT <p><b>The purpose</b> of this study is to test the efficacy of parathyroid hormone (PTH) mono-therapy and PTH+ anti-catabolic combination therapies on <i>Nmp4</i><sup>-/-</sup> and wild type (WT) mice. <b>The scope</b> of the research comprises the following specific aims: (i &amp; ii) to determine the impact of <i>Nmp4</i> on the efficacy of PTH mono- and combination therapies with various anti-catabolics in ovariectomized (ovx) mice; (iii) to determine the cell type-specific contributions to the enhanced response of the <i>Nmp4</i><sup>-/-</sup> mouse to these osteoporosis therapies. In <b>YEAR 2</b> we completed experiments comparing the response of ovx WT and <i>Nmp4</i><sup>-/-</sup> mice to PTH+anti-catabolic therapies. <b>The most significant findings during the YEAR 2 period include the following:</b></p> <ul style="list-style-type: none"> <li>• <b>KEY FINDING:</b> Mice receiving PTH+RAL (raloxifene) and PTH+ZOL (zoledronate) showed the largest BMD (bone mineral density) increase.</li> <li>• <b>KEY FINDING:</b> The PTH+RAL therapy was the only treatment to exhibit a synergistic effect on total WB (whole body) and spine BMD</li> <li>• <b>KEY FINDING:</b> Disabling <i>Nmp4</i> enhanced PTH+RAL-induced increases in femoral BV/TV and increased the synergistic action of PTH with RAL and ZOL in both the femur and spine.</li> <li>• <b>KEY FINDING:</b> Disabling <i>Nmp4</i> enhanced the distinction between the PTH+RAL-induced increase in cortical bone area and the other treatments</li> <li>• <b>KEY FINDING:</b> <i>Nmp4</i><sup>-/-</sup> mice under the PTH+RAL therapy harbored more bone marrow osteoprogenitors than mice under the other treatments</li> <li>• <b>KEY FINDING:</b> Raloxifene enhanced WT mesenchymal stem/progenitor cell (MSPC) mineralization</li> </ul> <p><b>Our key discovery</b> in YEAR 2 is that disabling <i>Nmp4</i> in a pre-clinical osteoporosis model improves the bone-forming efficacy of PTH+RAL therapy.</p>					
15. SUBJECT TERMS Nmp4-knockout (KO) mice, osteoporosis, ovariectomy, PTH combination therapies					
16. SECURITY CLASSIFICATION OF:			17. LIMITATION OF ABSTRACT	18. NUMBER OF PAGES	19a. NAME OF RESPONSIBLE PERSON
a. REPORT	b. ABSTRACT	c. THIS PAGE			USAMRMC
U	U	U	UU	167	19b. TELEPHONE NUMBER (include area code)

## Table of Contents

	<u>Page</u>
<b>Introduction.....</b>	<b>4</b>
<b>Body.....</b>	<b>4</b>
<b>Key Research Accomplishments.....</b>	<b>12</b>
<b>Reportable Outcomes.....</b>	<b>12</b>
<b>Conclusion.....</b>	<b>13</b>
<b>References.....</b>	<b>13</b>
<b>Appendices.....</b>	<b>15</b>

**INTRODUCTION:** The subject of this research is the need for improved osteoporosis therapies. The purpose of this study is to test the efficacy of parathyroid hormone (PTH) mono-therapy and PTH + anti-catabolic combination therapies on *Nmp4*<sup>-/-</sup> and wild type (WT) mice. We have previously determined that *Nmp4* represses the response of bone to osteoanabolics<sup>1-3</sup>. The scope of this research comprises the following specific aims: (i & ii) to determine the impact of *Nmp4* on the efficacy of PTH mono- and combination therapies with bisphosphonates and the selective estrogen receptor modulator (SERM) raloxifene in ovariectomized (ovx) mice; (iii) to determine the cell type-specific contributions to the enhanced response of the *Nmp4*<sup>-/-</sup> mouse to these osteoporosis therapies.

#### **BODY:**

During Year 2 we successfully accomplished a number of objectives in the following Tasks and Subtasks:

- i. *Task 2: Conduct PTH mono-therapy and PTH combination therapies with bisphosphonates:* A revised manuscript describing the impact of *Nmp4* on ovx-induced bone loss and the response of ovx mice to PTH mono-therapy is in review at Molecular Endocrinology (see Appendix Manuscript Number ME-14-1406R1). Note: this manuscript contains all details for the materials and methods used to generate the PTH+anti-catabolic data described below.
- ii. *Task 3: Conduct PTH combination therapy with raloxifene:* The treatment of the WT and *Nmp4*<sup>-/-</sup> mice with the PTH + anti-catabolic therapies (raloxifene and bisphosphonates) is finished and the analyses underway. The PTH+raloxifene combination therapy has been identified as the optimum combination treatment to be used in Task 4 (see below for details of results and ongoing analyses).
- iii. *Subtasks 4.2.a and 4.3.a: Breed 54 female Nmp4<sup>fl/fl</sup>3.6Col-Cre<sup>+</sup> & 54 Nmp4<sup>fl/fl</sup>-Cre<sup>-</sup> mice:* We are backcrossing our *Nmp4*<sup>flox/flox</sup> mice onto a C57BL/6J for production of conditional knockout animals (see below for details).
- iv. *Subtask 6.2: Culture, expand, and characterize the phenotype of both WT and Nmp4<sup>-/-</sup> mesenchymal stem/progenitor cells (MSPCs):* These experiments are described in the revised manuscript ME-14-1406R1 (Appendix) and we have started experiments designed to characterize the impact of raloxifene on MSPCs (see below)

#### **Overview of Objectives and Results During Year 2:**

During Year 1 we determined that the exaggerated response to anabolic doses of PTH was preserved in ovx *Nmp4*<sup>-/-</sup> mice but that disabling this transcription factor did not protect them from ovx-induced bone loss without therapy. During Year 2 we addressed whether various PTH+anti-catabolic combination therapies are more efficacious in osteoporotic *Nmp4*<sup>-/-</sup> than wild type (WT) mice. Animals were ovx at 12wks. Therapies were initiated at 16wks of age including PTH only, alendronate (ALN) only, raloxifene (RAL) only, zoledronate (ZOL) only, and the combination treatments PTH+ALN, PTH+RAL, PTH+ZOL. The vehicle control (VEH) was comprised of all the carriers used in the study. At 24wks of age (8wks treatment) mice were euthanized for analysis.

#### **Doses:**

- PTH: 30µg/kg/d
- ALN: 1µg/kg/d
- ZOL: 80µg/kg 1x dose:
- RAL: 1mg/kg/d

Doses of anti-resorptive agents are based on human clinical doses.

The standard ALN dose for treatment of osteoporosis typically given as either a daily (10mg) or weekly (70mg) dose. Based on a 60kg individual this is roughly 1.17 mg/kg/week. The human dose is oral and has an estimated bioavailability of around 0.6%, meaning that the absorbed dose is roughly 0.007 mg/kg/week (or 7 µg/kg/week). We dosed via injection, assuming 100% absorption, thus we delivered ALN at 1µg/kg/day<sup>4-6</sup>.

RAL is typically given as a 60 mg daily dose. Based on a 60 kg patient, the dose would be 1 mg/kg/day. The assumption is 100% absorption thus the full dose is used when injecting<sup>5, 7</sup>.

ZOL is typically given yearly at a dose of 5 mg. Based on a 60 kg patient, the dose is 0.083 mg/kg. Our single dose of 80 µg/kg approximates this amount<sup>8, 9</sup>.

## SUMMARY OF KEY FINDINGS FOR YEAR 2:

We have generated an extensive data set from the combination experiments and although the analysis is not complete the preliminary statistical evaluation provides an exciting emerging picture, which is presented here. Note that *Nmp4* targets cancellous bone thus we will specify what skeletal compartments comprise the endpoint under consideration.

- The PTH+RAL combination therapy typically added more bone to both WT and *Nmp4*<sup>-/-</sup> ovx skeletons than the other treatments (whole body [WB] and spine BMD and femoral and spine BV/TV)
- The PTH+RAL treatment was the most effective at out-performing the PTH mono-therapy in both genotypes (whole body [WB] and spine BMD and femoral and spine BV/TV)
- Disabling *Nmp4* significantly improved the efficacy of the PTH+RAL therapy but typically had little to no effect on the PTH+bisphosphonate treatments (whole body [WB] and spine BMD and femoral and spine BV/TV)
- The anti-catabolic mono-therapies, as expected, added only a modest amount of bone to the ovx WT and *Nmp4*<sup>-/-</sup> skeletons, compared to PTH mono-therapy. Disabling *Nmp4* did not enhance the response of the ovx skeleton to the anti-catabolic mono-therapies.
- The *Nmp4*<sup>-/-</sup> PTH+RAL treatment group exhibited the largest pool of bone marrow osteoprogenitors [identified by CD45<sup>-</sup>/CD105<sup>+</sup>/Nestin<sup>+</sup>/CD146<sup>+</sup>].
- Raloxifene enhanced the mineralization capacity of WT mesenchymal stem/progenitor cells (MSPCs) but did not further augment the precocious *Nmp4*<sup>-/-</sup> MSPC mineralization.

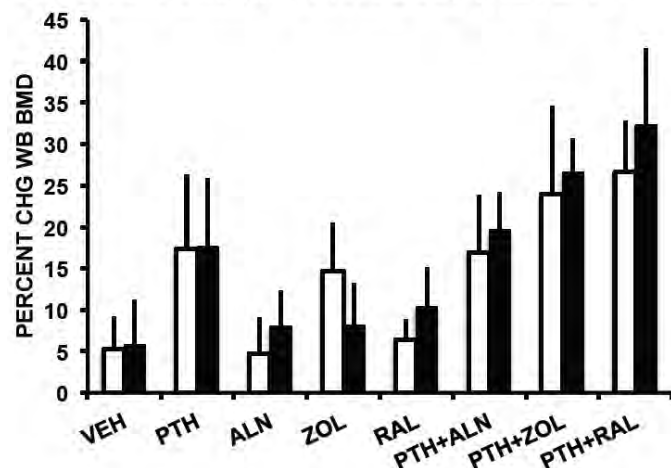
## STATSTICAL TREATMENT:

We have tested 7 therapies and a vehicle control using two genotypes of mice yielding a total of 16 treatment groups. To date we have used the following statistical methods:

- Raw data:
  - ◆ **μCT trabecular data:** Cancellous bone is the primary target of *Nmp4*. To determine if there was a genotype x treatment interaction for any of the combination treatments we performed a series of 2W ANOVAs using Genotype and Treatment (veh vs PTH+anti-catabolic; PTH vs PTH+anti-catabolic) as the independent variables and femoral BV/TV, femoral Tb N and Tb Th, or spine BV/TV as the dependent endpoints. We set  $p < 0.01$  to avoid Type I errors. Similarly, to determine if the combination treatments provided a synergistic effect over their respective mono-therapies we performed a series of 2W ANOVAs using PTH and the anti-catabolic treatments as the independent variables.
  - ◆ **μCT cortical data:** There was no indication of a genotype x treatment interaction therefore the raw cortical data was treated with a 1W ANOVA followed by a Tukey-Kramer HSD post hoc test to compare means.
- % Change BMD data: For these data we used the Kruskal–Wallis 1W ANOVA by ranks for non-parametric data.
- FACS data: The raw FACS data is reported as % of total cells analyzed. We used the Kruskal–Wallis 1W ANOVA followed by nonparametric comparisons with control using the Dunn method for joint ranking.

KEY FINDING: Mice receiving PTH+RAL and PTH+ZOL showed the largest BMD increase after ovx.

### A. Percent Change Whole Body (WB) BMD



### B. Percent Change Spine BMD

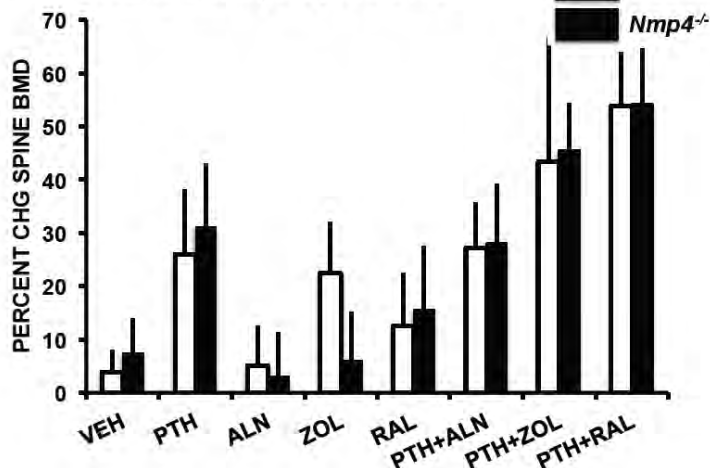
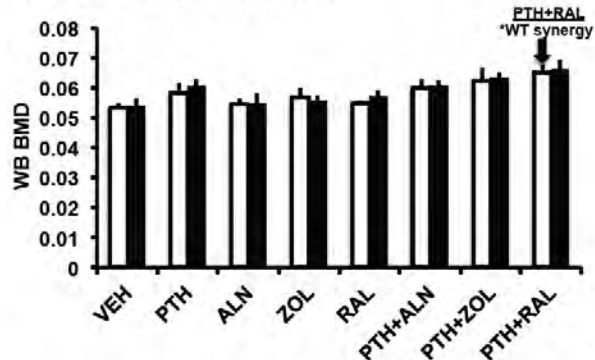


Figure 1: Percent change [A] whole body bone mineral density (WB BMD) (16wks to 24wks of age) and [B] spine BMD (L3-L5) for WT and *Nmp4*<sup>-/-</sup> [KO] mice under various treatment groups. The PTH+RAL and PTH+ZOL stimulated the largest changes in WB and spine BMD. The data were analyzed using the Kruskal-Wallis test for non-parametric statistics ( $p < 0.0001$ ) followed by a comparison for all pairs using Dunn method for joint ranking post hoc test. The data represents average  $\pm$  SD,  $n = 7-12$  mice/group.

### A. Whole Body BMD 24wks



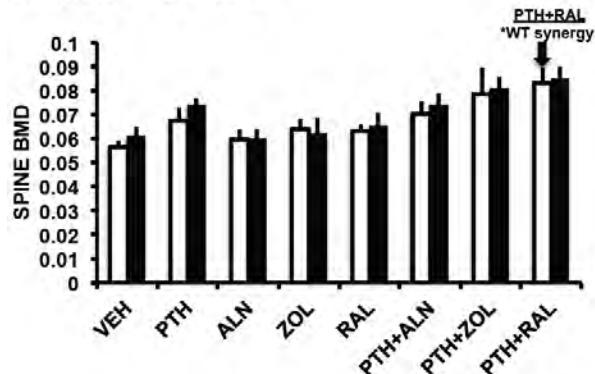
### B. 1W ANOVA

#### /Comparison of all pairs

KO-PTH+RAL	A
WT-PTH+RAL	A
KO-PTH+ZOL	A B
WT-PTH+ZOL	A B
KO-PTH+ALN	B C
KO-PTH	B C
WT-PTH+ALN	B C
WT-PTH	C D
KO-RAL	C D E
WT-ZOL	C D E
KO-ZOL	D E
KO-ALN	D E
WT-RAL	D E
WT-ALN	E
KO-VEH	E
WT-VEH	E

Levels not connected by the same letter are significantly different

### C. Spine BMD 24wks



### D. 1W ANOVA

#### /Comparison of all pairs

KO-PTH+RAL	A
WT-PTH+RAL	A
KO-PTH+ZOL	A B
WT-PTH+ZOL	A B
KO-PTH	B C
KO-PTH+ALN	B C
WT-PTH+ALN	C D
WT-PTH	C D E
KO-RAL	D E F
WT-ZOL	D E F G
WT-RAL	D E F G
KO-ZOL	D E F G
KO-VEH	E F G
KO-ALN	E F G
WT-ALN	F G
WT-VEH	G

Levels not connected by the same letter are significantly different

Figure 1 illustrates the percent change of WB and spine BMD of the WT and *Nmp4*<sup>-/-</sup> mice from the 16 different treatment groups. The use of the Kruskal-Wallis test for non-parametric statistics showed a significant difference between the groups ( $p < 0.0001$ ). The use of a Dunn's post-hoc test comparing all pair-wise comparisons indicated that the PTH+RAL and PTH+ZOL groups were distinct in that they were different from most of the other treatments (statistical output not shown in graphs for simplicity).

Figure 2 compares the raw WB and spine BMD of the different treatment groups at the end of the experiment (8wks of therapy, 24wks of age). The use of a 1W ANOVA followed by a Tukey-Kramer HSD shows that the PTH+RAL and the PTH+ZOL treatments were the most effective at adding bone after ovx.

Figure 2: [A] WB BMD (24wks of age) and [B] spine BMD (L3-L5) for WT and *Nmp4*<sup>-/-</sup> [KO] mice under various treatment groups. [C], [D] The data were analyzed using a 1W ANOVA followed by a comparison for all pairs using a Tukey-Kramer ( $p < 0.05$ ). The mice from the PTH+RAL (and PTH+ZOL) exhibited the largest WB and spine BMDs. The WT mice exhibited a synergistic response to the PTH+RAL combination therapy (see Table 1, next page). The data represents average  $\pm$  SD,  $n = 7-12$  mice/group.

These results raise the question as to whether any of the combination treatments show a synergistic response at the levels of WB and spine BMD.

KEY FINDING: The PTH+RAL therapy was the only treatment to exhibit a synergistic effect on total WB and spine BMD

TABLE 1

WHOLE BODY BMD			
THERAPY	p-value PTH Treatment	p-value Anti-catabolic Treatment	p-value PTH x Anti-catabolic interaction
PTH+ALN [WT mice]	<0.0001	0.04	0.65
PTH+ALN [ <i>Nmp4</i> <sup>-/-</sup> mice]	<0.0001	0.50	0.64
PTH+RAL [WT mice]	<0.0001	<0.0001	<b>0.0007</b>
PTH+RAL [ <i>Nmp4</i> <sup>-/-</sup> mice]	<0.0001	<0.0001	0.1025
PTH+ZOL [WT mice]	<0.0001	0.0003	0.8258
PTH+ZOL [ <i>Nmp4</i> <sup>-/-</sup> mice]	<0.0001	0.0023	0.3662
SPINE BMD (L3-L5)			
THERAPY	p-value PTH Treatment	p-value Anti-catabolic Treatment	p-value PTH x Anti-catabolic interaction
PTH+ALN [WT mice]	<0.0001	0.02	0.94
PTH+ALN [ <i>Nmp4</i> <sup>-/-</sup> mice]	<0.0001	0.69	0.79
PTH+RAL [WT mice]	<0.0001	<0.0001	<b>0.003</b>
PTH+RAL [ <i>Nmp4</i> <sup>-/-</sup> mice]	<0.0001	<0.0001	<b>0.0175</b>
PTH+ZOL [WT mice]	<0.0001	<0.0001	0.3807
PTH+ZOL [ <i>Nmp4</i> <sup>-/-</sup> mice]	<0.0001	0.0101	0.0561

To determine if the combination treatments provided a synergistic effect over their respective mono-therapies we performed a series of 2W ANOVAs using PTH and the anti-catabolic treatments as the independent variables and either WB BMD or spine BMD (at 8wks of therapy, 24wks of age) as the dependent endpoint (see Table 1). Note that these analyses used the actual BMD value and not the % change. We set p<0.01 to avoid Type I errors. Only the PTH+RAL combination therapy yielded a synergistic effect for the WT (WB BMD/spine BMD). The *Nmp4*<sup>-/-</sup> showed a nearly significant synergistic effect for spine BMD.

The PTH+ bisphosphonate therapies (ALN and ZOL) did not act synergistically on either the WT and *Nmp4*<sup>-/-</sup> mice. ALN induced the weakest response in both genotypes for these endpoints (% change BMD and BMD, Figures, 1, 2, and Table 1).

Potential interpretations of some of the data:

- WB BMD is primarily cortical bone (*Nmp4* non-target) whereas the spine BMD (L3-L5) has a comparatively larger proportion of cancellous bone (*Nmp4* target). This may explain the lack of a synergistic effect for the *Nmp4*<sup>-/-</sup> mice for the WB BMD parameter but near synergistic effect for spine BMD.
- The difference in the response to ALN mono-therapy between WT and *Nmp4*<sup>-/-</sup> mice is consistent with our previous observation that null osteoclasts are more active than WT cells<sup>2</sup>. These differences may be overwhelmed in the presence of the stronger bisphosphonate ZOL.



**KEY FINDING:** Disabling *Nmp4* enhanced PTH+RAL-induced increases in femoral BV/TV and increased the synergistic action of PTH with RAL and ZOL in both the femur and spine.

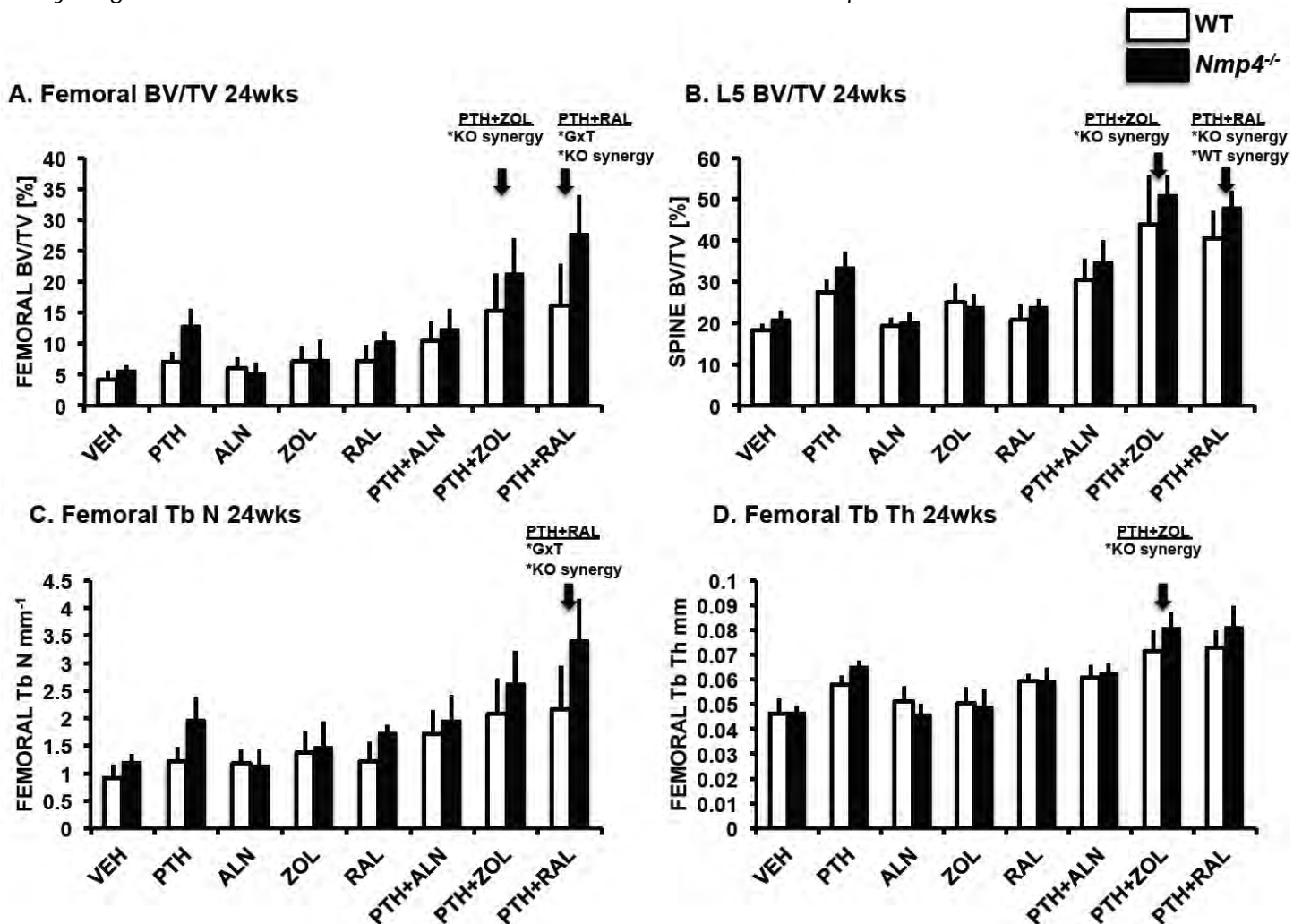


Figure 3: [A] Femoral BV/TV (24wks of age); [B] spine BV/TV (L5) [C] Femoral trabecular number (Tb N); and [D] Femoral trabecular thickness (Tb Th) for WT and *Nmp4*<sup>-/-</sup> mice under various treatment groups. The data were analyzed using a series of 2W ANOVAs. The PTH combination treatment groups were compared for genotype x treatment interactions (G x T). They were also compared for treatment synergy (PTH x anti-catabolic) for the WT and *Nmp4*<sup>-/-</sup> mice separately. The detailed results of the statistical analyses are shown in Tables 2-4. There was a G x T interaction in the PTH+RAL therapy (femoral BV/TV and Tb N, veh vs PTH+RAL). The *Nmp4*<sup>-/-</sup> mice exhibited a synergistic response to the PTH+RAL therapy (femoral BV/TV, femoral Tb N, L5 BV/TV) and to the PTH+ZOL therapy (femoral BV/TV, femoral Tb Th, spine BV/TV). The WT mice showed a synergistic response to PTH+RAL in the spine. The data represents average±SD, n=7-12 mice/group.

Table 2: FEMUR BV/TV

Therapy	Independent variable #1	Independent variable #2	Interaction var#1 x var#2
PTH+RAL: Gene x Treat <sup>a</sup>	Genotype: p<0.0001	Treatment: p<0.0001	G x T: p=0.0010
PTH+RAL: Gene x Treat <sup>b</sup>	Genotype: p<0.0001	Treatment: p<0.0001	G x T: p=0.0485
PTH+RAL: KO Synergy	PTH treatment: p<0.0001	RAL treatment: p<0.0001	PTH x RAL: p=0.0010
PTH+RAL: WT Synergy	PTH treatment: p<0.0001	RAL treatment: p<0.0001	PTH x RAL: p=0.0139
PTH+ZOL: Gene x Treat <sup>a</sup>	Genotype: p=0.0059	Treatment: p<0.0001	G x T: p=0.0760
PTH+ZOL: Gene x Treat <sup>b</sup>	Genotype: p=0.0059	Treatment: p<0.0001	G x T: p=0.9101
PTH+ZOL: KO Synergy	PTH treatment: p<0.0001	ZOL treatment: p<0.0001	PTH x ZOL: p=0.0067
PTH+ZOL: WT Synergy	PTH treatment: p<0.0001	ZOL treatment: p<0.0001	PTH x ZOL: p=0.0188
PTH+ALN: Gene x Treat <sup>a</sup>	Genotype: p=0.0295	Treatment: p<0.0001	G x T: p=0.7344
PTH+ALN: Gene x Treat <sup>b</sup>	Genotype: p<0.0001	Treatment: p=0.0779	G x T: p=0.0197
PTH+ALN: KO Synergy	PTH treatment: p<0.0001	ALN treatment: p=0.5540	PTH x ALN: p=0.9148
PTH+ALN: WT Synergy	PTH treatment: p<0.0001	ALN treatment: p=0.0001	PTH x ALN: p=0.1944

a: Genotype x treatment comparing vehicle-treated mice to PTH+ anti-catabolic therapy

b: Genotype x treatment comparing PTH-treated mice to PTH+ anti-catabolic therapy



Table 3: FEMUR Tb N and Tb Th

Therapy	Independent variable #1	Independent variable #2	Interaction var#1 x var#2
<i>Femur Tb N</i>			
PTH+RAL: Gene x Treat <sup>a</sup>	Genotype: p<0.0001	Treatment: p<0.0001	G x T: p=0.0090
PTH+RAL: Gene x Treat <sup>b</sup>	Genotype: p<0.0001	Treatment: p<0.0001	G x T: p=0.1641
PTH+RAL: KO Synergy	PTH treatment: p<0.0001	RAL treatment: p<0.0001	PTH x RAL: p<0.0001
PTH+RAL: WT Synergy	PTH treatment: p<0.0001	RAL treatment: p<0.0001	PTH x RAL: p=0.0313
PTH+ZOL: Gene x Treat <sup>a</sup>	Genotype: p=0.0046	Treatment: p<0.0001	G x T: p=0.4041
PTH+ZOL: Gene x Treat <sup>b</sup>	Genotype: p<0.0001	Treatment: p<0.0001	G x T: p=0.4838
PTH+ZOL: KO Synergy	PTH treatment: p<0.0001	ZOL treatment: p=0.0030	PTH x ZOL: p=0.1691
PTH+ZOL: WT Synergy	PTH treatment: p<0.0001	ZOL treatment: p=0.0004	PTH x ZOL: p=0.1415
<i>Femur Tb Th</i>			
PTH+RAL: Gene x Treat <sup>a</sup>	Genotype: p=0.0337	Treatment: p<0.0001	G x T: p=0.0422
PTH+RAL: Gene x Treat <sup>b</sup>	Genotype: p<0.0001	Treatment: p<0.0001	G x T: p=0.7730
PTH+RAL: KO Synergy	PTH treatment: p<0.0001	RAL treatment: p<0.0001	PTH x RAL: p=0.3820
PTH+RAL: WT Synergy	PTH treatment: p<0.0001	RAL treatment: p<0.0001	PTH x RAL: p=0.6140
PTH+ZOL: Gene x Treat <sup>a</sup>	Genotype: p=0.0127	Treatment: p<0.0001	G x T: p=0.0166
PTH+ZOL: Gene x Treat <sup>b</sup>	Genotype: p<0.0001	Treatment: p<0.0001	G x T: p=0.5458
PTH+ZOL: KO Synergy	PTH treatment: p<0.0001	ZOL treatment: p<0.0001	PTH x ZOL: p=0.0002
PTH+ZOL: WT Synergy	PTH treatment: p<0.0001	ZOL treatment: p<0.0001	PTH x ZOL: p=0.0172

a: Genotype x treatment comparing vehicle-treated mice to PTH+ anti-catabolic therapy

b: Genotype x treatment comparing PTH-treated mice to PTH+ anti-catabolic therapy

Table 4: L5 BV/TV

Therapy	Independent variable #1	Independent variable #2	Interaction var#1 x var#2
PTH+RAL: Gene x Treat <sup>a</sup>	Genotype: p=0.0002	Treatment: p<0.0001	G x T: p=0.0417
PTH+RAL: Gene x Treat <sup>b</sup>	Genotype: p<0.0001	Treatment: p<0.0001	G x T: p=0.5999
PTH+RAL: KO Synergy	PTH treatment: p<0.0001	RAL treatment: p<0.0001	PTH x RAL: p<0.0001
PTH+RAL: WT Synergy	PTH treatment: p<0.0001	RAL treatment: p<0.0001	PTH x RAL: p=0.0002
PTH+ZOL: Gene x Treat <sup>a</sup>	Genotype: p=0.0205	Treatment: p<0.0001	G x T: p=0.2534
PTH+ZOL: Gene x Treat <sup>b</sup>	Genotype: p=0.0026	Treatment: p<0.0001	G x T: p=0.8175
PTH+ZOL: KO Synergy	PTH treatment: p<0.0001	ZOL treatment: p<0.0001	PTH x ZOL: p<0.0001
PTH+ZOL: WT Synergy	PTH treatment: p<0.0001	ZOL treatment: p<0.0001	PTH x ZOL: p=0.0235
PTH+ALN: Gene x Treat <sup>a</sup>	Genotype: p=0.0045	Treatment: p<0.0001	G x T: p=0.4050
PTH+ALN: Gene x Treat <sup>b</sup>	Genotype: p=0.0002	Treatment: p=0.1281	G x T: p=0.5125
PTH+ALN: KO Synergy	PTH treatment: p<0.0001	ALN treatment: p=0.8438	PTH x ALN: p=0.3830
PTH+ALN: WT Synergy	PTH treatment: p<0.0001	ALN treatment: p=0.0472	PTH x ALN: p=0.3131

a: Genotype x treatment comparing vehicle-treated mice to PTH+ anti-catabolic therapy

b: Genotype x treatment comparing PTH-treated mice to PTH+ anti-catabolic therapy

- To determine if the combination treatments provided a synergistic effect over their respective mono-therapies we performed a series of 2W ANOVAs using PTH and the anti-catabolic treatments as the independent variables and Femoral BV/TV (Table 2), Femoral Tb N and Tb Th (Table 3), or Spine BV/TV (Table 4) as the dependent endpoints (8wks of therapy, 24wks of age). We set p<0.01 to avoid Type I errors.
  - Nmp4<sup>-/-</sup> mice show a synergistic response to PTH+RAL (Femoral BV/TV, Femoral Tb N, and Spine BV/TV)
  - The WT mice show a synergistic response to PTH+RAL (Spine BV/TV)
  - Nmp4<sup>-/-</sup> mice show a synergistic response to PTH+ZOL (Femoral BV/TV, Femoral Tb Th, and Spine BV/TV)
- To determine if there was a genotype x treatment interaction for any of the combination treatments we performed a series of 2W ANOVAs using Genotype and Treatment (veh vs PTH+anti-catabolic; PTH vs PTH+anti-catabolic) as the independent variables and Femoral BV/TV (Table 2), Femoral Tb N and Tb Th (Table 3), or Spine BV/TV (Table 4) as the dependent endpoints. We set p<0.01 to avoid Type I errors.
  - Genotype x treatment interactions were observed for femoral BV/TV and femoral Tb N under the PTH+RAL therapy when compared to the vehicle-treated mice
  - No genotype x treatment interactions were obtained for the PTH+ZOL therapy

KEY FINDING: *Disabling Nmp4 enhanced the distinction between the PTH+RAL-induced increase in cortical bone area and the other combination treatments*

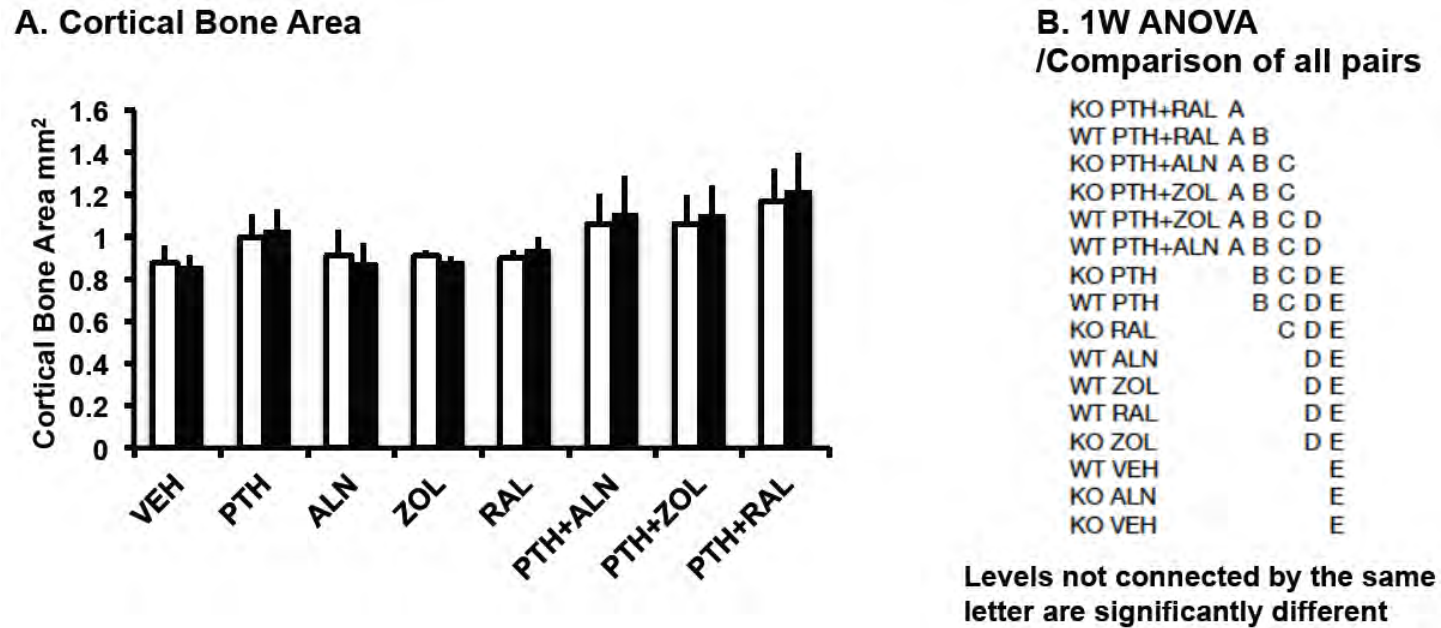


Figure 4: [A] Femoral cortical bone area of ovx WT and *Nmp4*<sup>-/-</sup> mice at 24wks of age, 8wks of treatment. Statistical analysis included a 1W ANOVA ( $p < 0.0001$ ) followed by a Tukey-Kramer HSD post-hoc test. Data are average  $\pm$  SD, number of mice/experimental group = 9-13.

We have previously shown that disabling *Nmp4* enhances the response of trabecular bone to PTH without compromising the cortical compartment<sup>3</sup>. This is consistent with our observation that *Nmp4*<sup>-/-</sup> mice from the PTH+RAL therapy group had the largest cortical bone area (Figures 4A and 4B). However, there was no evidence of synergy in this or any of the combination treatments for this parameter nor was there a genotype  $\times$  treatment effect.

KEY FINDING: *Nmp4*<sup>-/-</sup> mice under the PTH+RAL combination therapy harbored more bone marrow osteoprogenitors than mice under the other treatments

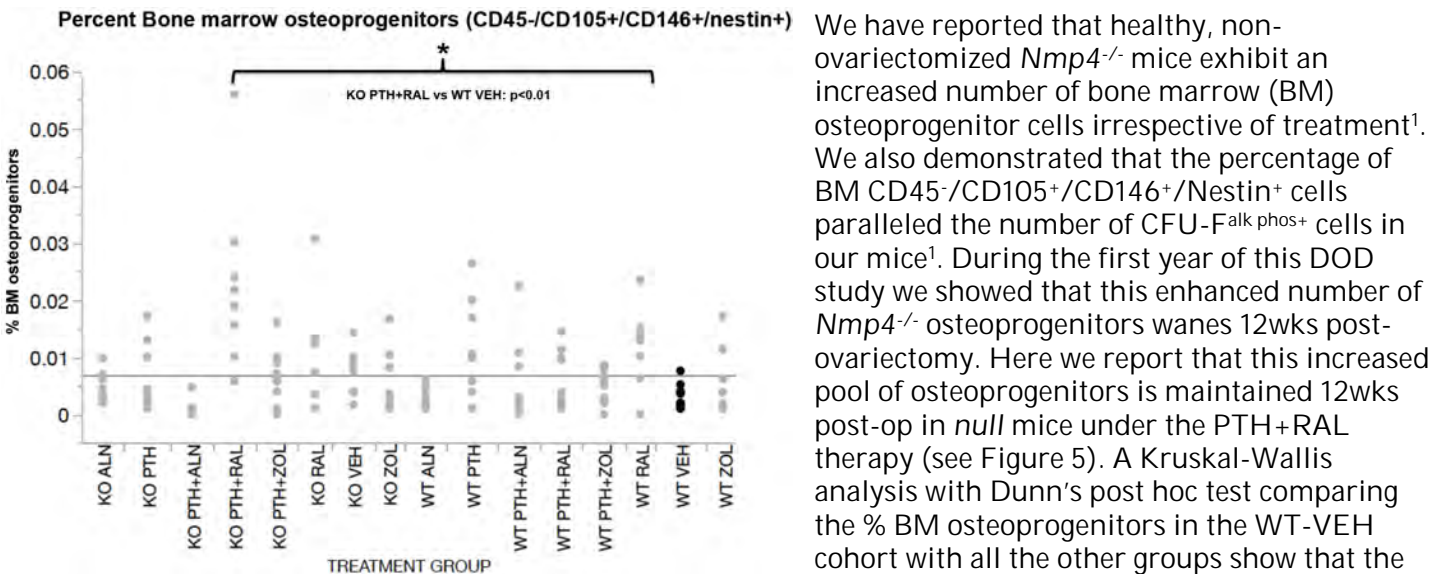


Figure 5: Percent bone marrow (BM) osteoprogenitors as evaluated by CD45-/CD105+/CD146+/Nestin+ cells. Statistical analysis used a non-parametric Kruskal-Wallis test followed by a Dunn's post hoc. See text for details.

**KEY FINDING:** *Raloxifene enhanced WT mesenchymal stem/progenitor cell (MSPC) mineralization*  
 We have shown that *Nmp4*<sup>-/-</sup> expanded MSCs exhibit a precocious mineralization (see Appendix Manuscript Number ME-14-1406R1). The null cells begin to mineralize by Days 4-7 in culture whereas the WT cells have a very weak mineralization response. There are a number of studies showing that osteoprogenitors and osteoblasts respond directly to raloxifene<sup>10-15</sup>. It has also been demonstrated that raloxifene has a mineralization-promoting effect on female mesenchymal stem cells<sup>13</sup>. As part of Subtask 6.2: Phenotype analyses of WT and *Nmp4*<sup>-/-</sup> mesenchymal stem progenitor cells (MSPCs) we addressed whether raloxifene enhances the mineralization response to ex vivo cultures of expanded MSCs. Figure 6 outlines the experimental protocol and results

These cells were derived from bone marrow mononuclear cells of male mice and expanded in MesenCult for 5 passages before use in osteogenic differentiation studies. Cells are used between passages 5 and 10<sup>16</sup>.

- **Day 0:** Seed 25K cells into each well in αMEM complete as shown in the Figure. [03/16/15]
- **Day 2:** Transfer cells to osteogenic medium [VEH3] or RAL+osteogenic medium.
- **For RAL supplement, add 1.02μl of Raloxifene Secondary Stock to 1mls of complete medium. To VEH3 add 1.02μl RAL diluent/1ml of complete medium.**
- **Feed the cells every MWF.**
- **Day 5, Day 9, and Day 16, stain the cells with alizarin red.**

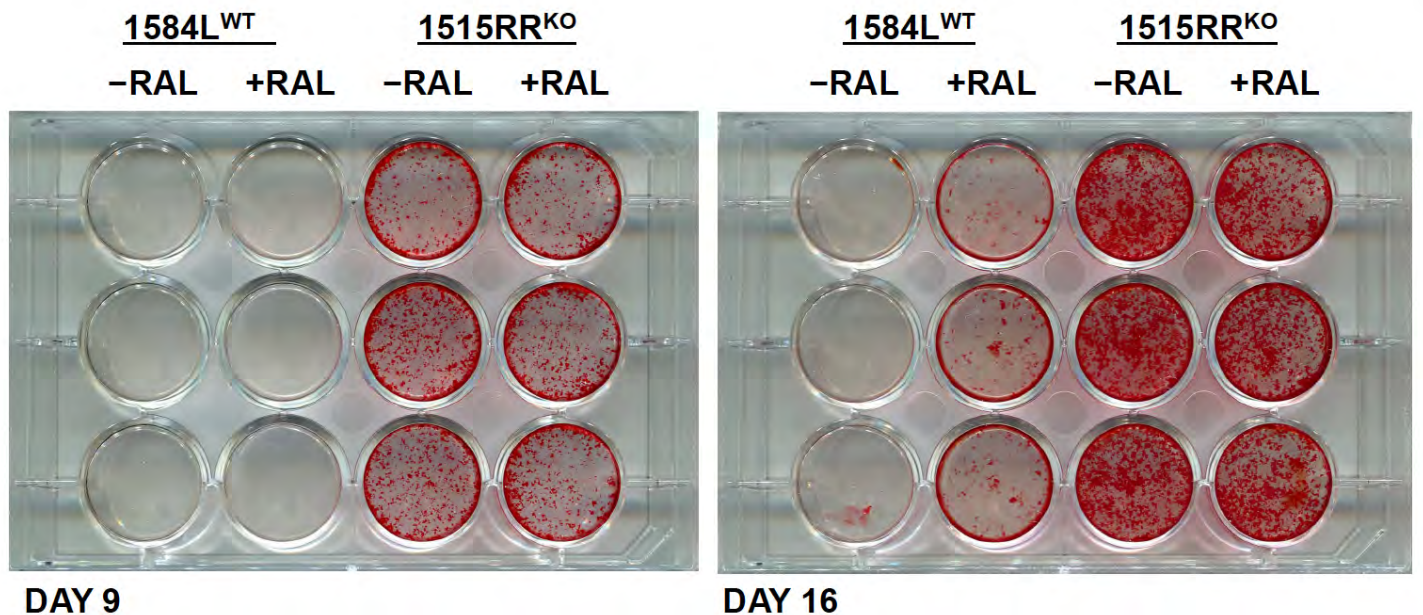


Figure 6: Raloxifene (100nM) clearly enhances WT MSPC mineralization. Whether it has an impact on the precocious mineralization of the *Nmp4*<sup>-/-</sup> (KO) remains to be determined. See text for details

We made the following observations from this single preliminary experiment:

- At Day 9, post-seeding the *Nmp4*<sup>-/-</sup> cells show a strong mineralization response in both the presence and absence of raloxifene (100nM), but the WT cells have little to no evidence of mineralization.
- At Day 16 the WT cells in raloxifene are showing a significant increase in mineralization compared to the cells in the absence of this drug
- The *Nmp4*<sup>-/-</sup> cells have mineralized to the point of obscuring any potential effect of the drug using this qualitative assay



#### ADDITIONAL RESEARCH ACTIVITIES:

##### *Breeding of conditional knockout (KO) mice*

The objectives for subtasks 4.2.a and 4.3.a are the breeding of *Nmp4<sup>fl/fl</sup> 3.6Col-Cre+*, *Nmp4<sup>fl/fl</sup> Cathepsin K-Cre+*, and *Nmp4<sup>fl/fl</sup>-Cre-* mice. After breeding our germline transmission mice with the B6.129S4-Gt(ROSA)26Sortum2(FLP)Sor/J mice to remove the Neo gene we obtained evidence that the 5' floxed site was absent in the offspring. We are currently repeating these analyses and if necessary will devise a strategy for restoring this site.

#### KEY RESEARCH ACCOMPLISHMENTS FOR 2<sup>ND</sup> YEAR:

- KEY FINDING: Mice receiving PTH+RAL and PTH+ZOL showed the largest BMD increase after ovx.
- KEY FINDING: The PTH+RAL therapy was the only treatment to exhibit a synergistic effect on total WB and spine BMD
- KEY FINDING: Disabling *Nmp4* enhanced PTH+RAL-induced increases in femoral BV/TV and increased the synergistic action of PTH with RAL and ZOL in both the femur and spine.
- KEY FINDING: Disabling *Nmp4* enhanced the distinction between the PTH+RAL-induced increase in cortical bone area and the other combination treatments
- KEY FINDING: *Nmp4*<sup>-/-</sup> mice under the PTH+RAL combination therapy harbored more bone marrow osteoprogenitors than mice under the other treatments
- KEY FINDING: Raloxifene enhanced WT mesenchymal stem/progenitor cell (MSPC) mineralization

#### REPORTABLE OUTCOMES:

*Abstract presentations in which the DOD support was acknowledged:*

1. American Society for Bone & Mineral Research:
  - a. Date/location: October 9-12 2015, Seattle, WA
  - b. Title: Improving PTH/Raloxifene Combination Osteoporosis Therapy In a Preclinical Model
  - c. Authors: Yu Shao, Selene Hernandez-Buquer, Paul Childress, Dan Brown, Yongzheng He, Marta Alvarez, Feng-chun Yang, Stuart J Warden, Matthew R Allen, Joseph P Bidwell

*Manuscripts submitted:*

1. Molecular Endocrinology:
  - a. Date: July 8, 2015 [revised, see Appendix]
  - b. Title: Genome-wide mapping and interrogation of the *Nmp4* anti-anabolic bone axis
  - c. Authors: Paul Childress, Keith Stayrook, Marta B Alvarez, Zhiping Wang, Yu Shao, Selene Hernandez-Buquer, Justin K Mack, Zachary R Grese, Yongzheng He, Daniel Horan, Fredrick M Pavalko, Stuart J Warden, Alexander G Robling, Feng-chun Yang, Matthew R Allen, Venkatesh Krishnan, Yunlong Liu, Joseph P Bidwell

*Funding applied for based on work supported by this award:*

Agency: NIH

Program: NIAMS

Title: Boosting Bone Anabolism and Bone Regeneration

Date submitted: 10/05/2014

Total costs & dates if funding awarded: \$3,010,660 [03/01/2015-02/28/2020]

CONCLUSION: Key experimental discovery for 2<sup>nd</sup> year of DOD study

*Our key discovery is that disabling Nmp4 significantly improves PTH+raloxifene combination therapy in an ovariectomized preclinical osteoporosis model but does not have a strong impact on PTH+bisphosphonate combination treatments*

"So what?"

Women comprise the fastest growing group of the US veterans contributing to the looming osteoporosis epidemic within the veteran population. The Veterans Affairs (VA) health care system will be in high demand by female veterans of Operation Enduring Freedom and Operation Iraqi Freedom. PTH is the only FDA-approved anabolic osteoporosis therapy and adds significant amounts of bone to the osteoporotic skeleton. Therefore, this drug has the potential to restore the bone lost in a variety of VA clinical settings. However, a drawback to PTH use is that potency declines within 2 years and thus it is not suitable as a long-term therapy, which is problematic in treating a chronic degenerative disease. Clinicians have attempted to improve PTH therapy by adding an anti-catabolic (e.g. raloxifene or a bisphosphonate) to the treatment. This has not met with success. The present discovery supports our contention that disabling Nmp4 or some component of its pathway will unlock the block on PTH combination therapies and enhance/extend regeneration of osteoporotic bone in post-menopausal female veterans.

#### REFERENCES:

1. He Y, Childress P, Hood M Jr, Alvarez M, Kacena MA, Hanlon M, McKee B, Bidwell JP, Yang FC. 2013 Nmp4/CIZ suppresses the parathyroid hormone anabolic window by restricting mesenchymal stem cell and osteoprogenitor frequency. *Stem Cells Dev.* 22(3):492-500
2. Childress P, Philip BK, Robling AG, Bruzzaniti A, Kacena MA, Bivi N, Plotkin LI, Heller A, Bidwell JP. 2011 Nmp4/CIZ suppresses the response of bone to anabolic parathyroid hormone by regulating both osteoblasts and osteoclasts. *Calcif Tissue Int.* 89(1):74-89.
3. Robling AG, Childress P, Yu J, Cotte J, Heller A, Philip BK, Bidwell JP. 2009 Nmp4/CIZ suppresses parathyroid hormone-induced increases in trabecular bone. *J Cell Physiol* 129(3):734-43.
4. Lui PP, Lee YW, Mok TY, Cheuk YC, Chan KM. 2013 Alendronate reduced peri-tunnel bone loss and enhanced tendon graft to bone tunnel healing in anterior cruciate ligament reconstruction. *Eur Cell Mater.* 25:78-96.
5. Ettinger B, San Martin J, Crans G, Pavo I. 2004 Differential effects of teriparatide on BMD after treatment with raloxifene or alendronate. *J Bone Miner Res.* 19(5):745-51.
6. Muschitz C, Kocijan R, Fahrleitner-Pammer A, Lung S, Resch H. 2013 Antiresorptives overlapping ongoing teriparatide treatment result in additional increases in bone mineral density. *J Bone Miner Res.* 28(1):196-205.
7. Cano A, Dapía S, Noguera I, Pineda B, Hermenegildo C, del Val R, Caeiro JR, García-Pérez MA. 2008 Comparative effects of 17beta-estradiol, raloxifene and genistein on bone 3D microarchitecture and volumetric bone mineral density in the ovariectomized mice. *Osteoporos Int.* 19(6):793-800.
8. Cosman F, Eriksen EF, Recknor C, Miller PD, Guañabens N, Kasperk C, Papanastasiou P, Readie A, Rao H, Gasser JA, Bucci-Rechtweg C, Boonen S. 2011 Effects of intravenous zoledronic acid plus subcutaneous teriparatide [rhPTH(1-34)] in postmenopausal osteoporosis. *J Bone Miner Res.* 26(3):503-11.
9. Sheng ZF1, Xu K, Ma YL, Liu JH, Dai RC, Zhang YH, Jiang YB, Liao EY. 2009 Zoledronate reverses mandibular bone loss in osteoprotegerin-deficient mice. *Osteoporos Int.* 20(1):151-9.
10. Viereck V, Gründker C, Blaschke S, Niederkleine B, Siggelkow H, Frosch KH, Raddatz D, Emons G, Hofbauer LC. 2003 Raloxifene concurrently stimulates osteoprotegerin and inhibits interleukin-6 production by human trabecular osteoblasts. *J Clin Endocrinol Metab.* 88(9):4206-13.
11. Taranta A, Brama M, Teti A, De luca V, Scandurra R, Spera G, Agnusdei D, Termine JD, Migliaccio S. 2002 The selective estrogen receptor modulator raloxifene regulates osteoclast and osteoblast activity in vitro. *Bone.* 30(2):368-76.
12. Lin Y, Liu LJ, Murray T, Sodek J, Rao L.J 2004 Effect of raloxifene and its interaction with human PTH on bone formation. *Endocrinol Invest.* 27(5):416-23.
13. Matsumori H, Hattori K, Ohgushi H, Dohi Y, Ueda Y, Shigematsu H, Satoh N, Yajima H, Takakura Y. 2009 Raloxifene: its ossification-promoting effect on female mesenchymal stem cells. *J Orthop Sci.* 14(5):640-5.
14. Giner M, Rios MJ, Montoya MJ, Vázquez MA, Miranda C, Pérez-Cano R. 2011 Alendronate and raloxifene affect the osteoprotegerin/RANKL system in human osteoblast primary cultures from patients with osteoporosis and osteoarthritis. *Eur J Pharmacol.* 15;650(2-3):682-7.

15. Somjen D, Katzburg S, Sharon O, Knoll E, Hendel D, Stern N. 2011 Sex specific response of cultured human bone cells to ER $\alpha$  and ER $\beta$  specific agonists by modulation of cell proliferation and creatine kinase specific activity. *J Steroid Biochem Mol Biol.* 125(3-5):226-30.
16. Wu X, Estwick SA, Chen S, Yu M, Ming W, Nebesio TD, Li Y, Yuan J, Kapur R, Ingram D, Yoder MC, Yang FC. 2006 Neurofibromin plays a critical role in modulating osteoblast differentiation of mesenchymal stem/progenitor cells. *Hum Mol Genet.* 15(19):2837-45.

#### APPENDIX:

Note: Full copy of the submitted manuscript to MOL ENDO that includes details for materials and methods used to generate the data described is appended.



# Molecular Endocrinology

## Genome-wide mapping and interrogation of the Nmp4 anti-anabolic bone axis --Manuscript Draft--

Manuscript Number:	ME-14-1406R1
Article Type:	Research Paper
Full Title:	Genome-wide mapping and interrogation of the Nmp4 anti-anabolic bone axis
Order of Authors:	Paul Childress, MS Ketih Stayrook, BS Marta B Alvarez, DDS, PhD Zhiping Wang, PhD Yu Shao, BS Selene Hernandez-Buquer, MS Justin K Mack, BS Zachary R Grese, BS Yongzheng He, PhD Daniel Horan, BS Fredrick M Pavalko, PhD Stuart J Warden, PhD Alexander G Robling, PhD Feng-chun Yang, MD, PhD Matthew R Allen, PhD Venkatesh Krishnan, PhD Yunlong Liu, PhD Joseph Bidwell, PhD
Author Comments:	Disclosure statement: PC, MBA, ZW, YS, SHB, YH, DH, FMP, AGR, SJW, FCY, YL have nothing to disclose. Eli Lilly and Company has awarded research funds to JPB and MRA. Eli Lilly and Company funded part of this work. VK is an employee of Eli Lilly & Co and owns stock in this company. KS, JKM, and ZRG are employees of Eli Lilly & Co
Abstract:	<p>Parathyroid hormone (PTH) is an osteoanabolic for treating osteoporosis but its potency wanes. Disabling the transcription factor Nmp4 in healthy, ovary-intact mice enhances bone response to PTH and BMP2 and protects from unloading-induced osteopenia. These Nmp4<sup>-/-</sup> mice exhibit expanded bone marrow (BM) populations of osteoprogenitors and supporting CD8<sup>+</sup> T cells. To determine whether the Nmp4<sup>-/-</sup> phenotype persists in an osteoporosis model we compared PTH response in ovariectomized (ovx) wild type (WT) and Nmp4<sup>-/-</sup> mice. To identify potential Nmp4 target genes we performed bioinformatic/pathway profiling on Nmp4 ChIP-seq data. Mice (12wks) were ovx or sham-operated 4wks before the initiation of PTH therapy. Skeletal phenotype analysis included <math>\mu</math>CT, histomorphometry, serum profiles, FACS sorting and the growth/mineralization of cultured WT and Nmp4<sup>-/-</sup> BM mesenchymal stem progenitor cells (MSPCs). ChIP-seq data were derived using MC3T3-E1 pre-osteoblasts, murine embryonic stem cells, and two blood cell lines. OvX Nmp4<sup>-/-</sup> mice exhibited an improved response to PTH coupled with elevated numbers of osteoprogenitors and CD8<sup>+</sup> T cells, but were not protected from ovx-induced bone loss. Cultured Nmp4<sup>-/-</sup> MSPCs displayed enhanced proliferation and accelerated mineralization. ChIP-seq/gene ontology analyses identified target genes likely under Nmp4 control as enriched for negative regulators of biosynthetic processes. Interrogation of mRNA transcripts in non-differentiating and osteogenic differentiating</p>

	WT and Nmp4-/- MSPCs was performed on 90 Nmp4 target genes and differentiation markers. These data suggest that Nmp4 suppresses bone anabolism, in part, by regulating insulin-like growth factor binding protein expression. Changes in Nmp4 status may lead to improvements in osteoprogenitor response to therapeutic cues.
<b>Additional Information:</b>	
<b>Question</b>	<b>Response</b>
<p>Do you confirm that your submission meets the standards described in the Instructions to Authors, <a href="#">Cell Line Authentication?</a> as follow-up to "CELL LINES:</p> <p>Does your submission include cell lines? (If you have questions, please contact the editorial staff at <a href="mailto:molendo@endocrine.org">molendo@endocrine.org</a>)</p> <p>"</p>	Yes
<p>FUNDING SOURCES:</p> <p>Please list all sources of funding for this manuscript. This should be included on the title page of your manuscript as well. If no funding, then respond NOT APPLICABLE.</p>	DOD and Eli Lilly
<p>STEROID HORMONE ASSAYS:</p> <p>Does your submission include steroid hormone assays? (If you have questions, please contact the editorial staff at <a href="mailto:molendo@endocrine.org">molendo@endocrine.org</a>)</p>	No
<p>CELL LINES:</p> <p>Does your submission include cell lines? (If you have questions, please contact the editorial staff at <a href="mailto:molendo@endocrine.org">molendo@endocrine.org</a>)</p>	No

**INDIANA UNIVERSITY****DEPARTMENT OF ANATOMY AND CELL BIOLOGY**

School of Medicine

07/06/15

Stephen R. Hammes, M.D., Ph.D.

Editor-in-Chief, Molecular Endocrinology

Dear Dr Hammes;

We are pleased to submit our revised manuscript Ref.: Ms. No. ME-14-1406 “*Genome-wide mapping and interrogation of the Nmp4 anti-anabolic bone axis*” for your consideration. We thank the reviewers for their insightful and helpful comments. We have made a substantial effort to comprehensively address their concerns (see separate file RESPONSE TO REVIEWERS). This includes the addition of a study to evaluate gene expression in non-differentiating and in osteogenic-differentiating WT and *Nmp4*<sup>-/-</sup> MPSCs during a 16-day culture period at five time-points using a custom Taqman Low-Density Array system designed for 96 genes including Nmp4 target genes identified by our genome-wide ChIP-seq profiling, non-target genes that drive osteogenic differentiation and marker genes of this process. These results provide considerable new information on how Nmp4 may suppress the anabolic response to PTH. Additionally, these new data strengthen our assertion that further interrogation of the Nmp4 anti-anabolic network will identify pharmacologically accessible pathways for adding new bone to the old skeleton. The supplemental files are intended for online publication. **Note that the revised/new text is in red font with a black line in the right margin.** Finally, there is no requirement for a PDB number and we are not reporting a new structure or compounds.

Sincerely,

Joseph Bidwell  
Professor

## RESPONSE TO REVIEWERS

Ms. No. ME-14-1406 “*Genome-wide mapping and interrogation of the Nmp4 anti-anabolic bone axis*”

We thank the reviewers for the helpful and insightful comments. We believe that following their advice has made this a more powerful and informative study. Please note **that the revised/new text is in red font with a black line in the right margin.**

### **Comment: The phenotypic studies in the current work are merely confirmative**

**Response:** The reviewers raise an important issue and we clearly failed to emphasize the significance of the questions addressed by these experiments.

- Our data are a key and obligatory *preclinical extension* of the *Nmp4*<sup>-/-</sup> phenotype. An overriding objective of the *Nmp4* studies is to determine if this network of pathways harbor potential targets for treating postmenopausal osteoporosis. Therefore we addressed two central phenotype questions in the present study:
  - (i) Does disabling *Nmp4* protect mice from ovariectomy-induced bone loss as it does in disuse-induced osteopenia?
  - (ii) Does the exaggerated response to PTH therapy in *Nmp4*<sup>-/-</sup> mice persist after ovariectomy?

Our findings that the null mice are not protected from ovariectomy-induced bone loss yet maintain the amplified response to PTH therapy is an important discovery. These data begin to demarcate the potential *Nmp4*-based therapeutic strategies. We have revised both the Introduction and Discussion to emphasize these points.

### **Comment: If *Nmp4* suppresses *Igf1* and *Bmp2*, and cellular synthetic process, why there is no difference between WT vs. *Nmp4*<sup>-/-</sup> mice under either basal or OVX-challenged conditions? Why is there only enhanced response to PTH treatment?**

**Response:** The reviewer raises a significant question about features of the *Nmp4*<sup>-/-</sup> phenomenon. Although a definitive answer requires further study, we address this query in the Discussion. The key concepts of our response follow:

- The *Nmp4* phenomenon differs from the results of recent clinical trials in which neutralizing sclerostin, an inhibitor of the Wnt signaling pathway and osteoblast differentiation, significantly increases baseline bone mineral density.
- Apparently disabling *Nmp4* is not sufficient for driving excess bone formation but instead enlarges the number of osteoprogenitors that can be recruited once activated by an anabolic cue. The downregulation of *Cxcl12* in the *Nmp4*<sup>-/-</sup> cells may contribute to the increased number of CFU-F<sup>alk phos+</sup> osteoprogenitors (see low-density array data below).
- Once activated by an anabolic cue, e.g. PTH, the *Nmp4*<sup>-/-</sup> cells produce autocrine/paracrine factors that enhance the replication and differentiation of neighboring osteoprogenitors, a key early event driving the PTH anabolic response (see below).
- The occasionally observed elevated trabecular volume in untreated *Nmp4*<sup>-/-</sup> mice may be due to the sporadic local release of growth factors, e.g., *Igf1* and/or *Bmp2*.
- However exogenous pharmacological doses of PTH provide a stronger stimulus for triggering the response leading to an enhanced bone formation.
- The enhanced mineralization in *Nmp4*<sup>-/-</sup> MSPC culture is only observed upon the addition of the anabolic cue dexamethasone, an *Nmp4* target pathway.

**Comment: Table 1, why didn't the CTX bone resorption marker and P1NP bone formation marker show significant differences between the pre-op and post-op group, even in WT mice?**

**Response:**

- Surgery-induced changes in serum bone markers took longer than 4wks to be detected. Our mice showed the appropriate ovx-induced significant increases in body weight, decreases in uterine weight, and significant bone loss during the first 4wks post-op. Nevertheless, our study was not a longitudinal design in which repeated measures on each animal at numerous time points were obtained, thus the typical small increases in serum CTX seen in other ovx mouse studies may have been obscured. A more extensive time course for harvesting histomorphometry and serum samples is required to more fully characterize the anticipated differences in WT and *Nmp4<sup>-/-</sup>* dynamic bone remodeling. However, removal of a single outlier in the serum P1NP data indicated there was a 21% decline in serum P1NP in the *Nmp4<sup>-/-</sup>* mice during the first 4wks post-op but no significant change in the WT animals (Genotype p=0.37; Treatment p=0.16; GxT p=0.05, 2W ANOVA, see Results and Table 1 [revised]). Additionally, from pre-op to post-op 12wks (*vehicle-treated mice*) there was an approximately 50% decline in P1NP (genotype p=0.95; treatment p<0.0001; GxT p=0.36) and an approximate 20% decline in serum CTX (genotype p=0.14; treatment p=0.0003; GxT p=0.18). This suggests a decrease in bone remodeling in the untreated mice predominantly in the bone formation arm. We further address this issue in the revised Discussion.

**Comment: Figures 1 and 2, The *Nmp4<sup>-/-</sup>* mice without PTH seems to lose more bone at 12wks compared to the WT without PTH treatment. Why does this happen?**

**Comment: The difference of FEMUR BV/TV between WT and *Nmp4<sup>-/-</sup>* at 12 wks seems to be smaller (or the same) comparing to the difference of FEMUR BV/TV between WT and *Nmp4<sup>-/-</sup>* at 8wks. This phenomenon also can be found for the L5 BV/TV. Can authors explain this?**

**Response:**

- We agree that the graphical data suggest the vehicle-treated *Nmp4<sup>-/-</sup>* mice lose more bone between 8-12wks and that the difference between BV/TV in the two genotypes is smaller at the later time point, however stringent statistical analysis does not support this interpretation. Comparison of the femoral BV/TV data derived from the vehicle-treated mice at the 8wk and 12wk time points indicates a significant decline in both genotypes but no genotype or genotype x time interaction (Genotype p=0.44; Time p= 0.03; G x T 0.06, 2W ANOVA). A similar result is obtained with the L5 BV/TV data. This indicates that the modest enhanced bone loss in the *Nmp4<sup>-/-</sup>* mice observed 4wks post-op was stabilized or stabilizing by 8wks post-op.

**Comment: I wonder if the difference of the PTH treatment between *Nmp4<sup>-/-</sup>* and WT will be less when the follow-up time is longer than 12 weeks?**

**Response:**

- The reviewer's query whether the enhanced PTH-induced bone formation in the *Nmp4<sup>-/-</sup>* mice will decline after 12wks is very interesting. Although the elevated number of *Nmp4<sup>-/-</sup>* osteoprogenitors declined at 12wks post-op, the higher number of *Nmp4<sup>-/-</sup>* CD8+ T cells did not decrease. Therefore, although the augmented response to PTH might be weakened in these mice, it may not disappear since the persistent increased lymphocyte number would provide extra Wnt10b. We have revised the Discussion to incorporate this talking point.

**Comment:** The identification of *Nmp4* target genes relied solely on ChIP-seq analysis. As binding to the promoter may lead to either gene activation or repression, this approach can only reveal the binding properties, but does not reveal functional outcome. Gene expression analysis by either microarray or RNA-seq in parallel would be more informative.

**Comment:** The findings from ChIP-seq and bioinformatics analysis should be more extensively validated by ChIP-QPCR, mutagenesis and functional analysis, followed by rescuing experiments to determine whether the potential targets are truly functionally significant.

**Comment:** Although authors spent a great effort to create chip-seq data and the data is very interesting, but, regarding the specific genes/pathways that *Nmp4* may be involved in PTH treatment, findings from chip-seq data seem to fall short and is inconclusive. I am wondering if there are *Nmp4* targeted genes that are relevant to osteogenesis, bone mineralization, PTH and/or PTH treatment relevant pathways? In addition, have authors performed transcriptome profiling in relevant cells/tissues on those four experiment groups of animals? Did IGF1 or BMP express differently?

**Response:**

- We have added significantly more functional data to the revised manuscript. To evaluate gene expression in non-differentiating and in osteogenic-differentiating WT and *Nmp4*<sup>-/-</sup> MPSCs, RNA was isolated at five time points from both genotypes over the 16-day culture period. Individual cDNAs were quantified by qRT-PCR using a custom Taqman Low-Density Array system (Format 96a, Applied Biosystems, Foster City, CA) designed for 96 genes including *Nmp4* target genes identified by our genome-wide ChIP-seq profiling, non-target genes that drive osteogenic differentiation and marker genes of this process. Our results are presented in Figures 9, 10 and Supplemental Figure 2A-2E. These data are very informative and suggest a mechanism underlying the enhanced PTH-induced anabolism in the *Nmp4*<sup>-/-</sup> mice. Briefly, the *Nmp4*<sup>-/-</sup> cells showed a dramatic surge in the expression of *Igfbp2* and downregulation of *Igfbp4* during the early stages of differentiation, both *Nmp4* target genes. *Igfbp2* is a strong autocrine/paracrine anabolic signal and a recent study demonstrated that over-expression of this gene accelerated mineralization and enhanced osteocalcin (*Bglap*) expression in bone cells [Xi et al., 2014], strikingly similar to the phenotype of our null osteoprogenitors. *Igfbp4* is a potent inhibitor of osteogenesis [Miyakoshi et al., 1999]. Interestingly, disabling *Nmp4* had no impact on the mRNA expression of the target genes *Igf1* and *Igfr1* but did elevate expression of *Pdk1*, a key component of the *Igf1*/insulin signaling pathway. Near the end of the 16-day differentiation period the *Nmp4*<sup>-/-</sup> cells exhibited an enhanced anabolic profile and expressed elevated levels of the non-target genes *Bmp2*, *Pth1r*, and *Bglap*. We also described the markedly downregulation of *Cxcl12* in the *Nmp4*<sup>-/-</sup> cells, a gene that plays a significant role in MSPC osteolineage commitment. Other differences between the WT and *Nmp4*<sup>-/-</sup> mRNA expression profiles are described. We agree that mutagenesis and rescuing experiments are the next step in analyzing the *Nmp4* network but we respectfully contend that they are beyond the scope of the present study.
- Our *Nmp4* ChIP-seq-derived map is the vital first step for deciphering the gene regulatory networks underlying the biological processes of this novel anti-anabolic axis. Our low-density array results are the first step in validating the reliability of this map.

**Comment: Tables 1 and 2: It would be great to know the number of animals in each group.**

**Response:** We have placed this information in Tables 1 and 2.



1                   **Genome-wide mapping and interrogation of the Nmp4 anti-anabolic bone axis**  
2     Paul Childress<sup>1</sup>, Keith R. Stayrook<sup>2</sup>, Marta B Alvarez<sup>3</sup>, Zhiping Wang<sup>4, 5</sup>, Yu Shao<sup>4</sup>, Selene Hernandez-  
3     Buquer<sup>1</sup>, **Justin K Mack<sup>2</sup>**, **Zachary R Grese<sup>2</sup>**, Yongzheng He<sup>6, 7</sup>, Daniel Horan<sup>1</sup>, Fredrick M Pavalko<sup>8</sup> |  
4     Stuart J Warden<sup>9, 10</sup>, Alexander G Robling<sup>1</sup>, Feng-Chun Yang<sup>6, 7</sup> Matthew R Allen<sup>1</sup>, Venkatesh Krishnan<sup>2</sup>,  
5     Yunlong Liu<sup>4, 5</sup>, Joseph P Bidwell<sup>1, 4¶</sup>

- 6  
7             1. Department of Anatomy & Cell Biology, Indiana University School of Medicine (IUSM),  
8             Indianapolis, IN, 46202  
9             2. Lilly Research Laboratories, Eli Lilly and Company, Indianapolis, Indiana, USA.  
10            3. Orthopaedic Surgery IUSM  
11            4. Department of Medical and Molecular Genetics, IUSM  
12            5. Center for Computational Biology and Bioinformatics, IUSM  
13            6. Department of Pediatrics, IUSM  
14            7. Herman B Wells Center for Pediatric Research  
15            8. Cellular & Integrative Physiology  
16            9. Center for Translational Musculoskeletal Research, School of Health and Rehabilitation Sciences,  
17             IN University  
18            10. Department of Physical Therapy, School of Health and Rehabilitation Sciences, IN University

19  
20     **Abbreviated title:** The Nmp4 anti-anabolic axis  
21     **Key terms:** bioinformatics, ChIP-seq, gene ontology, **low-density arrays**, osteoporosis, |  
22     osteoprogenitors, ovariectomy  
23     **Word count:** Main text: 8,075; Abstract 250; References 2203; Figure legends 1193; Supplemental  
24     legends 516]  
25     **Number of figures and tables:** Ten figures + Two supplementary figures, Five tables + Three  
26     supplementary tables

¶Corresponding Author:

Joseph P. Bidwell

Department of Anatomy & Cell Biology

Indiana University School of Medicine

Medical Science Bldg 5035, 635 Barnhill Drive

Indianapolis, IN 46202

E-mail: [jbidwell@iupui.edu](mailto:jbidwell@iupui.edu)

**Disclosure statement:** PC, MBA, ZW, YS, SHB, YH, DH, FMP, AGR, SJW, FCY, YL have nothing to disclose. Eli Lilly and Company has awarded research funds to JPB and MRA. Eli Lilly and Company funded part of this work. VK is an employee of Eli Lilly & Co and owns stock in this company. KS, JKM, and ZRG are employees of Eli Lilly & Co

**ABSTRACT:**

Parathyroid hormone (PTH) is an osteoanabolic for treating osteoporosis but its potency wanes. Disabling the transcription factor *Nmp4* in healthy, ovary-intact mice enhances bone response to PTH and BMP2 and protects from unloading-induced osteopenia. These *Nmp4*<sup>-/-</sup> mice exhibit expanded bone marrow (BM) populations of osteoprogenitors and supporting CD8<sup>+</sup> T cells. To determine whether the *Nmp4*<sup>-/-</sup> phenotype persists in an osteoporosis model we compared PTH response in ovariectomized (ovx) wild type (WT) and *Nmp4*<sup>-/-</sup> mice. To identify potential *Nmp4* target genes we performed bioinformatic/pathway profiling on *Nmp4* ChIP-seq data. Mice (12wks) were ovx or sham-operated 4wks before the initiation of PTH therapy. Skeletal phenotype analysis included  $\mu$ CT, histomorphometry, serum profiles, FACS sorting and the growth/mineralization of cultured WT and *Nmp4*<sup>-/-</sup> BM mesenchymal stem progenitor cells (MSPCs). ChIP-seq data were derived using MC3T3-E1 pre-osteoblasts, murine embryonic stem cells, and two blood cell lines. OvX *Nmp4*<sup>-/-</sup> mice exhibited an improved response to PTH coupled with elevated numbers of osteoprogenitors and CD8<sup>+</sup> T cells, but were not protected from ovx-induced bone loss. Cultured *Nmp4*<sup>-/-</sup> MSPCs displayed enhanced proliferation and accelerated mineralization. ChIP-seq/gene ontology analyses identified target genes likely under *Nmp4* control as enriched for negative regulators of biosynthetic processes. **Interrogation of mRNA transcripts in non-differentiating and osteogenic differentiating WT and *Nmp4*<sup>-/-</sup> MSPCs was performed on 90 *Nmp4* target genes and differentiation markers. These data suggest that *Nmp4* suppresses bone anabolism, in part, by regulating insulin-like growth factor binding protein expression.** Changes in *Nmp4* status may lead to improvements in osteoprogenitor response to therapeutic cues.

250 words

## INTRODUCTION:

Patients with severe osteoporosis are often treated with parathyroid hormone (PTH), a potent osteoanabolic agent [Kraenzlin & Meier, 2011], however, the bone-building ability of this drug or its ‘anabolic window’ wanes, likely due to latent increases in bone resorption. [Cipriani et al., 2012; Baron & Hesse, 2012; Yu et al., 2011]. This limits its effectiveness to treat a chronic degenerative disease. Recent advances in bone-forming agents have shown that one can increase the extent of bone mass accrual with anti-SOST treatment compared to PTH (McClung et al., 2014). However, there may be unique pathways triggered by PTH, which allows for sustained targeting of early osteogenesis as evidenced by serum markers of bone formation such as N-terminal propeptide of type 1 procollagen (P1NP) and osteocalcin (OCN, Padhi et al., 2011; Saag et al., 2009). In contrast to PTH, anti-SOST antibodies may have a limited capacity for targeting osteoprogenitors as evidenced by a relatively transient up-regulation of collagen-based markers such as P1NP (McClung et al., 2014). Therefore given PTH’s unique mode of action, therapies that could enhance PTH-mediated recruitment of osteoprogenitors may add value to some patients. How to achieve this enhancement is not clear. For example, attempts to extend and enhance PTH efficacy by combining treatment with anti-resorptive medications have met with mixed success and have generally been underwhelming [Cosman et al., 2011; Finkelstein et al., 2010; Black et al., 2003].

Blocking the activity of Nmp4/CIZ (nuclear matrix protein 4/cas interacting zinc finger protein, ‘Nmp4’) in mice dramatically enhanced their response to anabolic doses of PTH [He et al., 2013; Childress et al., 2011; Robling et al., 2009], suggesting a potential strategy for an adjuvant therapy [Krane, 2005]. Intermittent exogenous doses of hormone stimulated equivalent new bone formation in wild type (WT) and *Nmp4*<sup>-/-</sup> mice during the first 2wks of challenge, but at 3wks of treatment the null mice exhibited greater than a 2-fold increase in new trabecular bone compared to their WT littermates [Childress et al., 2011]. This augmented skeletogenesis in the *Nmp4*<sup>-/-</sup> mice was extended to 7wks of treatment and was observed in the femur, tibia, and vertebra. Serum osteocalcin continued to rise at this time point in the *Nmp4*<sup>-/-</sup> mice but had decreased in the WT animals [Childress et al., 2011]. However, the PTH response of the cortical compartment was equivalent throughout treatment in the WT and null mice

[Robling et al., 2009]. This suggests that disabling *Nmp4* accelerates and enhances the response of bone to intermittent PTH [Childress et al., 2011].

*Nmp4*<sup>-/-</sup> bone may have a generalized accelerated and heightened response to systemic or local anabolic cues. For example, these mice also exhibited augmented BMP2-induced ectopic bone formation compared to their WT littermates [Morinobu et al., 2005]. The *Nmp4*-null mice showed an accelerated osseous regeneration after marrow ablation [Morinobu et al., 2005] and did not lose bone during hind limb unloading, which appeared to derive from an enhanced osteoblast activity [Hino et al., 2007].

Prerequisite for an adjuvant therapy target, disabling *Nmp4* has little impact on the health, longevity, or global baseline phenotype of the mouse, with a few exceptions. The *Nmp4*<sup>-/-</sup> baseline skeletal phenotype (i.e., bone mineral density and/or content and trabecular architecture) is generally equivalent compared to WT animals], although we have occasionally observed an unprovoked increase in bone properties in *Nmp4*<sup>-/-</sup> mice [He et al., 2013, Childress et al., 2011; Robling et al., 2009; Morinobu et al., 2005]. Similarly, male *Nmp4*<sup>-/-</sup> mice exhibit variable degrees of spermatogenic cell degeneration resembling germinal-cell aplasia with focal spermatogenesis resulting in *sporadic* infertility [Nakamoto et al., 2004].

Our recent work suggests that the cellular basis of the osteoanabolic repressor function of *Nmp4* is due to its effect on the bone marrow derived stromal stem/progenitor cells aka mesenchymal stem progenitor cells (MSPCs) [He et al., 2013]. *Nmp4*<sup>-/-</sup> mice have significantly more osteoprogenitor cells in their marrow, which lie in wait to be quickly mobilized to differentiate into active osteoblasts upon stimulation with various osteoanabolic stimuli [He et al., 2013]. There was no difference between WT and *Nmp4*<sup>-/-</sup> BM cellularity or profiles of several blood elements however, the null mouse exhibited a 4-fold increase in CD45<sup>-</sup>/CD105<sup>+</sup>/nestin<sup>+</sup>/CD146<sup>+</sup> BM osteoprogenitor cells. These markers are a common hallmark to CFU-F cells with osteogenic potential [Isern et al., 2013; Méndez-Ferrer et al., 2010] and indeed 4-fold more CFU-F<sup>Alk<sup>phos</sup>+</sup> and CFU-F<sup>Ob</sup> cells have been recovered from these mice compared to the WT animals [He et al., 2013; Morinobu et al., 2005]. A second, related phenomenon we have observed in *Nmp4*<sup>-/-</sup> mice is a 2-fold increase in the prevalence of CD8<sup>+</sup> T-cells in the femoral marrow—

the lymphocyte population that provides potent input to induce MSPCs down the osteoblast differentiation pathway [He et al., 2013; Bedi et al., 2012; Terauchi et al., 2009; Li et al., 2014]. These blood cells express the PTHR1 receptor and support the PTH anabolic response via the release of Wnt10b upon hormone challenge, which drives osteoprogenitor differentiation to pre-osteoblasts and mature matrix-producing bone cells [Bedi et al., 2012; Terauchi et al., 2009; Li et al., 2014].

There is little information on the molecular mechanisms and cellular pathways that mediate the anti-anabolic action of Nmp4. This transcription factor is a Cys<sub>2</sub>His<sub>2</sub> zinc finger protein that primarily localizes to the nucleus although there is evidence for cytoplasmic activity [Bidwell et al., 2012; Nakamoto et al., 2000]. The zinc fingers recognize the DNA minor groove of an AT-rich consensus sequence and two transactivation domains can suppress or activate transcription depending on the cellular context [Shah et al., 2004; Torrungruang et al., 2002; Thunyakitpisal et al., 2001; Nakamoto et al., 2000; Alvarez et al., 1998]. The amino terminus of the rodent protein contains an SH3-binding domain that associates with the adaptor signaling protein p130Cas [Nakaomoto et al., 2000], but the functional significance of this interaction remains unknown.

The *Nmp4*<sup>-/-</sup> progenitor cells and their progeny have an exaggerated stimulus response at the levels of transcription and cell signaling [Alvarez et al., 2012; Yang et al., 2010; Shen et al., 2002]. *Nmp4*-null bone marrow stromal cells (BMSCs) show an enhanced transcriptional response to PTH and BMP2 [Alvarez et al., 2012; Shah et al., 2004; Shen et al., 2002]. The *Nmp4*<sup>-/-</sup> derived calvarial cells exhibit an increased load-induced phosphorylation of Pi3k and Akt and beta-catenin nuclear translocation [Yang et al., 2010]. Analogous to heightened response to anabolic signals in *Nmp4*<sup>-/-</sup> osteolineage cells, osteoclast preparations from the null mice exhibited a heightened response to the remodeling signals of RANKL and M-CSF (Childress et al., 2011).

Two essential genotype-phenotype questions remaining to be addressed are (i) whether the *Nmp4*-null mouse is resistant to ovariectomy (ovx)-induced bone loss and (ii) if disabling *Nmp4* improves PTH-based bone therapy in the OVX model. This is a focal preclinical extension of the *Nmp4*<sup>-/-</sup> phenotype necessary before this gene and its associated pathways can be considered potential targets for an adjuvant



therapy. Additionally, we used expanded cultures of WT and *Nmp4*<sup>-/-</sup> mesenchymal stem/progenitor cells (MSPCs) to probe the cell autonomous proliferative and mineralization activities of this cell population. To delineate the framework of the Nmp4 anti-anabolic network we performed genome-wide chromatin immunoprecipitation sequencing (ChIP-seq) on MC3T3-E1 cells and combined these data with the data available for Nmp4 (a.k.a. Znf384) from the Mouse Encyclopedia of DNA Elements (ENCODE) Consortium for transcription factors [Stamatoyannopoulos et al., 2012]. Bioinformatic profiling, gene ontology (GO), and pathway analysis were performed on these data sets to infer a map of the negative regulation of bone anabolism under Nmp4 control. Interrogation of mRNA transcripts in non-differentiating and osteogenic differentiating WT and *Nmp4*<sup>-/-</sup> MSPCs was performed on 90 Nmp4 target genes and differentiation markers to inaugurate validation of the Nmp4 anti-anabolic network.

## MATERIALS AND METHODS:

*Mice:* Male and female *Nmp4*<sup>-/-</sup> mice, backcrossed onto a C57BL/6J background for 7 generations [He et al., 2013, Childress et al., 2011; Robling et al., 2009], and their WT littermates were produced and maintained in our colony at Indiana University Bioresearch Facility, Indiana University School of Dentistry. Our local Institutional Animal Care and Use Committee approved all husbandry practices and experimental procedures and regimens described in this investigation.

*Bilateral ovariectomy surgery:* 12wk-old virgin mice were anesthetized using isoflurane inhalation followed by a mixture of xylazine and ketamine administered intraperitoneally. A 1-2cm dorsal incision was made in the midline below the level of the last rib and the skin bluntly dissected from the muscle on either side of the incision. Through the skin incision, the muscle wall was incised 1cm lateral to the midline 1-2cm below the last rib to enter the abdominal cavity. The periovarian fat pad was located and gently grasped and exteriorized. Care was taken not to directly handle the ovary to avoid abdominal implantation of ovarian tissue. While holding the periovarian fat pad with forceps, the fallopian tube between the fat pad and uterus was clamped and crushed using mosquito hemostats. The crushed area was

cut with scissors and the fat pad with ovary removed. The procedure was repeated on the contralateral side. The skin incision was closed with one or two surgical wound clips. The sham surgeries involved all the outlined steps except the crushing the fallopian tubes and the actual removal of the ovaries. To confirm the efficacy of OVX, uteri were weighed following euthanasia.

*PTH treatment:* At 16 wks of age, ovx animals were sorted into four treatment groups based on equivalent mean-group-body weight. These four groups included 1) vehicle-treated WT; 2) PTH-treated WT; 3) vehicle-treated *Nmp4<sup>-/-</sup>* and 4) PTH-treated *Nmp4<sup>-/-</sup>* mice. Mice were injected subcutaneously (sc) with synthetic human PTH 1-34 acetate salt (Bachem Bioscience Inc, PA) at 30µg/kg/day, daily or vehicle control (0.2% BSA/1.0µN HCl in saline, Abbott Laboratory, North Chicago, IL) for the length of time indicated.

*Cell culture:* Cells from ATCC (MC3T3-E1 subclone 4) were maintained in  $\alpha$ -MEM medium supplemented with 100 IU/ml penicillin, 100 µg/ml streptomycin, 25 µg/ml amphotericin, 2 mM L-glutamine (Gibco BRL, Grand Island, NY), ascorbic acid (50µg/ml, Sigma-Aldrich, St Louis, MO), and 10% fetal bovine serum (FBS; Sigma-Aldrich, St Louis, MO). Expanded mesenchymal stem/progenitor cell (MSPC) cultures were established as previously described [Wu et al., 2006]. Briefly, long bone BM was isolated from euthanized mice 6-8wks of age and the mononuclear cells (BMMNCs) were isolated using a Ficoll gradient. These cells were plated in Mesencult™ Media + Mesencult™ Stimulatory Supplement (StemCell™ Technologies, Vancouver BC, Canada) and maintained in culture for 3-4wks without passage and fed every 5-7 days by removing 50% of the old media and adding 50% fresh media, very gently so as not to disturb the cells. At approximately 80% confluence, the cells were passaged at 1:3 dilution for two more passages before use or were frozen for storage. Cells were used for experiments between passages 5-10. For comparing cell proliferation rates between WT and *Nmp4<sup>-/-</sup>* MSPCs, the cells were transferred to  $\alpha$ -MEM medium without the ascorbic acid in 12-well plates at 5,000 cells/well (Day

0). Cells were counted on Day 2, 4, and 6 post-seeding prior to refreshing the medium for the remaining cells. To evaluate mineralizing capacity cells were transferred to osteogenic differentiation medium and after 48hrs (Day 0), which was comprised of  $\alpha$ -MEM supplemented with ascorbic acid (5-50 $\mu$ g/ml, Sigma Aldrich), dexamethasone (0-10nM, Sigma-Aldrich), and 10mM glycerol 2-phosphate disodium salt hydrate (BGP, Sigma-Aldrich). For controls, cells were passaged into fresh MesenCult medium without the osteogenic/mineralization supplements. Cells were stained for alkaline phosphatase activity using naphthol AS-MX phosphate and fast red violet B salt following the manufacturer's instructions (Sigma cat# 85L3R-1KT) or for mineralization using alizarin red.

To compare mRNA expression profiles of select genes in non-differentiating and osteogenic-differentiating WT and *Nmp4*<sup>-/-</sup> MSPCs, cells were seeded into 12-well plates at either 10,000 or 25,000 cells/well in Mesencult™ Media + Mesencult™ Stimulatory Supplement. Those cells at the lower seeding density were harvested on Day 3 post-seeding (non-differentiating). The remaining cells were transferred to osteogenic differentiation medium 48hrs post-seeding and harvested on Days 5, 7, 9, and 16.

*Flow cytometry*: Cellular surface marker profiles from BM and peripheral blood (PBL) were assessed as previously described [He et al., 2013]. The antibodies employed for flow cytometry were obtained from BD Biosciences (San Jose, CA). Stained cells were analyzed on an FACS Calibur (BD Biosciences) and results were quantified using FlowJo Version 8.8.6 software (TreeStar Inc, Ashland OR).

*Micro computed tomography ( $\mu$ CT)*: Trabecular bone architecture was analyzed as we have previously described [He et al., 2013; Childress et al., 2011]. Briefly, femurs and L5 vertebra were excised from the WT and *Nmp4*<sup>-/-</sup> mice after euthanasia, the muscle and connective tissue removed, and the bones transferred to 10% buffered formalin, 4°C for 48 hr, after which the bones were placed in 70% ethanol (4°C) until analyzed. For femur analysis a 2.6-mm span (~5 mm<sup>3</sup> of medullary space) of the excised distal femoral metaphysis was scanned in 70% ethanol on a desktop  $\mu$ CT ( $\mu$ CT 35; Scanco Medical AG, Bassersdorf, Switzerland) at 10  $\mu$ m resolution using 55-kVp tube potential and 400-msec integration time,

to measure three-dimensional morphometric properties. The entire vertebra (L5) were scanned using standard methods (Skyscan 1172). Bones were reconstructed and analyzed using the manufacturer's software. The trabecular bone between the two growth plates was isolated from the cortical shell via manual tracing and assessed for trabecular architecture. From the three dimensional reconstructions the following parameters were obtained using the Scanco and Skyscan software analyses: trabecular bone volume per total volume (BV/TV, %), connectivity density (Conn.D,  $\text{mm}^{-3}$ ), structure model index (SMI), trabecular number (Tb.N,  $\text{mm}^{-1}$ ), trabecular thickness (Tb.Th, mm), and spacing (Tb.Sp, mm) [Bouxsein et al., 2010].

*Bone histomorphometry:* All histomorphometric parameters were obtained as previously described [Childress et al., 2011] following the ASBMR guidelines [Dempster et al., 2013]. Briefly, mice were administered intraperitoneal injections of calcein green (20 mg/kg; Sigma-Aldrich) and alizarin red (25 mg/kg, Sigma-Aldrich) 6 and 3 days before euthanasia, respectively. The femur marrow cavity was exposed via cutting the anterior face of the epiphyseal plate. Bones were embedded in methyl-methacrylate subsequent to dehydration with graded alcohols, sectioned (4 $\mu\text{m}$ ) with a Leica RM2255 microtome (Leica Microsystems, Wetzlar, Germany), and mounted unstained on microscope slides and imaged under fluorescent light with a microscope system [Childress et al., 2011]. Bone formation rate (BFR), mineral apposition rate (MAR), and mineralizing surface (MS/BS) were obtained from a 0.03 $\text{mm}^2$  metaphyseal region of interest from 250 $\mu\text{m}$  to 1750 $\mu\text{m}$  below the growth plate using ImagePro 3.1 software (Media Cybernetics, Bethesda, MD, USA).

*Serum biochemistry:* We analyzed serum N-terminal propeptide of type 1 procollagen (P1NP) to evaluate global bone formation in our experimental mice using the Rat/Mouse P1NP EIA from IDS Immunodiagnostic Systems (Scottsdale, AZ) following the manufacturer's instructions. To follow bone resorption we analyzed serum C-terminal telopeptides (CTX) with the RatLaps<sup>TM</sup> ELISA (Immunodiagnostic Systems Inc) [Childress et al., 2011].

*Quantitative real-time PCR (qRT-PCR) analysis:* ChIP-qPCR was used to authenticate select ChIP-seq profiles employing SYBR Green assays and SYBR Green Supermix (Bio-rad, Hercules, CA). qRT-PCR reactions were carried out in triplicate on specific genomic regions. The resulting signals were normalized for primer efficiency by carrying out qRT-PCR reactions for each primer pair using Input DNA.

To evaluate gene expression in non-differentiating and in osteogenic-differentiating WT and *Nmp4*<sup>-/-</sup> MPSCs, RNA was isolated with RNAeasy columns according to the manufacturer's instructions (Qiagen, Gaithersburg, MD). The RNA was reverse-transcribed via the High-Capacity cDNA Reverse Transcription Kit (Applied Biosystems, Foster City, CA). RNA expression profiling was performed on three-four replicates per time point for both genotypes over the 16-day culture period. Individual cDNAs were quantified by qRT-PCR using a custom TLDA system (Format 96a, Applied Biosystems, Foster City, CA) designed for 96 genes including *Nmp4* target genes identified by our genome-wide ChIP-seq profiling, osteogenic differentiation marker genes, and candidate normalizer genes. All experiments were performed in biological quadruplicate or triplicate with TaqMan fast advanced master mix (Applied Biosystems) on a QuantStudio™ 7 Flex Real-Time PCR System. The probes used are listed in Supplemental Table 1. We used the ExpressionSuite v1.0.4™ analysis software (Applied Biosystems) to analyze these data. This software utilizes the comparative threshold cycle ( $\Delta\Delta CT$ ) method to quantify relative gene expression across a large number of genes and samples. The software provides options to normalize expression data using either global normalization or endogenous controls and calculates fold changes with P values. Gene expression data were normalized to five endogenous controls (*I8S*, *Gusb*, *Rplp2*, *B2m*, and *Hprt*) although we report *Gusb* and *Rplp2* data here. In all experiments, the CT upper limit was set to 40, meaning that all mRNA detectors with a CT value greater than or equal to 40 were excluded. The multiple-comparisons correction (Benjamini-Hochberg method for false-discovery rate) was applied to the data and a P value of  $\leq 0.05$  was considered significant. Additionally, individual qRT-PCR reactions were performed to monitor the expressions of *Sp7* (osterix, Mm00504574\_m1) and *Bglap* (osteocalcin, Mm03413826\_mH) using *Rplp2* as the normalizer (Mm03059047\_gH). The prepared

cDNA was used to set up qRT-PCR reactions using FastStart Universal Probe Master mix (Rox) (Roche Life Science, Indianapolis, IN).

*Chromatin immunoprecipitation sequencing (ChIP-seq) and ChIP analysis:* Cells from ATCC (MC3T3-E1 subclone 4) were seeded into twenty-one 150mm plates at an initial density of 50,000 cells/plate (320 cells/cm<sup>2</sup>) and maintained in  $\alpha$ MEM complete medium + ascorbic acid. On Day 14 post-seeding, cells were treated with 25nM hPTH(1-34) or vehicle control for 1hr before harvest. Subsequent to treatment cells were fixed with 1% formaldehyde for 15min and quenched with 0.125M glycine. Cell pellets were frozen in an ethanol dry ice bath and shipped to Active Motif for FactorPath™ analysis. The chromatin was isolated from the pellets by adding lysis buffer followed by disruption with a Dounce homogenizer. Lysates were sonicated and the DNA sheared to an average length of 300-500 bp. Genomic DNA (Input) was prepared by treating aliquots of chromatin with RNase, proteinase K and heat for de-crosslinking, followed by ethanol precipitation. Pellets were resuspended and the resulting DNA was quantified on a NanoDrop spectrophotometer. Extrapolation to the original chromatin volume allowed quantitation of the total chromatin yield. An aliquot of chromatin (30 $\mu$ g) was precleared with protein A agarose beads (Invitrogen, ThermoFisher Scientific, Waltham, MA). Genomic DNA regions of interest were isolated using 4 $\mu$ g antibody against ZNF384 (Sigma HPA004051, Lot A57874). Complexes were washed, eluted from the beads with SDS buffer, and subjected to RNase and proteinase K treatment. Crosslinks were reversed by incubation overnight at 65°C, and ChIP DNA was purified by phenol-chloroform extraction and ethanol precipitation.

*ChIP Sequencing (Illumina):* ChIP and Input DNAs were prepared for amplification by converting overhangs into phosphorylated blunt ends and adding an adenine to the 3'-ends. Illumina genomic adapters were ligated and the sample was size-fractionated (200-300 bp) on an agarose gel. After a final PCR amplification step (18 cycles), the resulting DNA libraries were quantified and sequenced on HiSeq 2000. Sequences (50nt reads, single end) were aligned to the mouse genome (mm10) using the BWA



algorithm. Alignments were extended in silico at their 3'-ends to a length of 150 bp, which is the average genomic fragment length in the size-selected library, and assigned to 32-nt bins along the genome. The resulting histograms (genomic "signal maps") were stored in BAR and bigWig files. ZNF384 peak locations were determined using the MACS algorithm (v1.4.2) with a cutoff of  $pvalue = 1e-7$  [Li and Durbin, 2009].

*Bioinformatic profiling:* In addition to generating our own Nmp4 ChIP-seq data from the MC3T3-E1 cells we used Nmp4 (Znf384) ChIP-seq data from murine embryonic stem cell line (ES-E14) and the B-cell lymphoma cell lines Ch12 and MEL from the ENCODE Consortium for transcription factors 2011 Freeze data sets in NarrowPeak format (Rosenbloom et al., 2013). To assign an Nmp4 peak to a promoter region it had to be within -5kb to +2kb from a transcription start site (TSS). To assign a peak to an intragenic region it had to be located within the range defined by the TSS and the transcription end site (TES), and not within the promoter range of the same gene. To assign a peak to an intergenic region it had to be -10,000kb from the TSS and +10,000kb from the TES, and not within the promoter range of the same gene. A peak could be assigned to multiple functional regions in an area of the genome harboring multiple genes. A common example of this is an area with genes on both strands. A peak may not fit any of these definitions and was assigned to the classification "other". This methodology yielded 34,317 functional assignments for the peaks in the MC3T3-E1 cells.

*GEM analysis:* Genome wide Event finding and Motif discovery (GEM) [Guo et al., 2012] was used to derive the Nmp4 consensus sequence. The latest mouse genome build (mm10) was employed together with the GEM default ChIP-seq read distribution file and a minimal k-mer width of 6 and maximum of 20.

*Gene Ontology:* Gene ontology analysis was conducted using DAVID [Huang et al., 2009], and terms summarized using REVIGO [Supek et al., 2011]. The ENCODE ChIP-Seq Significance Tool was employed to identify enriched transcription factors in our Nmp4 gene target list [Auerbach et al., 2013]. Additionally some functional analysis was also generated through the use of QIAGEN's Ingenuity Pathway Analysis (IPA®, QIAGEN Redwood City, [www.qiagen.com/ingenuity](http://www.qiagen.com/ingenuity)).

*Bone phenotype statistical analysis:* Statistical evaluations were processed using the program JMP version 7.0.1 (SAS Institute, Cary, NC). The animal studies employed a two-way ANOVA using genotype and treatment as the independent variables followed by either a Tukey HSD or LS Means post hoc test if a genotype x treatment interaction was indicated. Statistical significance was set at  $p \leq 0.05$ . To compare growth rates of the WT and *Nmp4*<sup>-/-</sup> MSPCs derived from various experimental mice, we evaluated the slopes of log-transformed cell counts regressed onto experimental day using a t-test. The numbers of mice per treatment group and replicates/treatment for the cell studies are indicated in the appropriate figures and tables.

## RESULTS:

### *Nmp4*<sup>-/-</sup> mice are not protected from ovx-induced bone loss

To determine whether genetically disabling Nmp4 activity protects mice from ovx-induced bone loss as it does from unloading-associated osteopenia [Hino et al., 2007], we removed the ovaries or performed sham operations on both WT and *Nmp4*<sup>-/-</sup> mice (Figure 1). Both the ovx WT and ovx *Nmp4*<sup>-/-</sup> mice experienced significant weight gain at 4wks post-op (Table 1) consistent with previous mouse studies [Vieira Potter et al., 2012]. Additionally, ovx resulted in a significant decrease in uterine weight in both genotypes (Table 1). There was no genotype x treatment interaction in either of these parameters.

Both WT and *Nmp4*<sup>-/-</sup> mice exhibited significant bone loss 4wks after ovx surgery as measured in the trabecular bone compartment of the distal femur and the L5 vertebra (Table 1). The *Nmp4*<sup>-/-</sup> mice exhibited a trend towards enhanced loss of bone that neared significance in the distal femur (BV/TV, genotype x treatment interaction = 0.06, Table 1) and reached significance in the L5 vertebra (BV/TV, genotype x treatment interaction <0.05, Table 1). Despite this enhanced (or nearly enhanced) rate of bone loss the *Nmp4*<sup>-/-</sup> animals maintained more trabecular bone compared to WT mice during the first 4wks after ovariectomy. The *Nmp4*<sup>-/-</sup> mice exhibited a decrease in the serum bone formation marker PINP at 4wks post-op and both genotypes showed significant decreases in this marker at 12wks post-op in the

vehicle-treated mice. A small decrease in the serum bone resorption marker CTX was observed at 12wks post-op in the vehicle-treated mice.

*Ovx Nmp4<sup>-/-</sup> mice show an enhanced bone gain response to PTH therapy*

With a separate group of ovx mice we initiated treatment of both WT and *Nmp4*-null ovx animals with PTH (30µg/kg/day) or vehicle control 4wks after surgery. The duration of hormone therapy lasted 4wks (8wks post-op) and 8wks (12wks post-op). The ovx *Nmp4<sup>-/-</sup>* mice showed an enhanced PTH-induced gain in femoral BV/TV and Conn D at 4wks and 8wks of therapy compared to their ovx WT littermates as well as an augmented gain in trabecular thickness at 8wks (Figure 2, Table 2). The null mice also showed an enhanced PTH response at the L5 vertebra at 8wks of treatment (Figure 3, Table 2). Specifically the 2-way ANOVA indicated strong genotype x treatment effects for the distal femur for both 4wks and 8wks therapy and for the L5 vertebra for 8wks therapy (see Figures 2A and 3A); the post-hoc tests concluded that the difference between the genotypes was within the hormone-treated groups. The vehicle-treated ovx WT and ovx *Nmp4<sup>-/-</sup>* groups showed no difference in BV/TV (Figures 2 and 3) at the end of the treatment regimens indicating that the modest enhanced loss in bone in the *Nmp4<sup>-/-</sup>* mice was stabilized by 4wks therapy. PTH significantly elevated MAR, MS/BS, and BFR at the end of 4wks treatment as shown by strong treatment effects (Table 3). However, there was no genotype effect or genotype x treatment interaction for any of these parameters (Table 3). Hormone significantly elevated serum levels of the bone formation marker P1NP and the resorption marker CTX at 8wks of therapy, but there was no treatment x genotype interaction for either of these parameters (Table 3).

FACS analysis of the BM CD45<sup>-</sup>/CD105<sup>+</sup>/CD146<sup>+</sup>/nestin<sup>+</sup> osteoprogenitors revealed a significant elevation in the number of these cells in the BM obtained from the *Nmp4<sup>-/-</sup>* mice at the end of 4wk therapy, irrespective of treatment (Figure 4A). This is consistent with our previous observation in the ovary-intact null mice [He et al., 2013]. By the end of 8wks treatment (12wks post-op) the observed increase in the number of these *Nmp4<sup>-/-</sup>* cells in the BM failed to reach statistical significance, but there was a significant elevation in the number of the PBL *Nmp4<sup>-/-</sup>* osteoprogenitors in the vehicle-treated mice (Figure 4D). The

*Nmp4*<sup>-/-</sup> mice showed a significant elevation in CD8<sup>+</sup> T cells in both the BM and the PBL throughout the entire therapy regimen (Figure 4B and 4E). PTH significantly decreased the numbers of these cells in the BM at 8wks therapy in both genotypes (Figure 4B) but had no impact on the number of these cells in the PBL (Figure 4E). Disabling *Nmp4* had little to no effect on CD4<sup>+</sup> T cells, nor did treatment with PTH (Figure 4C and 4F). The modest increase in BM CD4<sup>+</sup> T cells approached significance ( $p < 0.06$ ) but this was not reflected in the PBL, just as we previously observed in the ovary-intact mice [He et al., 2013].

To determine if the enhanced osteogenic potential of the BM could be reliably and reproducibly maintained in vitro in MSPC cultures over several passages and in the absence of supporting cells (e.g. T-cells) we established expanded WT and *Nmp4*<sup>-/-</sup> MSPCs from ovary-intact mice. The expanded *Nmp4*<sup>-/-</sup> MSPCs from ovary-intact mice exhibited modest but significantly enhanced proliferation compared to the WT cells (Figure 5A). Both the null and WT expanded MSPCs showed strong alkaline phosphatase expression (Figure 5B). However, the expanded *Nmp4*<sup>-/-</sup> MSPCs typically showed an accelerated and enhanced mineralization compared to WT cells under various concentrations of dexamethasone and ascorbic acid (Figure 5B). Finally, the expanded *Nmp4*<sup>-/-</sup> and WT MSPCs exhibited varying degrees of alkaline phosphatase staining while maintained in MesenCult medium, depending on the confluence of the cells and time in culture (3-9 days), however no mineralization was observed in these control cultures (data not shown).

*Genome-wide ChIP-seq/gene ontology analysis reveals Nmp4 target genes and potential pathways of the anti-anabolic axis.*

*Nmp4* is expressed in nearly all cells, yet the most singular consequence of globally disabling this protein is the enhanced mobilization of bone cells upon osteoanabolic induction [He et al., 2013; Childress et al., 2011; Robling et al., 2009; Morinobu et al., 2005]. As a first step in understanding the origins of this phenotype, which may have clinical significance, we needed the following information: (1) the identity of the *Nmp4* target genes including ‘core’ target genes common to multiple cell types; (2) identify common functions of these core genes to distinguish pathways that make osteoprogenitors

particularly vulnerable to the effects of Nmp4 and (3) experimental confirmation of some of these pathways. To begin to understand how Nmp4 works we set out to understand (4) whether Nmp4 targets functional regions of the genome, (5) if it binds directly to DNA or via other proteins, and (6) whether osteoanabolic agents, e.g. PTH, alter Nmp4 DNA-binding along target genes.

The potential Nmp4 target genes identified by ChIP-seq in the MC3T3-E1 (vehicle-treated) cells and those established in the three ENCODE cell lines were compared using those genes that had one or more peaks associated with the TSS. A Venn diagram of these genes showed that 2114 Nmp4 ‘core’ target genes were common to the four cell lines (Figure 6A, and Supplemental Table 1). These core target genes were classified into functionally related categories using gene ontology (GO) analysis with the Database for Annotation, Visualization, and Integrated Discovery (DAVID) tool [Huang et al, 2009]. The functional annotation-clustering algorithm was applied to the target list, which is able to give a more insightful view of the relationships between annotation categories and terms compared to other analytic modules [Huang et al., 2009]. The significance of group classification was defined by enrichment scores based on Fisher exact statistics (false discovery rate, FDR  $p < 0.05$ ). The DAVID-derived biological profile was further summarized using REVIGO [Supek et al., 2011]. GO analysis of the core target genes designated Nmp4 as a negative regulator of cellular biosynthetic processes showing significant enrichment for genes involved in the regulation of transcription, chromatin modification, protein catabolic processes, regulation of the cell cycle, and mRNA processing/splicing (Figure 6B). Interestingly, the genes *specific* to any one particular cell line or specific to vehicle-treated or PTH-treated MC3T3-E1 cells did not yield a distinct biological process profile that reached statistical significance as obtained with the core target genes (data not shown). However, peak-associated genes common to the vehicle- and PTH-treated MC3T3-E1 cells yielded a profile nearly identical to that obtained with the core target genes.

Next we probed existing datasets for enriched transcription factors within our Nmp4 core target gene list using the ENCODE ChIP-seq Significance Tool [Auerbach et al., 2013] (Table 4). This profile shows that Nmp4 binding in the promoter regions of its target genes predominantly co-occurs with proteins that regulate chromatin organization and with proteins that contribute to maintaining

stem/progenitor pluripotency/multipotency and the poised gene state, e.g. CHD2, SIN3a, and GCN5 [Harada et al., 2012; Nascimento et al., 2011; Lin et al., 2007].

In an effort to gain further understanding of how Nmp4 regulates gene expression we prepared a genome-wide functional region map of the Nmp4 binding sites for all four cell types as described in Materials and Methods. The majority of the occupancy peaks were located in or near the TSS or in intragenic regions, areas typically associated with regulatory functions (Figure 7A). To determine if Nmp4 binds directly to DNA or can associate with the genome via other proteins we used the discovery algorithm GEM to derive the Nmp4 consensus-binding site from the MC3T3-E1 data. In support of previous studies by our lab and others the derived binding site matched the unusual homopolymeric (dA·dT) consensus sequence previously derived by cyclic amplification and electrophoretic mobility shift assay [Alvarez et al., 1998; Nakamoto et al., 2000] (Figure 7B). No other consensus sequences were identified suggesting a single and direct mode of genome association, mediated by the Cys2His2 DNA-binding domain [Torrunguang et al., 2002]. To determine whether PTH challenge altered Nmp4 DNA-binding along target genes we generated genome-wide Nmp4 ChIP-seq profiles using the pre-osteoblast cell line MC3T3-E1 treated with hPTH(1-34) or vehicle control for 1hr. We used the 1hr time point because we observed the most significant differences in femoral mRNA expression profiles between WT and *Nmp4*<sup>-/-</sup> mice 1hr after injection [Childress et al., 2011]. Hormone reduced Nmp4 genome-wide occupancy from a total of 15,446 to 13,109 binding sites. However, at the level of the single gene there was a diversity of changes in Nmp4 occupancy, i.e. PTH was observed to remove (e.g. *Nid2*), induce (e.g. *Ccdc53*) or have no effect on Nmp4-DNA association (e.g. *Akt2*, *Arrb2*) (Figure 8; also see ChIP-qPCR confirmation of Nmp4 binding, Figure S1).

As a first step in the validation of the ChIP-seq-derived anti-anabolic map we interrogated 90 mRNA transcripts in non-differentiating and osteogenic differentiating WT and *Nmp4*<sup>-/-</sup> expanded MSCs at five different time points. The accelerated and enhanced mineralization of the *Nmp4*<sup>-/-</sup> MSCs (Figure 5) is consistent with our previous observation that in response to PTH *Nmp4*<sup>-/-</sup> mice add more bone and add it faster than WT mice [Childress et al., 2011]. Our choice of Nmp4 target genes (Supplemental Table

1) was based on our DAVID analysis. We chose both core target genes and *Nmp4* target genes identified in the MC3T3-E1 pre-osteoblasts. DAVID also uses KEGG (Kyoto Encyclopedia of Genes and Genomes) database to map large gene lists to signaling pathways [Huang et al., 2009]. For example the DAVID/KEGG profile of the *Nmp4* core target genes included the TOR and insulin/IGF1 signaling pathways (Table 5) and indeed the insulin/IGF1->IRS1->PI3K->PDK1->Akt signaling response limb is common to many of the pathways listed. This is also consistent with our IPA analysis (Supplemental Table 3). Also included were *Nmp4* target genes coding for proteins involved in the ubiquitin-proteasome system, chromatin remodeling, transcription regulation, and RNA processing. Finally we analyzed the expression of osteogenic differentiation markers.

Volcano plots (Supplemental Figure 2) identify genes that were statistically significantly upregulated or downregulated by at least 2-fold in the *Nmp4*<sup>-/-</sup> cells compared to the WT cohort on the same day of culture. Figures 9 and 10 compare the relative mRNA expression of select genes to the level of the transcript in WT cells on Day 3 of culture thus providing a time course view. The *Nmp4*<sup>-/-</sup> cells showed a strikingly elevated expression of the *Nmp4* target gene *Igfbp2* mRNA and downregulation of the target gene *Igfbp4* mRNA during the early differentiation period (Figures 9A and 9B). *Igfbp2* stimulates osteoblast differentiation whereas the *Igfbp4* is a potent inhibitor of Igf actions [Xi et al., 2014; Miyakoshi et al., 1999]. Phosphoinositide-dependent kinase 1 (*Pdk1*, target gene) a key component of the Igf1/insulin signaling pathway [Calleja et al., 2014] was upregulated in the *Nmp4*<sup>-/-</sup> cells throughout the developmental time course (Figure 9C). Interestingly, neither the target genes *Igf1* nor its receptor *Igf1r* exhibited striking differences in gene expression between the two genotypes (data not shown). The *Nmp4*<sup>-/-</sup> cells exhibited an enhanced anabolic profile during the latter differentiation period as evidenced by elevated expression levels of the non-target genes *Bmp2* (Figure 9D), *Pth1r* (Figure 9E), and *Bglap* (osteocalcin, Figure 9F).

*Cxcl12* expression (target gene), also known as stromal derived factor 1, was dramatically downregulated in the *Nmp4*<sup>-/-</sup> cells throughout development (Figure 10A) and the target gene *Plaur* (*uPAR*, urokinase plasminogen activator receptor) was upregulated in the null cells (Figure 10B). Both



genes play roles in MSPC osteogenic lineage commitment (Shahnazari et al., 2013; Sugiyama et al., 2006; Furlan et al., 2007; Kalbasi et al., 2014). *Spp1* (osteopontin, target gene) and *Thbs2* (thrombospondin 2, target gene) regulate aspects of mineralization [Hunter 2013; Alford et al., 2010] and the former was upregulated in our null cell whereas the latter was downregulated (Figures 10C and 10D). Type I collagen (*Col1a1*, target gene) expression was elevated in the *Nmp4*<sup>-/-</sup> cells throughout the developmental period (Figure 10E). Interestingly, we observed no substantial difference in the expression profiles of *Sp7* (osterix, Figure 10F) or the target gene *Runx2* (data not shown), essential transcription factors for osteoblast differentiation (Komori, 2011).

## DISCUSSION:

Our findings that the *Nmp4*<sup>-/-</sup> mice are not protected from ovariectomy-induced bone loss yet maintain the amplified response to PTH therapy is a key advance necessary for further consideration of *Nmp4*-based treatment strategies. The ovx *Nmp4*<sup>-/-</sup> mice displayed an enhanced hormone-induced recovery of femoral and L5 trabecular BV/TV despite delaying treatment until 4wks post-op to allow for significant bone loss. Both the ovx WT and ovx *Nmp4*<sup>-/-</sup> mice showed strong responses to PTH therapy. After 4wks and 8wks of treatment the WT mice displayed a 3.2-fold and 4.6-fold increase in femoral BV/TV over vehicle-treated mice, respectively. However the *Nmp4*<sup>-/-</sup> mice showed a 3.6-fold and 8.8-fold increase over the same time period resulting in a very strong genotype x treatment interaction. Differences in PTH-mediated BV/TV restoration efficacy between the WT and *Nmp4*<sup>-/-</sup> mice in the L5 vertebra and was less striking although statistically significant (1.3-fold vs 1.6-fold at 8wks in the WT and *Nmp4*<sup>-/-</sup> mice, respectively). We observed similar PTH-responsive femoral and L5 profiles between younger, ovary-intact WT and *Nmp4*-null mice [Robling et al., 2009; Childress et al., 2011; He et al., 2013]. The histomorphometry and serum data reported here tracked the PTH-induced increases in bone mass in the ovx animals showing strong treatment effects for bone formation parameters MAR, BFR, and MS/BS (at 4wks treatment) as well as strong increases in bone remodeling serum PINP and CTX (at 8wks treatment). However, these parameters did not distinguish the genotypes in regards to the amount of bone formed

over this time period as was achieved with the  $\mu$ CT data. Interestingly, the histomorphometry data did not distinguish the differences in PTH-induced bone formation in ovary-intact WT and *Nmp4*<sup>-/-</sup> mice [Childress et al., 2011]. Our present observation that *Nmp4*<sup>-/-</sup> MSPCs exhibit an accelerated and enhanced mineralization in response to anabolic cues, i.e. osteogenic medium suggests that the augmented bone formation is an early event. Similarly, we did not observe the expected ovx-induced small increase in serum CTX. Instead, the serum data of the vehicle-treated mice showed a large decrease in P1NP and a smaller decrease in CTX over the time course of the entire experiment, i.e. pre-op vs 12wks post-op. This suggests a decrease in bone remodeling in the untreated mice predominantly in the bone formation arm. A more extensive time course with earlier harvest points for histomorphometry and serum samples is required to more fully characterize the anticipated differences in WT and *Nmp4*<sup>-/-</sup> dynamic bone remodeling.

The most robust phenotypic characteristic of *Nmp4* ablation is the exaggerated bone formation response to PTH or BMP2, which suggests that the adult mice harbor an increased number of BM MSPCs with heightened sensitivity to osteoanabolic signals. Disabling *Nmp4* has no observable impact on embryonic or perinatal skeletal development. Adult MSPCs are a heterogeneous population of multipotent stem, progenitor, and stromal cells that contribute to BM homeostasis [Mizoguchi et al., 2014]. In mouse bone marrow much of the CFU-F activity is in the nestin<sup>+</sup> cell population and in the human marrow the CD146<sup>+</sup> population [Mizoguchi et al., 2014; Sacchetti et al., 2007]. In ovary-intact, *Nmp4*<sup>-/-</sup> mice we observed a 4-fold increase in the frequency of CD45<sup>-</sup>/CD105<sup>+</sup>/CD146<sup>+</sup>/nestin<sup>+</sup> cells irrespective of treatment (PTH vs vehicle control), which paralleled the magnitude increase in CFU-F and CFU-F<sup>alk phos</sup><sup>+</sup> cell number in culture [He et al., 2013]. Similarly, the ovx *Nmp4*<sup>-/-</sup> mice exhibited an approximate 3-fold increase in the CD45<sup>-</sup>/CD105<sup>+</sup>/CD146<sup>+</sup>/nestin<sup>+</sup> cells at 8wks post-op compared to the ovx WT animals.

The enhanced osteogenic potential of the *Nmp4*<sup>-/-</sup> BM as measured by the frequency of cells capable of becoming osteoprogenitors persists in expanded *Nmp4*<sup>-/-</sup> MSPC cultures over 5-10 passages and removed from the supporting CD8<sup>+</sup> T cells. In culture these cells displayed a modest increase in

proliferative activity and perhaps this aspect of the phenotype contributes to the observed expanded pool of osteoprogenitors in vivo. In an earlier study, Noda and colleagues demonstrated that *Nmp4*<sup>-/-</sup> BM yielded significantly more CFU-F<sup>Ob</sup> mineralizing colonies at passage P<sub>0</sub> than WT BM [Morinobu et al., 2005]. Our present data extend these observations and show that the serially passaged *Nmp4*<sup>-/-</sup> MSPCs maintain a strikingly enhanced capacity for mineralization compared to the capacity of the WT cultures. Taken together these observations suggest that there is a cell autonomous role of *Nmp4* for regulating MSPC osteogenesis.

Our -omics data combined with our low-density array results suggest that upon challenge with an anabolic cue *Nmp4*<sup>-/-</sup> MSPCs produce autocrine/paracrine factors that enhance the replication and differentiation of neighboring osteoprogenitors, a key early event driving the PTH anabolic response [Jilka, 2007]. We observed that once *Nmp4*<sup>-/-</sup> cells were transferred to osteogenic medium they expressed strikingly elevated levels of the *Nmp4* target gene *Igfbp2*, a strong autocrine/paracrine factor that enhances osteogenesis (Xi et al., 2014). Consistent with our observations, overexpression of *Igfbp2* in MC3T3-E1 cells accelerated the time course of differentiation and mineralization as well as increased the total number of differentiating cells. By Day 6 in this previous study, *Igfbp2*-overexpressing cells expressed twice as much osteocalcin as control cultures and this difference persisted [Xi et al., 2014]. This is a strikingly similar phenotype to the *Nmp4*<sup>-/-</sup> cells. Interestingly, the expression of the *Nmp4* target gene *Igfbp4* was decreased in the null cells. This binding protein is a strong inhibitor of osteoblast differentiation [Miyakoshi et al., 1999] and thus its suppression may further accelerate and enhance the differentiation of the null cells. *Igf1* is a key mediator of the PTH anabolic response [Bikle & Wang, 2012; Elis et al., 2010] and although there was no notable alteration in the expression profiles of *Igf1* or *Igf1r* in the null cells, the expression of *Pdk1*, a target of *Nmp4* and a key kinase component of the *Igf1*/insulin signaling pathway was elevated. This may enhance the sensitivity of the *Nmp4*<sup>-/-</sup> cells to this growth factor. At the end of the 16-day culture period the *Nmp4*<sup>-/-</sup> cells exhibited an enhanced anabolic profile as evidenced by the elevated expressions of the non-target *Nmp4* genes *Bmp2*, *Pth1r*, and *Bglap*. Perhaps this is an autocrine/paracrine response to the earlier surge in *Igfbp2* expression. Indeed the *Igf1*

pathway plays a significant role in MSPC proliferation and mineralization [Kumar and Ponnazhagan, 2012; Xian et al., 2012] and the null cells exhibited alterations in the expression not only of *Bglap* but the *Nmp4* target extracellular matrix proteins *Colla1*, *Spp1*, and *Thbs2*. Although the molecular mechanisms underlying mineralization remain to be elucidated, *Spp1* is an anionic phosphoprotein expressed in mineralizing tissues that appears to regulate crystal size, shape, and location [Hunter, 2013]. *Thbs2* is an extracellular matrix glycoprotein that has pleiotropic effects on bone phenotype. This protein appears to suppress the MSPC osteoprogenitor pool but also supports mineralization [Alford et al., 2010; Hankenson et al., 2002; Hankenson et al., 2000]. Therefore whether the decrease in *Thbs2* expression in the *Nmp4*<sup>-/-</sup> cells impacts the observed alteration in the number of osteoprogenitors, alterations in mineralization or impacts cell phenotype in other ways remains to be determined. Finally, we observed no striking differences in the expression of the transcription regulators *Sp7* and *Runx2* between the genotypes. This suggests that disabling *Nmp4* alters select aspects of the developing osteoblast phenotype.

The dramatic decrease in *Cxcl12* expression in the *Nmp4*<sup>-/-</sup> cells raises the question as to whether this plays a role in the observed increase in CFU-F<sup>alk phos+</sup> osteoprogenitors in the null mice [He et al., 2013; Morinobu et al., 2005 and the present work]. *Cxcl12* and its receptor *Cxcr4* play key roles in maintaining the bone marrow niche and *Cxcl12* is expressed by bone marrow stromal cells and cells of the osteoblast lineage [Jung et al., 2006; Sugiyama et al., 2006]. Ablation of the receptor *Cxcr4* in mature osteoblasts increased the number of CFU-F<sup>alk phos+</sup> osteoprogenitors recovered from these mice although the phenotype also included a decrease in BV/TV [Shahnazari et al., 2013]. Our results suggest that suppressing the expression of the *Cxcr4* ligand *Cxcl12* results in a similar impact on osteoprogenitor number but a different bone phenotype. The upregulation of *Plaur* expression in the *Nmp4*<sup>-/-</sup> MSPCs may potentially contribute to the increased number of CFU-F<sup>alk phos+</sup> cells since abrogating the activity of this GPI-anchored receptor suppressed MSPC osteogenic differentiation [Kalbasi et al., 2014]. Finally mutagenesis and rescuing experiments to determine whether the potential targets are truly functionally significant is the next required step for authenticating this new anti-anabolic network.

Further parsing of the enhanced *Nmp4*<sup>-/-</sup> BM osteogenic potential implicates the elevated frequency of CD8<sup>+</sup> T cells in both ovary-intact and ovx *Nmp4*<sup>-/-</sup> mice, although this requires functional confirmation in these models. The ovx null animals exhibited elevated numbers of CD8<sup>+</sup> T cells in both BM and PBL compartments throughout the entire treatment regimen, similar to what we previously observed in the younger ovary-intact *Nmp4*<sup>-/-</sup> mice, although this increase was limited to the BM [He et al., 2013]. The elevated number of CD8<sup>+</sup> T cells is intriguing since these cells are documented to amplify the PTH anabolic response [Bedi et al., 2012; Terauchi et al., 2009]. MSPCs regulate T cell proliferation and survival [Wang et al., 2012] and perhaps disabling *Nmp4* de-represses this aspect of the cell-cell interaction, although this apparent alteration in proliferation/survival may be a cell autonomous feature of the *Nmp4*<sup>-/-</sup> T cell phenotype. Although the elevated number of *Nmp4*<sup>-/-</sup> osteoprogenitors declined at 12wks post-op, the higher number of *Nmp4*<sup>-/-</sup> CD8<sup>+</sup> T cells did not decrease. Therefore, although the augmented response to PTH might be weakened in the *Nmp4*<sup>-/-</sup> mice, it may not disappear since the persistent increased lymphocyte number might provide extra Wnt10b as a potent osteoprogenitor differentiation factor.

Why is there typically no difference between the amount of baseline trabecular bone in WT and *Nmp4*<sup>-/-</sup> mice despite the presence of an expanded pool of osteoprogenitors and CD8<sup>+</sup> T cells in the null bone marrow? This phenomenon differs from the results of recent clinical trials in which neutralizing sclerostin, an inhibitor of the Wnt signaling pathway and osteoblast differentiation, significantly increases baseline bone mineral density [reviewed in Becker, 2014]. Apparently disabling *Nmp4* is not sufficient for driving excess bone formation but instead primes the aforementioned cells for activation by an anabolic cue. The occasionally observed elevated trabecular volume in untreated *Nmp4*<sup>-/-</sup> mice may be due to the sporadic local release of growth factors, e.g., Igf1, Igfbp2 or Bmp2. However exogenous pharmacological doses of PTH provide a strong stimulus for triggering the response leading to the enhanced bone formation. Once activated by the anabolic cue, the *Nmp4*<sup>-/-</sup> cells produce the autocrine/paracrine factors that enhance the anabolic response.

Consistent with the requirement for a strong anabolic cue to trigger enhanced bone formation in the *Nmp4*<sup>-/-</sup> mice, disabling this transcription factor did not protect the animals from ovx-induced bone loss, indeed the initial rate of loss during the first 4wks after ovariectomy was higher (L5) or nearly higher (distal femur) in the *Nmp4*<sup>-/-</sup> mice. These animals harbor a modestly elevated number of osteoclast progenitors (CFU-GM) [He et al., 2013] that upon differentiation exhibit an enhanced bone-resorbing activity in vitro [Childress et al., 2011]. Therefore a decrease in estrogen might accentuate this aspect of the phenotype. Moreover, differences in sex steroid levels may underlie why intact male *Nmp4*<sup>-/-</sup> mice did not lose bone under hind limb suspension [Hino et al., 2007]. As mentioned, the *Nmp4*<sup>-/-</sup> baseline phenotype includes an occasional unprovoked enhancement in trabecular architecture, which we observed in the present study. That is to say, despite the elevated initial bone loss, the cohort of sham and ovx *Nmp4*<sup>-/-</sup> mice had more femoral and L5 trabecular bone compared to WT at the time of harvest (Table 3). However, there was no statistical difference between vehicle-treated animals in either the 4wk or 8wk hormone therapy cohorts (Figures 2 and 3). Longitudinal studies for serum turnover markers coupled with pQCT in live mice could be used to track the real-time dynamics of ovx-induced bone loss and subsequent therapy-induced bone gain between the WT and *Nmp4*<sup>-/-</sup> mice. In lieu of this, we employed a 2-way ANOVA, which incorporates differences in control groups, to evaluate whether there is an interaction between genotype and treatment.

The present data also contribute to our knowledge as to how Nmp4 works at the molecular level. Nmp4 binds throughout the genome but is primarily localized to regions near the TSS and within the gene, consistent with mediating a regulatory role. GEM analysis confirmed the AT-rich homopolymeric binding-site and did not identify other consensus sequences expected only if Nmp4 also interacted with the genome indirectly via other DNA-binding proteins. Nmp4 association with the genome is responsive to PTH since hormone decreased genome-wide occupancy in the MC3T3-E1 cells after 1hr of exposure. However, the impact of PTH on Nmp4 occupancy was gene and site-specific and hormone stimulation was observed to induce, remove, or have no effect on Nmp4 genomic occupancy. This may further

augment the fine control that this transcription factor has over the regulation of osteoprogenitor and/or bone-forming capacity.

There is a critical need for osteoanabolic agents [Lewiecki, 2011]. We have taken a two-pronged approach in our research to serve this clinical demand: (1) identify molecular and cellular mechanisms that could be used, for example in an adjuvant setting to promote enhanced efficacy or less frequent dosing with current osteoanabolic agents; and (2) identify innovative approaches to identify new drug targets/pathways or mechanisms of action that would provide needed substrate for the future drug discovery initiatives in bone disease, including osteoporosis. Our discovery-driven approaches have mapped a global network of Nmp4-regulated pathways potentially comprising a bone anti-anabolic axis. Further functional studies charting the hierarchy and interactions of these network pathways will provide a novel integrated mechanism underlying the natural constraints on bone formation. We postulate that the Nmp4 anti-anabolic network may constitute a novel strategy to identify and reveal pharmacologically accessible pathways for adding new bone to the old skeleton.

#### Acknowledgements:

This work was supported in part by the Department of Defense (PR120563, JPB); Eli Lilly (062079-00002B, JPB); NIH (CTSI pre-doctoral fellowship TL1 000162, PC)



## REFERENCES:

- Alford AI, Terkhorn SP, Reddy AB, Hankenson KD. 2010 Thrombospondin-2 regulates matrix mineralization in MC3T3-E1 pre-osteoblasts. *Bone*. 46(2):464-71.
- Alvarez MB, Childress P, Philip BK, Gerard-O'Riley R, Hanlon M, Herbert BS, Robling AG, Pavalko FM, Bidwell JP. 2012 Immortalization and characterization of osteoblast cell lines generated from wild-type and Nmp4-null mouse BM stromal cells using murine telomerase reverse transcriptase (mTERT). *J Cell Physiol*. 227(5):1873-82.
- Alvarez M, Thunyakitpisal P, Morrison P, Onyia J, Hock J, Bidwell JP. 1998 PTH-responsive osteoblast nuclear matrix architectural transcription factor binds to the rat type I collagen promoter. *J Cell Biochem*. 69(3):336-52
- Auerbach RK, Chen B, Butte AJ. 2013 Relating genes to function: identifying enriched transcription factors using the ENCODE ChIP-Seq significance tool. *Bioinformatics*. 29(15):1922-4.
- Baron R, Hesse E. 2012 Update on bone anabolics in osteoporosis treatment: rationale, current status, and perspectives. *J Clin Endocrinol Metab*. 97(2):311-25.
- Becker CB 2014 Sclerostin inhibition for osteoporosis--a new approach. *N Engl J Med*. 370(5):476-7.
- Bedi B, Li JY, Tawfeek H, Baek KH, Adams J, Vangara SS, Chang MK, Kneissel M, Weitzmann MN, Pacifici R. 2012 Silencing of parathyroid hormone (PTH) receptor 1 in T cells blunts the bone anabolic activity of PTH. *Proc Natl Acad Sci U S A*. 109(12):E725-33.

676 Bidwell JP, Childress P, Alvarez MB, Hood M Jr, He Y, Pavalko FM, Kacena MA, Yang FC. 2012  
 677 Nmp4/CIZ closes the parathyroid hormone anabolic window. *Crit Rev Eukaryot Gene Expr.* 22(3):205-18.  
 678  
 679 Bikle DD, Wang Y. 2012 Insulin like growth factor-I: a critical mediator of the skeletal response to  
 680 parathyroid hormone. *Curr Mol Pharmacol.* 5(2):135-42.  
 681  
 682 Black DM, Greenspan SL, Ensrud KE, Palermo L, McGowan JA, Lang TF, Garnero P, Bouxsein ML,  
 683 Bilezikian JP, Rosen CJ 2003 The effects of parathyroid hormone and alendronate alone or in  
 684 combination in postmenopausal osteoporosis. *N Engl J Med* 349: 1207–1215  
 685  
 686 Bouxsein ML, Boyd SK, Christiansen BA, Guldberg RE, Jepsen KJ, Müller R. 2010 Guidelines for  
 687 assessment of bone microstructure in rodents using micro-computed tomography. *J Bone Miner Res*  
 688 25:1468–86  
 689  
 690 Calleja V, Laguerre M, de Las Heras-Martinez G, Parker PJ, Requejo-Isidro J, Larijani B 2014 Acute  
 691 regulation of PDK1 by a complex interplay of molecular switches. *Biochem Soc Trans.* 42(5):1435-40.  
 692  
 693 Childress P, Philip BK, Robling AG, Bruzzaniti A, Kacena MA, Bivi N, Plotkin LI, Heller A, Bidwell JP.  
 694 2011 Nmp4/CIZ suppresses the response of bone to anabolic parathyroid hormone by regulating both  
 695 osteoblasts and osteoclasts. *Calcif Tissue Int.* 89(1):74-89.  
 696  
 697 Cipriani C, Irani D, Bilezikian JP. 2012 Safety of osteoanabolic therapy: a decade of experience. *J Bone*  
 698 *Miner Res.* 27(12):2419-28.  
 699

Cosman F, Eriksen EF, Recknor C, Miller PD, Guanabens N, Kasperk C, Papanastasiou P, Readie A,  
 Rao H, Gasser JA, Bucci-Rechtweg C, Boonen S 2011 Effects of intravenous zoledronic acid plus  
 subcutaneous teriparatide [rhPTH(1–34)] in postmenopausal osteoporosis. *J Bone Miner Res* 26:503–511  
 Dempster DW, Compston JE, Drezner MK, Glorieux FH, Kanis JA, Malluche H, Meunier PJ, Ott SM,  
 Recker RR, Parfitt AM. 2013 Standardized nomenclature, symbols, and units for bone histomorphometry:  
 a 2012 update of the report of the ASBMR Histomorphometry Nomenclature Committee. *J Bone Miner*  
*Res.* 28(1):2-17. doi: 10.1002/jbmr.1805.  
 Elis S, Courtland HW, Wu Y, Fritton JC, Sun H, Rosen CJ, Yakar S. 2010 Elevated serum IGF-1 levels  
 synergize PTH action on the skeleton only when the tissue IGF-1 axis is intact. *J Bone Miner Res.*  
 25(9):2051-8.  
 Finkelstein JS, Wyland JJ, Lee H, Neer RM 2010 Effects of teriparatide, alendronate, or both in women  
 with postmenopausal osteoporosis. *J Clin Endocrinol Metab* 95:1838–1845  
 Furlan F, Galbiati C, Jorgensen NR, Jensen JE, Mrak E, Rubinacci A, Talotta F, Verde P, Blasi F. 2007  
 Urokinase plasminogen activator receptor affects bone homeostasis by regulating osteoblast and  
 osteoclast function. *J Bone Miner Res.* 22(9):1387-96.  
 Guo Y, Mahony S, Gifford DK 2012 High resolution genome wide binding event finding and motif  
 discovery reveals transcription factor spatial binding constraints. *PLoS Computational Biology* 8(8):  
 e1002638.  
 Hankenson KD, Bornstein P 2002 The secreted protein thrombospondin 2 is an autocrine inhibitor of  
 marrow stromal cell proliferation. *J Bone Miner Res* 17:415–25.

726

727 Hankenson KD, Bain SD, Kyriakides TR, Smith EA, Goldstein SA, Bornstein P 2000 Increased marrow-

728 derived osteoprogenitor cells and endosteal bone formation in mice lacking thrombospondin 2. *J Bone*

729 *Miner Res* 15:851–62.

730

731 Harada A, Okada S, Konno D, Odawara J, Yoshimi T, Yoshimura S, Kumamaru H, Saiwai H, Tsubota T,

732 Kurumizaka H, Akashi K, Tachibana T, Imbalzano AN, Ohkawa Y. 2012 Chd2 interacts with H3.3 to

733 determine myogenic cell fate. *EMBO J.* 31(13):2994-3007.

734

735 He Y, Childress P, Hood M Jr, Alvarez M, Kacena MA, Hanlon M, McKee B, Bidwell JP, Yang FC.

736 2013 Nmp4/CIZ suppresses the parathyroid hormone anabolic window by restricting mesenchymal stem

737 cell and osteoprogenitor frequency. *Stem Cells Dev.* 22(3):492-500.

738

739 Hino K, Nakamoto T, Nifuji A, Morinobu M, Yamamoto H, Ezura Y, Noda M. 2007 Deficiency of CIZ,

740 a nucleocytoplasmic shuttling protein, prevents unloading-induced bone loss through the enhancement of

741 osteoblastic bone formation in vivo. *Bone.* 40(4):852-60.

742

743 Huang da W, Sherman BT, Lempicki RA. 2009 Systematic and integrative analysis of large gene lists

744 using DAVID bioinformatics resources. *Nat Protoc.* 4(1):44-57.

745

746 Hunter GK 2013 Role of osteopontin in modulation of hydroxyapatite formation. *Calcif Tissue Int.*

747 93(4):348-54.

748

749 Isern J, Martín-Antonio B, Ghazanfari R, Martín AM, López JA, del Toro R, Sánchez-Aguilera A, Arranz

750 L, Martín-Pérez D, Suárez-Lledó M, Marín P, Van Pel M, Fibbe WE, Vázquez J, Scheduling S, Urbano-

751 Ispizúa Á, Méndez-Ferrer S. 2013 Self-renewing human bone marrow mesenspheres promote  
 752 hematopoietic stem cell expansion. *Cell Rep.* 3(5):1714-24.  
 753  
 754 Jilka RL 2007 Molecular and cellular mechanisms of the anabolic effect of intermittent PTH. *Bone.* 2007  
 755 40(6):1434-46.  
 756 Kalbasi Anaraki P, Patecki M, Larmann J, Tkachuk S, Jurk K, Haller H, Theilmeier G, Dumler I. 2014  
 757 Urokinase receptor mediates osteogenic differentiation of mesenchymal stem cells and vascular  
 758 calcification via the complement C5a receptor. *Stem Cells Dev.* 23(4):352-62.  
 759  
 760 Jung Y, Wang J, Schneider A, Sun YX, Koh-Paige AJ, Osman NI, McCauley LK, Taichman RS 2006  
 761 Regulation of SDF-1 (CXCL12) production by osteoblasts; a possible mechanism for stem cell homing.  
 762 *Bone* 38: 497–508  
 763  
 764 Komori T. 2011 Signaling networks in RUNX2-dependent bone development. *J Cell Biochem.*  
 765 112(3):750-5.  
 766  
 767 Kraenzlin ME, Meier C. 2011 Parathyroid hormone analogues in the treatment of osteoporosis. *Nat Rev*  
 768 *Endocrinol.* 7(11):647-56.  
 769  
 770 Krane SM. 2005 Identifying genes that regulate bone remodeling as potential therapeutic targets. *J Exp*  
 771 *Med.* 201(6):841-3.  
 772  
 773 Kumar S, Ponnazhagan S. 2012 Mobilization of bone marrow mesenchymal stem cells in vivo augments  
 774 bone healing in a mouse model of segmental bone defect. *Bone* 50(4):1012-8.  
 775

776 Lewiecki EM 2011 New targets for intervention in the treatment of postmenopausal osteoporosis *Nature*  
 777 *Reviews Rheumatology* 7:631-638  
 778  
 779 Li H and Durbin R 2009 Fast and accurate short read alignment with Burrows-Wheeler Transform.  
 780 *Bioinformatics*, 25:1754-60.  
 781  
 782 Li JY, Walker LD, Tyagi AM, Adams J, Weitzmann MN, Pacifici R. 2014 The sclerostin-independent  
 783 bone anabolic activity of intermittent PTH treatment is mediated by T-cell-produced Wnt10b. *J Bone*  
 784 *Miner Res.* 29(1):43-54.  
 785  
 786 Lin W, Srajer G, Evrard YA, Phan HM, Furuta Y, Dent SY. 2007 Developmental potential of Gcn5(−/−)  
 787 embryonic stem cells in vivo and in vitro. *Dev Dyn.* 236:1547–1557.  
 788  
 789 McClung MR, Grauer A, Boonen S, Bolognese MA, Brown JP, Diez-Perez A, Langdahl BL, Reginster  
 790 JY, Zanchetta JR, Wasserman SM, Katz L, Maddox J, Yang YC, Libanati C, Bone HG. 2014  
 791 Romosozumab in postmenopausal women with low bone mineral density. *N Engl J Med.* 370(5):412-20.  
 792  
 793 Méndez-Ferrer S, Michurina TV, Ferraro F, Mazloom AR, Macarthur BD, Lira SA, Scadden DT,  
 794 Ma'ayan A, Enikolopov GN, Frenette PS. 2010 Mesenchymal and haematopoietic stem cells form a  
 795 unique bone marrow niche. *Nature.* 466(7308):829-34.  
 796  
 797 Miyakoshi N, Richman C, Qin X, Baylink DJ, Mohan S 1999 Effects of recombinant insulin-like growth  
 798 factor-binding protein-4 on bone formation parameters in mice. *Endocrinology* 140: 5719–5728  
 799

Mizoguchi T, Pinho S, Ahmed J, Kunisaki Y, Hanoun M, Mendelson A, Ono N, Kronenberg HM, Frenette PS. 2014 Osterix marks distinct waves of primitive and definitive stromal progenitors during bone marrow development. *Dev Cell*. 29(3):340-9.

Morinobu M, Nakamoto T, Hino K, Tsuji K, Shen ZJ, Nakashima K, Nifuji A, Yamamoto H, Hirai H, Noda M. 2005 The nucleocytoplasmic shuttling protein CIZ reduces adult bone mass by inhibiting bone morphogenetic protein-induced bone formation. *J Exp Med*. 201(6):961-70.

Nakamoto T, Shiratsuchi A, Oda H, Inoue K, Matsumura T, Ichikawa M, Saito T, Seo S, Maki K, Asai T, Suzuki T, Hangaishi A, Yamagata T, Aizawa S, Noda M, Nakanishi Y, Hirai H. 2004 Impaired spermatogenesis and male fertility defects in CIZ/Nmp4-disrupted mice. *Genes Cells* 9(6):575-89.

Nakamoto T, Yamagata T, Sakai R, Ogawa S, Honda H, Ueno H, Hirano N, Yazaki Y, Hirai H. 2000 CIZ, a zinc finger protein that interacts with p130(cas) and activates the expression of matrix metalloproteinases. *Mol Cell Biol*. 20(5):1649-58

Nascimento EM, Cox CL, MacArthur S, Hussain S, Trotter M, Blanco S, Suraj M, Nichols J, Kübler B, Benitah SA, Hendrich B, Odom DT, Frye M. 2011 The opposing transcriptional functions of Sin3a and c-Myc are required to maintain tissue homeostasis. *Nat Cell Biol*. 13(12):1395-405.

D. Padhi, G. Jang, B. Stouch, L. Fang, E. Posvar 2011 Single-dose, placebo-controlled, randomized study of AMG 785, a sclerostin monoclonal antibody *J Bone Miner Res*, 26: 19–26

Robling AG, Childress P, Yu J, Cotte J, Heller A, Philip BK, Bidwell JP. 2009 Nmp4/CIZ suppresses parathyroid hormone-induced increases in trabecular bone. *J Cell Physiol*. 219(3):734-43.



826 Rosenbloom KR, Sloan CA, Malladi VS, Dreszer TR, Learned K, Kirkup VM, Wong MC, Maddren M,  
827 Fang R, Heitner SG, Lee BT, Barber GP, Harte RA, Diekhans M, Long JC, Wilder SP, Zweig AS,  
828 Karolchik D, Kuhn RM, Haussler D, Kent WJ. 2013 ENCODE data in the UCSC Genome Browser: year  
829 5 update. *Nucleic Acids Res.* 41(Database issue):D56-63.  
830  
831 Saag KG, Zanchetta JR, Devogelaer JP, Adler RA, Eastell R, See K, Krege JH, Krohn K, Warner MR.  
832 2009 Effects of teriparatide versus alendronate for treating glucocorticoid-induced osteoporosis: thirty-  
833 six-month results of a randomized, double-blind, controlled trial. *Arthritis Rheum.* 60(11):3346-55.  
834  
835 Sacchetti B, Funari A, Michienzi S, Di Cesare S, Piersanti S, Saggio I, Tagliafico E, Ferrari S, Robey PG,  
836 Riminucci M, Bianco P. 2007 Self-renewing osteoprogenitors in bone marrow sinusoids can organize a  
837 hematopoietic microenvironment. *Cell.* 131(2):324-36  
838  
839 Shah R, Alvarez M, Jones DR, Torrungruang K, Watt AJ, Selvamurugan N, Partridge NC, Quinn CO,  
840 Pavalko FM, Rhodes SJ, Bidwell JP. 2004 Nmp4/CIZ regulation of matrix metalloproteinase 13 (MMP-  
841 13) response to parathyroid hormone in osteoblasts. *Am J Physiol Endocrinol Metab.* 287(2):E289-96.  
842  
843 Shahnazari M, Chu V, Wronski TJ, Nissenson RA, Halloran BP 2013 CXCL12/CXCR4 signaling in the  
844 osteoblast regulates the mesenchymal stem cell and osteoclast lineage populations. *FASEB J.* 27(9):3505-  
845 13.  
846  
847 Shen ZJ, Nakamoto T, Tsuji K, Nifuji A, Miyazono K, Komori T, Hirai H, Noda M. 2002 Negative  
848 regulation of bone morphogenetic protein/Smad signaling by Cas-interacting zinc finger protein in  
849 osteoblasts. *J Biol Chem.* 277(33):29840-6.  
850

Stamatoyannopoulos JA, et al., [Mouse ENCODE Consortium] 2012 An encyclopedia of mouse DNA elements (Mouse ENCODE). *Genome Biol.* 13(8):418.

Sugiyama T., Kohara H., Noda M., Nagasawa T 2006 Maintenance of the hematopoietic stem cell pool by CXCL12-CXCR4 chemokine signaling in bone marrow stromal cell niches. *Immunity* 25: 977–988

Supek F, Bošnjak M, Škunca N, Šmuc T. 2011 REVIGO summarizes and visualizes long lists of gene ontology terms. *PLoS One.* 6(7):e21800.

Terauchi M, Li JY, Bedi B, Baek KH, Tawfeek H, Galley S, Gilbert L, Nanes MS, Zayzafoon M, Guldberg R, Lamar DL, Singer MA, Lane TF, Kronenberg HM, Weitzmann MN, Pacifici R. 2009 T lymphocytes amplify the anabolic activity of parathyroid hormone through Wnt10b signaling. *Cell Metab.* 10(3):229-40.

Thunyakitpisal P, Alvarez M, Tokunaga K, Onyia JE, Hock J, Ohashi N, Feister H, Rhodes SJ, Bidwell JP. 2001 Cloning and functional analysis of a family of nuclear matrix transcription factors (NP/NMP4) that regulate type I collagen expression in osteoblasts. *J Bone Miner Res.* 16(1):10-23

Torrunguang K, Alvarez M, Shah R, Onyia JE, Rhodes SJ, Bidwell JP. 2002 DNA binding and gene activation properties of the Nmp4 nuclear matrix transcription factors. *J Biol Chem.* 277(18):16153-9.

Vieira Potter VJ, Strissel KJ, Xie C, Chang E, Bennett G, Defuria J, Obin MS, Greenberg AS. 2012 Adipose tissue inflammation and reduced insulin sensitivity in ovariectomized mice occurs in the absence of increased adiposity. *Endocrinology.* 153(9):4266-77.

Wang L, Zhao Y, Shi S. 2012 Interplay between mesenchymal stem cells and lymphocytes: implications for immunotherapy and tissue regeneration. *J Dent Res.* 91(11):1003-10.

Wu X, Estwick SA, Chen S, Yu M, Ming W, Nebesio TD, Li Y, Yuan J, Kapur R, Ingram D, Yoder MC, Yang FC. 2006 Neurofibromin plays a critical role in modulating osteoblast differentiation of mesenchymal stem/progenitor cells. *Hum Mol Genet.* 15(19):2837-45.

Xi G, Wai C, DeMambro V, Rosen CJ, Clemmons DR 2014 IGFBP-2 directly stimulates osteoblast differentiation. *J Bone Miner Res.* 29(11):2427-38

Xian L, Wu X, Pang L, Lou M, Rosen CJ, Qiu T, Crane J, Frassica F, Zhang L, Rodriguez JP, Xiaofeng Jia, Shoshana Yakar, Shouhong Xuan, Argiris Efstratiadis, Mei Wan, Xu Cao. 2012 Matrix IGF-1 maintains bone mass by activation of mTOR in mesenchymal stem cells. *Nat Med.* 18(7): 1095-101.

Yang Z, Bidwell JP, Young SR, Gerard-O'Riley R, Wang H, Pavalko FM. 2010 Nmp4/CIZ inhibits mechanically induced beta-catenin signaling activity in osteoblasts. *J Cell Physiol.* 223(2):435-41.

Yu EW, Neer RM, Lee H, Wyland JJ, de la Paz AV, Davis MC, Okazaki M, Finkelstein JS. 2011 Time-dependent changes in skeletal response to teriparatide: escalating vs. constant dose teriparatide (PTH 1-34) in osteoporotic women. *Bone.* 48(4):713-9.

## FIGURE LEGENDS

**Figure 1:** Schematic of treatment regimen for WT and *Nmp4*<sup>-/-</sup> mice; Group 1 mice were subjected to ovariectomy (ovx) or sham operation at 12wks of age and evaluated for bone loss 4wks post-op (16wks of age). Group 2 mice were ovx at 12wks of age and began PTH or vehicle therapy at 16wks of age for a duration of 4wks and 8wks. Endpoint analyses included micro-computed tomography  $\mu$ CT, serum analysis for N-terminal propeptide of type 1 procollagen (P1NP) and C-terminal telopeptides (CTX), and dynamic histomorphometry.

**Figure 2:** Disabling *Nmp4* enhances PTH restorative therapy in the distal femur of ovx *Nmp4*<sup>-/-</sup> mice [A] Interaction plots of femoral trabecular bone volume/total volume (BV/TV) of ovx WT and ovx *Nmp4*<sup>-/-</sup> mice as determined by  $\mu$ CT at 4wks of treatment and 8wks of treatment. Data are average  $\pm$  SD, number of mice/experimental group = 8-9). Statistical differences were determined using a 2-way ANOVA and significance was set at  $p \leq 0.05$ . The Tukey's HSD post hoc test was used to determine differences between the treatment groups. There were genotype, treatment and genotype x treatment interaction at both time points. There was no difference between the vehicle-treated WT and *Nmp4*<sup>-/-</sup> mice. [B]  $\mu$ CT images showing PTH-induced improvements in distal femur trabecular architecture in ovx WT and *Nmp4*<sup>-/-</sup> mice after 8 weeks of treatment (12wks post-op, 24wks of age).

**Figure 3:** The exaggerated response to anabolic PTH persists in the L5 vertebra of ovx *Nmp4*<sup>-/-</sup> mice. [A] Interaction plots of L5 vertebra bone volume/total volume (BV/TV) of ovx WT and ovx *Nmp4*<sup>-/-</sup> mice as determined by  $\mu$ CT at 4wks of treatment and 8wks of treatment. Data are average  $\pm$  SD, number of mice/experimental group = 8-9). Statistical differences were determined using a 2-way ANOVA and significance was set at  $p \leq 0.05$ . The LS Means Student t post hoc test was used to determine differences between the treatment groups. There were genotype, treatment effects at both time points and a genotype x treatment interaction at 8wks therapy. There was no difference between the vehicle-treated WT and

*Nmp4*<sup>-/-</sup> mice. [B]  $\mu$ CT images showing PTH-induced improvements in L5 trabecular architecture in ovx WT and *Nmp4*<sup>-/-</sup> mice after 8 weeks of treatment (12wks post-op, 24wks of age).

**Figure 4:** OvX does not abrogate the expanded population of osteoprogenitors and CD8<sup>+</sup> T cells in *Nmp4*<sup>-/-</sup> mice. FACS analysis of BM and PBL osteoprogenitors, CD8<sup>+</sup> T cells, and CD4<sup>+</sup> T cells. [A, D] The frequency of femoral BM and PBL CD45<sup>-</sup>/CD105<sup>+</sup>/CD146<sup>+</sup>/CD105<sup>+</sup>/nestin<sup>+</sup> osteoprogenitor cells in WT and *Nmp4*<sup>-/-</sup> mice at the end of 4wks and 8wks treatment with intermittent PTH or vehicle control; [B, E] the frequency of BM and PBL CD8<sup>+</sup> T cells from the WT and *Nmp4*<sup>-/-</sup> mice; [C, F] the frequency of BM and PBL CD4<sup>+</sup> T cells from the WT and null mice. Data are average  $\pm$  SD, number of mice/experimental group = 8–9; Statistical differences were determined using a 2-way ANOVA and significance was set at  $p \leq 0.05$ .

**Figure 5:** Expanded *Nmp4*<sup>-/-</sup> MSPCs exhibit enhanced proliferation and mineralization in culture. [A] Comparative growth rates of expanded WT and *Nmp4*<sup>-/-</sup> MSPCs. Cell counts/day (n=4 lines per genotype log<sub>10</sub> cells/well, 3 wells/sample, average  $\pm$  SD, t test,  $t < 0.05$ ). Note: each ‘line’ is derived from a single mouse [B] Alkaline phosphatase (alk phos) and alizarin red staining of a WT and *Nmp4*<sup>-/-</sup> MSPC cultures from Day7-Day28. See text for details

**Figure 6:** *Nmp4* associates with core target genes common to multiple cell types and acts as a *negative regulation of cellular biosynthetic processes* [A] Venn diagram illustrating the shared *Nmp4* target genes in the MC3T3-E1 osteoblast-like cells (vehicle-treated), and the three ENCODE cells lines, ES-E14 (embryonic stem cells), MEL, and CH12 cells (B-cell lymphomas). [B] DAVID/REVIGO gene ontology (GO) profile of *Nmp4* core target genes

**Figure 7:** *Nmp4* binds to AT-rich DNA typically proximal to TSS sites or within intragenic regions. [A] Genome-wide mapping of the *Nmp4* binding sites show that most sites are distributed in the TSS and

intragenic regions of the genome. ChIP-seq analysis included vehicle-treated and PTH-treated MC3T3-E1 osteoblast-like cells (vMC and pMC, respectively) and three murine cell lines from the ENCODE Consortium including ES-E14 (Es14), which are E14 undifferentiated mouse embryonic stem cells, and two mouse erythroleukemia cell lines (Ch12 and MEL) derived from B-cell lymphomas. [B] GEM analysis for the Nmp4 consensus sequence derived from MC3T3-E1 cells. A minimal k-mer width of 6 and maximum of 20 were used. The optimal position weight matrix (PWM) score for the MC3T3-E1 data was 10.07. The hypergeometric P-value (hgp) was 1e-1466.1.

**Figure 8:** ChIP-seq reveals Nmp4 binding profiles at specific gene loci. Mouse MC3T3-E1 cells were seeded into twenty-one 150mm plates at an initial density of 50,000 cells/plate (320 cells/cm<sup>2</sup>) and maintained in  $\alpha$ MEM complete medium + ascorbic acid for 14 days. Prior to harvest cells were treated with 25nM hPTH(1-34) or vehicle control for 1hr. Processing for ChIP-seq analysis was performed as described in the Materials and Methods. Sequences (50nt reads, single end) were aligned to the mouse genome (mm10) using the BWA algorithm. Alignments were extended in silico at their 3'-ends to a length of 150bp, which is the average genomic fragment length in the size-selected library, and assigned to 32-nt bins along the genome. Nmp4 (Znf384) peak locations were determined using the MACS algorithm (v1.4.2) with a cutoff of pvalue = 1e-7. The genomic loci including the chromosome number and nucleotide interval are indicated. Read scales are indicated on the Y-axis. An arrow indicates the transcriptional start sites and direction of transcription for each of the genes; vertical boxes within the gene indicate exons. The Nmp4 ChIP-seq gene profiles include (A) *Nid2* (B) *Akt2*, (C) *Pdk1* (D) *ccdc53*, (E) *Arrb2* and (F) *Irs1*. The input DNA profiles were devoid of peaks.

**Figure 9:** Comparison of mRNA expression profiles derived from non-differentiating (Day 3) and osteogenic-differentiating (Days 5-16) WT and *Nmp4*<sup>-/-</sup> cells. All transcript levels are compared to WT Day 3 providing a time course of expression. mRNA profiles [A] *Igfbp2*; [B] *Igfbp4*; [C] *Pdk1*; [D] *Bmp2*; [E] *Pth1r* were derived from the TLDA system (Format 96a, Applied Biosystems, Foster City,

CA) performed on a QuantStudio™ 7 Flex Real-Time PCR System and normalized with GusB. Profile [F] *Bglap* mRNA profile qRT-PCR reactions were performed on an Eppendorf Mastercycler® RealPlex<sup>2</sup> using *Rplp2* as the normalizer as previously described [Robling et al, 2009]. Comparison of profiles using *GusB* and *Rplp2* as the normalizer showed no differences in the shape of the expression profiles

**Figure 10:** Comparison of mRNA expression profiles derived from non-differentiating (Day 3) and osteogenic-differentiating (Days 5-16) WT and *Nmp4*<sup>-/-</sup> cells. All transcript levels are compared to WT Day 3 providing a time course of expression. mRNA profiles [A] *Cxcl12*; [B] *Plaur*; [C] *Spp1*; [D] *Thbs2*; [E] *Col1a1* were derived from the TLDA system (Format 96a, Applied Biosystems, Foster City, CA) performed on a QuantStudio™ 7 Flex Real-Time PCR System and normalized with GusB. Profile [F] *Sp7* mRNA profile qRT-PCR reactions were performed on an Eppendorf Mastercycler® RealPlex<sup>2</sup> using *Rplp2* as the normalizer as previously described [Robling et al., 2009]. The Day 16 WT sample is the average of two replicates. Comparison of profiles using GusB and *Rplp2* as the normalizer showed no differences in the shape of the expression profiles

**Supplemental Figure S1:** qRT-PCR validates the ChIP-seq profiles. [A] The *Nmp4* ChIP-seq profile for the gene *Col1a1*. The genomic loci including the chromosome number and nucleotide interval are indicated. Read scale is indicated on the Y-axis. An arrow marks the transcriptional start site and direction of transcription; vertical boxes within the gene identify exons. [B] qRT-PCR was used to authenticate the ChIP-seq peaks as described in the Materials and Methods.

**Supplemental Figure 2:** Volcano plots derived from gene expression profiles of non-differentiating (Day 3) and osteogenic-differentiating (Days 5-16) WT and *Nmp4*<sup>-/-</sup> as described in the Materials and Methods. RNA expression profiling was performed on a QuantStudio™ 7 Flex Real-Time PCR System and data analyzed using the ExpressionSuite v1.0.4™ analysis software (Applied Biosystems) as described in the Materials and Methods. [A] WT vs *Nmp4*<sup>-/-</sup> cells at Day 3 post-seeding. mRNA transcript expression was



compared to WT cells (Day 3). Cells maintained in Mesencult™ Media + Mesencult™ Stimulatory Supplement. [B] WT vs *Nmp4*<sup>-/-</sup> cells at Day 5 post-seeding. mRNA transcript expression was compared to WT cells (Day 5). Cells maintained in differentiation medium for 48hrs [C] WT vs *Nmp4*<sup>-/-</sup> cells at Day 7 post-seeding. mRNA transcript expression was compared to WT cells (Day 7). Cells maintained in differentiation medium for 96hrs [D] WT vs *Nmp4*<sup>-/-</sup> cells at Day 9 post-seeding. mRNA transcript expression was compared to WT cells (Day 9). Cells maintained in differentiation medium for 144hrs [E] WT vs *Nmp4*<sup>-/-</sup> cells at Day 16 post-seeding. mRNA transcript expression was compared to WT cells (Day 16). Cells maintained in differentiation medium for 192hrs. Genes indicated with green dots (left of center) and above the X-axis exhibited a significant downregulation by over 2-fold. Genes indicated with the red dots (right of center) and above the X-axis exhibited a significant upregulation by over 2-fold.

**Supplemental TABLE 1:** 96 *Nmp4* ‘core’ target genes, non-core target genes, and non-target genes including 5 candidate normalizer genes. Individual cDNAs were quantified by qRT-PCR using a custom TLDA system (Format 96a, Applied Biosystems, Foster City, CA) as described in the Materials and Methods on a QuantStudio™ 7 Flex Real-Time PCR System. We used the ExpressionSuite v1.0.4™ analysis software (Applied Biosystems) to analyze these data.

**Supplemental TABLE 2:** 2114 *Nmp4* ‘core’ target genes common to the four cell lines MC3T3-E1 osteoblast-like cells, and three murine cell lines from the ENCODE Consortium including ES-E14 (Es14), which are E14 undifferentiated mouse embryonic stem cells, and two mouse erythroleukemia cell lines (Ch12 and MEL) derived from B-cell lymphomas.

**Supplemental TABLE 3:** IPA analysis of 2114 *Nmp4* ‘core’ target genes common to the four cell lines MC3T3-E1 osteoblast-like cells, and three murine cell lines from the ENCODE Consortium including ES-E14 (Es14), which are E14 undifferentiated mouse embryonic stem cells, and two mouse erythroleukemia cell lines (Ch12 and MEL) derived from B-cell lymphomas.

Table 1: Bone loss data.

	WT		<i>Nmp4</i> <sup>-/-</sup>		2-WAY ANOVA p-values		
	SHAM	OVX	SHAM	OVX	Genotype	Treatment	Gene x Treat
%Δ Body weight	2.48±7.73	8.65±5.48	4.14±4.70	5.66±2.94	0.69	0.03	0.17
Uterine weight (g)	0.10±0.05	0.04±0.02	0.10±0.02	0.05±0.02	0.30	<0.0001	0.34
<b><u>Distal Femur</u></b>							
BV/TV	0.019±0.004	0.012±0.004	0.038±0.011	0.021±0.010	<0.0001	<0.0001	0.06
SMI	3.818±0.250	4.055±0.357	3.387±0.263	3.810±0.294	0.0008	0.0011	0.32
Tb.N (mm <sup>-1</sup> )	2.554±0.239	2.165±0.385	3.128±0.218	2.797±0.276	<0.0001	0.0004	0.76
Tb.Th (mm)	0.040±0.005	0.041±0.005	0.039±0.003	0.037±0.004	0.08	0.87	0.23
Tb.Sp (mm)	0.393±0.036	0.477±0.097	0.317±0.026	0.359±0.037	<0.0001	0.0012	0.25
<b><u>L5 Vertebra</u></b>							
BV/TV	0.189±0.028	0.177±0.013	0.253±0.019	0.212±0.019	<0.0001	0.0004	0.05
Tb.N (mm <sup>-1</sup> )	3.797±0.513	3.580±0.285	4.491±0.345	4.022±0.254	<0.0001	0.0091	0.32
Tb.Th (mm)	0.050±0.003	0.049±0.002	0.056±0.002	0.053±0.002	<0.0001	0.0032	0.02
Tb.Sp (mm)	0.227±0.023	0.229±0.013	0.202±0.020	0.214±0.012	0.0013	0.25	0.44
<b><u>Serum P1NP</u></b>							
		WT : <i>Nmp4</i> <sup>-/-</sup>				p-values [G; T; G x T] <sup>4wks</sup>	p-values [G; T; G x T] <sup>12wks</sup>
Pre-op		Post-op <sup>4wks</sup>		Post-op <sup>12wks</sup>			
5.62±1.21 : 6.02±1.41		5.83±1.41 : 4.77±1.22		3.15±0.65 : 2.81±0.76		0.34; 0.16; 0.05      0.95; <0.0001; 0.36	
<b><u>Serum CTX</u></b>							
		WT : <i>Nmp4</i> <sup>-/-</sup>				p-values [G; T; G x T] <sup>4wks</sup>	p-values [G; T; G x T] <sup>12wks</sup>
Pre-op		Post-op <sup>4wks</sup>		Post-op <sup>12wks</sup>			
13.66±2.43 : 13.37±1.88		12.96±3.04 : 13.53±2.58		11.47±2.24 : 9.36±1.22		0.92; 0.46; 0.96      0.14; 0.0003; 0.18	

The % change body weight, uterine weight, and microCT of distal femur and L5 vertebra from WT and *Nmp4*<sup>-/-</sup> mice after ovx or sham operation 4wks post-op. Serum bone formation [P1NP] and bone resorption [CTX] marker levels were compared in mice previous to the operation (Pre-op) and 4wks and 12wks subsequent to surgery (Post-op). The 12wks post-op data was obtained from the vehicle-control treatment groups. Data are average ± SD, number of mice/experimental group=8-14 [4 mice in WT SHAM uterine weight]). Statistical significance was set at p≤0.05 and differences were determined using a 2-way ANOVA.

Table 2: PTH-induced bone gain data.

	WT		<i>Nmp4<sup>-/-</sup></i>		2-WAY ANOVA p-values		
<u>Distal Femur</u>							
<b>4wks</b>	VEH	PTH	VEH	PTH	Genotype	Treatment	Gene x Treat
Conn D (mm <sup>-3</sup> )	3.180±3.870	33.230±26.730	9.681±15.979	67.533±14.111	0.0018	<0.0001	0.03
SMI	3.752±0.437	3.013±0.384	3.472±0.327	2.514±0.113	0.0025	<0.0001	0.36
Tb.N (mm <sup>-1</sup> )	2.100±0.519	2.441±0.281	2.712±0.241	2.833±0.224	0.0002	0.06	0.36
Tb.Th (mm)	0.039±0.010	0.042±0.007	0.033±0.003	0.044±0.003	0.54	0.004	0.09
Tb.Sp (mm)	0.510±0.157	0.409±0.051	0.370±0.036	0.342±0.032	0.0019	0.04	0.24
<b>8wks</b>							
Conn D (mm <sup>-3</sup> )	3.123±5.307	38.658±14.910	0.982±1.103	58.128±13.570	0.03	<0.0001	0.0064
SMI	3.808±0.479	2.470±0.284	3.589±0.218	2.262±0.141	0.05	<0.0001	0.96
Tb.N (mm <sup>-1</sup> )	2.132±0.297	2.164±0.431	2.286±0.145	2.552±0.277	0.02	0.17	0.28
Tb.Th (mm)	0.037±0.006	0.048±0.005	0.030±0.004	0.049±0.003	0.12	<0.0001	0.02
Tb.Sp (mm)	0.476±0.072	0.471±0.109	0.438±0.033	0.378±0.045	0.01	0.20	0.27
<u>L5 Vertebra</u>							
<b>4wks</b>	VEH	PTH	VEH	PTH	Genotype	Treatment	Gene x Treat
Tb.N (mm <sup>-1</sup> )	3.453±0.451	4.875±0.587	3.891±0.504	5.518±0.381	0.0049	<0.0001	0.56
Tb.Th (mm)	0.051±0.002	0.049±0.002	0.054±0.004	0.051±0.001	0.04	0.03	0.60
Tb.Sp (mm)	0.246±0.021	0.224±0.030	0.229±0.021	0.197±0.021	0.02	0.0036	0.52
<b>8wks</b>							
Tb.N (mm <sup>-1</sup> )	4.046±0.917	5.648±1.191	3.627±0.235	5.906±0.754	0.79	<0.0001	0.26
Tb.Th (mm)	0.053±0.003	0.049±0.004	0.055±0.001	0.054±0.001	0.0018	0.0044	0.09
Tb.Sp (mm)	0.239±0.021	0.206±0.037	0.256±0.020	0.186±0.023	0.86	<0.0001	0.05

MicroCT (distal femur and L5 vertebra) from ovx WT and ovx *Nmp4<sup>-/-</sup>* mice after 4 wks and 8wks PTH/VEH therapy. Data are average ± SD, number of mice/experimental group = 8-9. Statistical significance was set at p≤0.05 and differences were determined using a 2-way ANOVA.

Table 3: Histomorphometry and serum analyses.

	WT		<i>Nmp4<sup>-/-</sup></i>		2-WAY ANOVA p-values		
	VEH	PTH	VEH	PTH	Genotype	Treatment	Gene x Treat
<b><u>Dynamic histo</u></b>							
MAR (µm/day)	2.28±0.37	3.80±0.73	2.29±0.37	3.61±0.40	0.70	<0.0001	0.66
MS/BS (%)	0.41±0.09	0.55±0.05	0.44±0.10	0.52±0.06	0.98	0.01	0.45
BFR (µm <sup>2</sup> /µm/day)	0.95±0.28	2.09±0.52	1.01±0.25	1.86±0.22	0.60	<0.0001	0.37
<b><u>Serum</u></b>							
	WT		<i>Nmp4<sup>-/-</sup></i>		2-WAY ANOVA p-values		
	VEH <sup>8wks</sup>	PTH <sup>8wks</sup>	VEH <sup>8wks</sup>	PTH <sup>8wks</sup>	Genotype	Treatment	Gene x Treat
P1NP (ng/ml)	3.147±0.653	10.066±2.659	2.806±0.760	8.042±3.304	0.19	<0.0001	0.34
CTX (ng/ml)	11.466±2.239	15.147±3.518	9.361±1.222	14.157±1.532	0.12	0.0002	0.56

Dynamic bone histomorphometry data of the distal femur from WT and *Nmp4<sup>-/-</sup>* mice treated with intermittent PTH or vehicle for 4wks (8wks post-op). Sera data were collected at the end of 8wks treatment (12wks post-op). The parameters include mineral apposition rate (MAR), mineralizing surface/bone surface (MS/BS), and bone formation rate (BFR). Data are average ± SD, number of mice/experimental group = 4-7. A 2-way ANOVA was used to determine statistical differences and significance was set at p≤0.05.

**Table 4:** ENCODE ChIP-Seq Significance Tool profile for enriched transcription factors [TFs] within the Nmp4 target core gene list

Factor	Q-value*	Factor	Q-value
Nmp4	0.00E+00	Max	0.00E+00
CHD2	0.00E+00	Mxi1	0.00E+00
CTCF	0.00E+00	NELFe	0.00E+00
GCN5	0.00E+00	Pol2	0.00E+00
HCFC1	0.00E+00	SIN3A	0.00E+00
MAZ	0.00E+00	TBP	0.00E+00
p300	0.00E+00	c-Myc	7.352e-317

\* Hypergeometric test; Benjamini-Hochberg; (select TFs from 72 entries).

**Table 5:** DAVID profile of KEGG pathway mapping.

<b>GO Term Pathways</b>	<b>FDR</b>
TOR signaling pathway	0.003
Insulin signaling pathway	0.004
Chronic myeloid leukemia	0.026
JAK-STAT signaling pathway	0.026
Neurotrophin signaling pathway	0.034

Only pathways with an FDR of  $p < 0.05$  are listed

Figure 1  
[Click here to download Figure: FIGURE 1.tif](#)

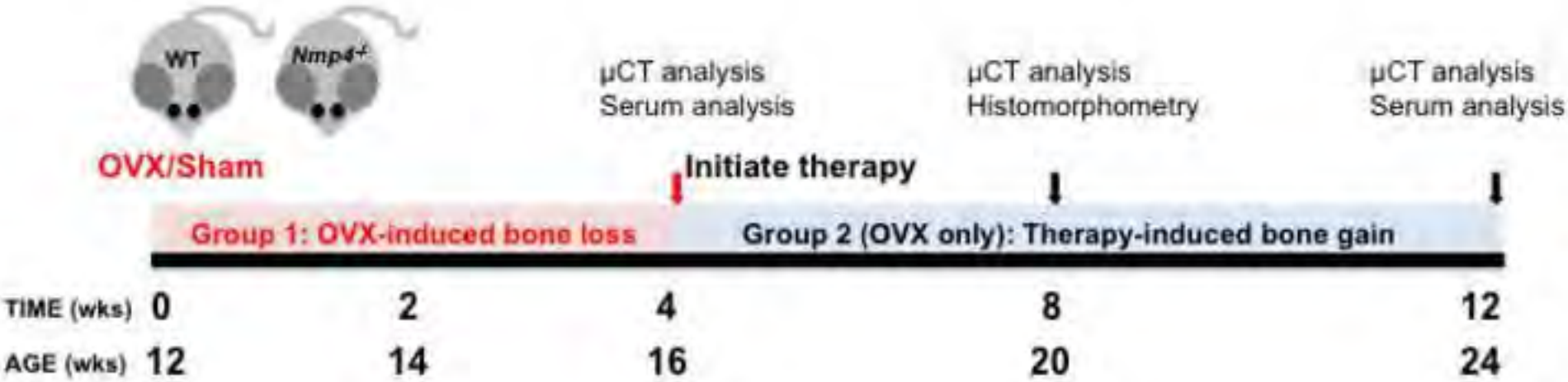


Figure 2

[Click here to download Figure: FIGURE 2.tif](#)

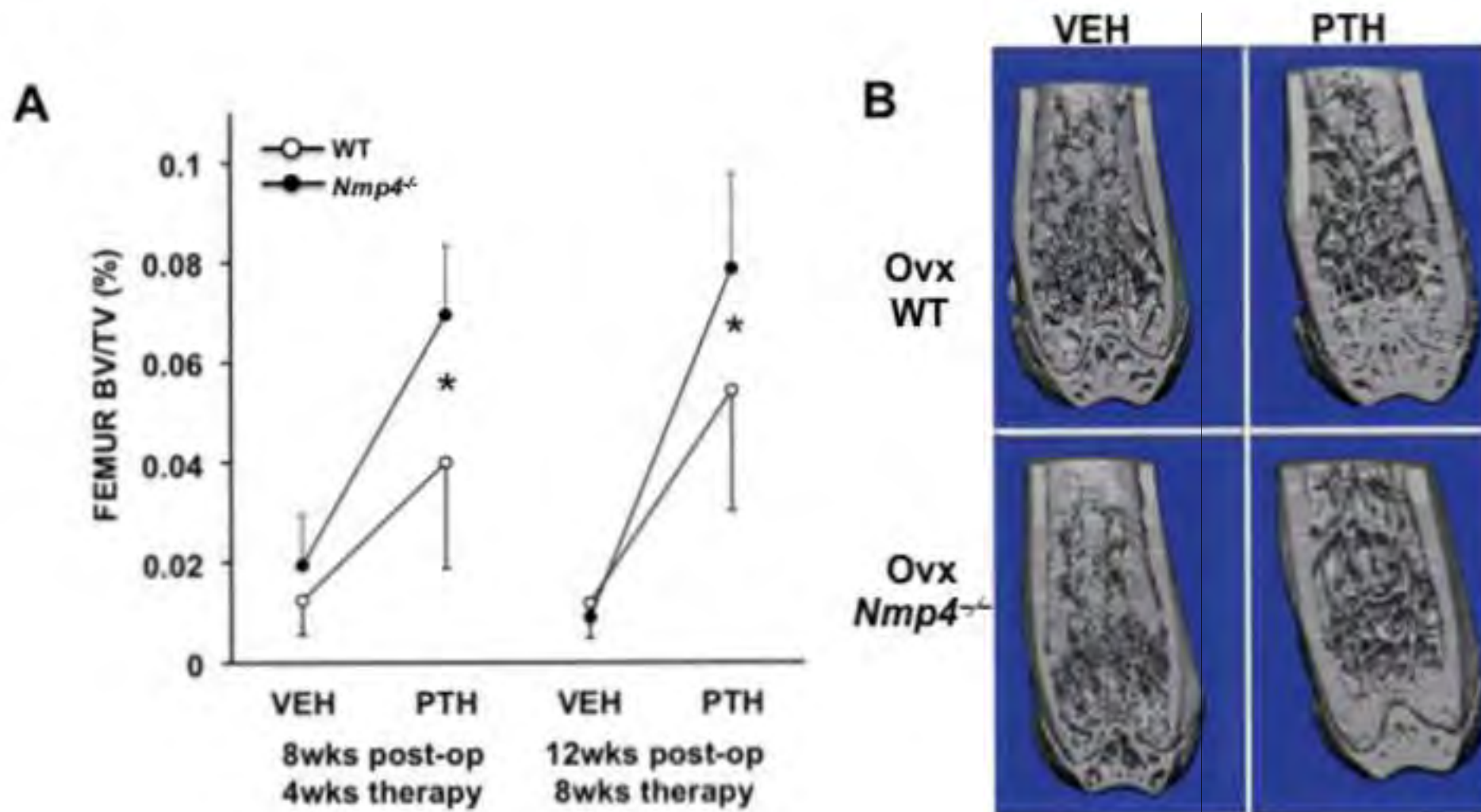




Figure 3  
[Click here to download Figure: FIGURE 3.tif](#)

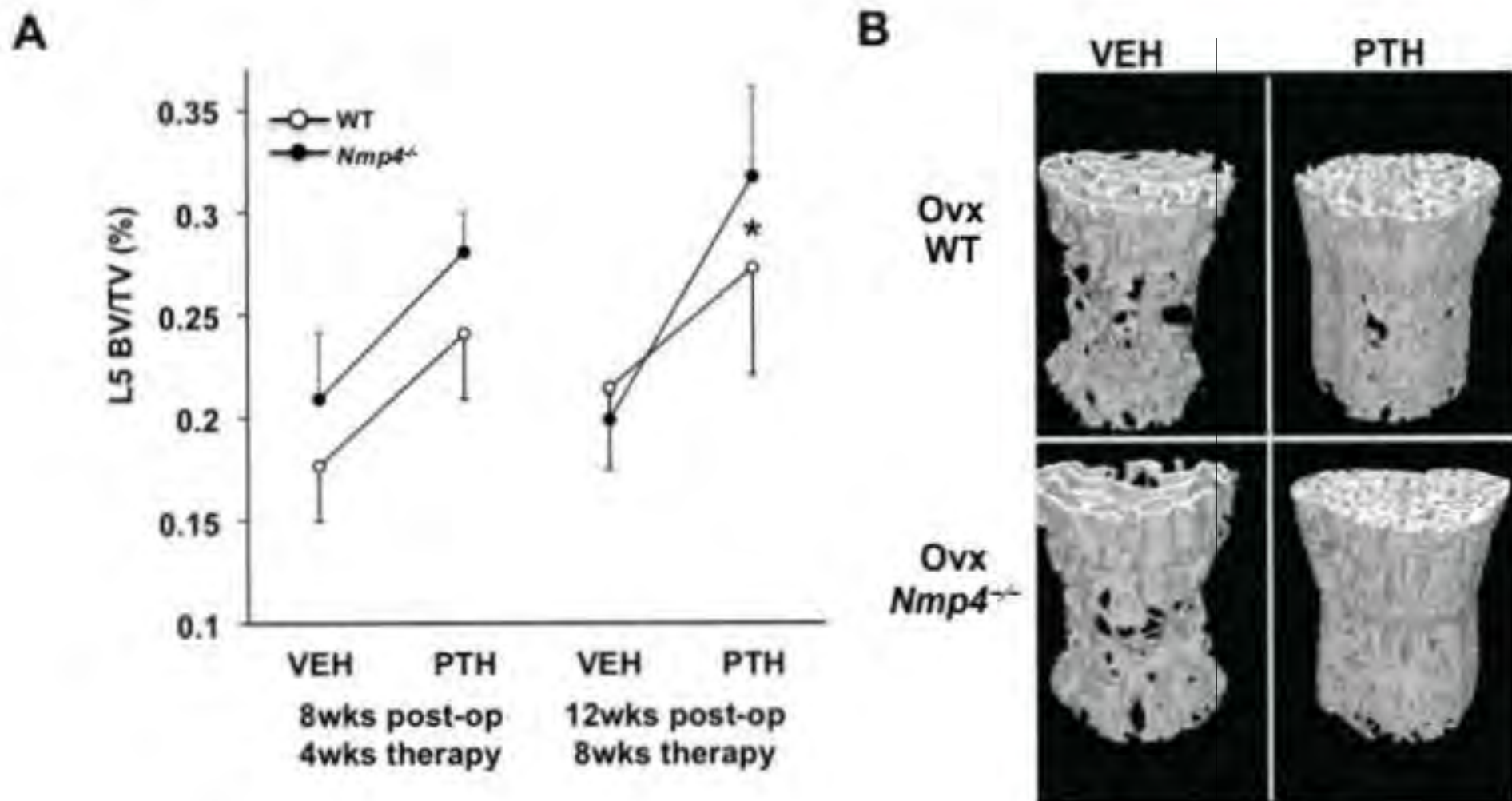


Figure 4  
Click here to download Figure: FIGURE 4.tif

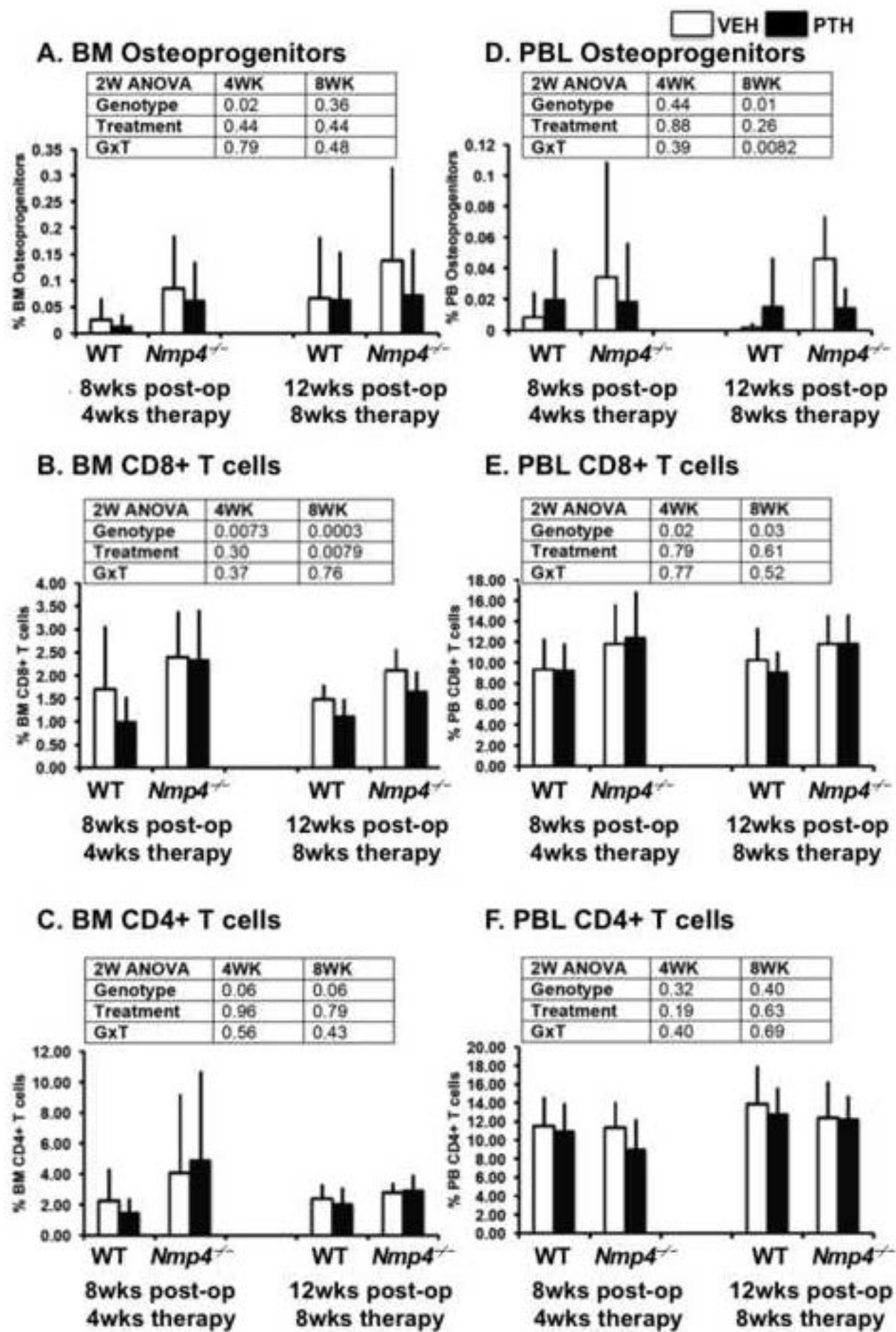


Figure 5  
[Click here to download Figure: FIGURE 5.tif](#)

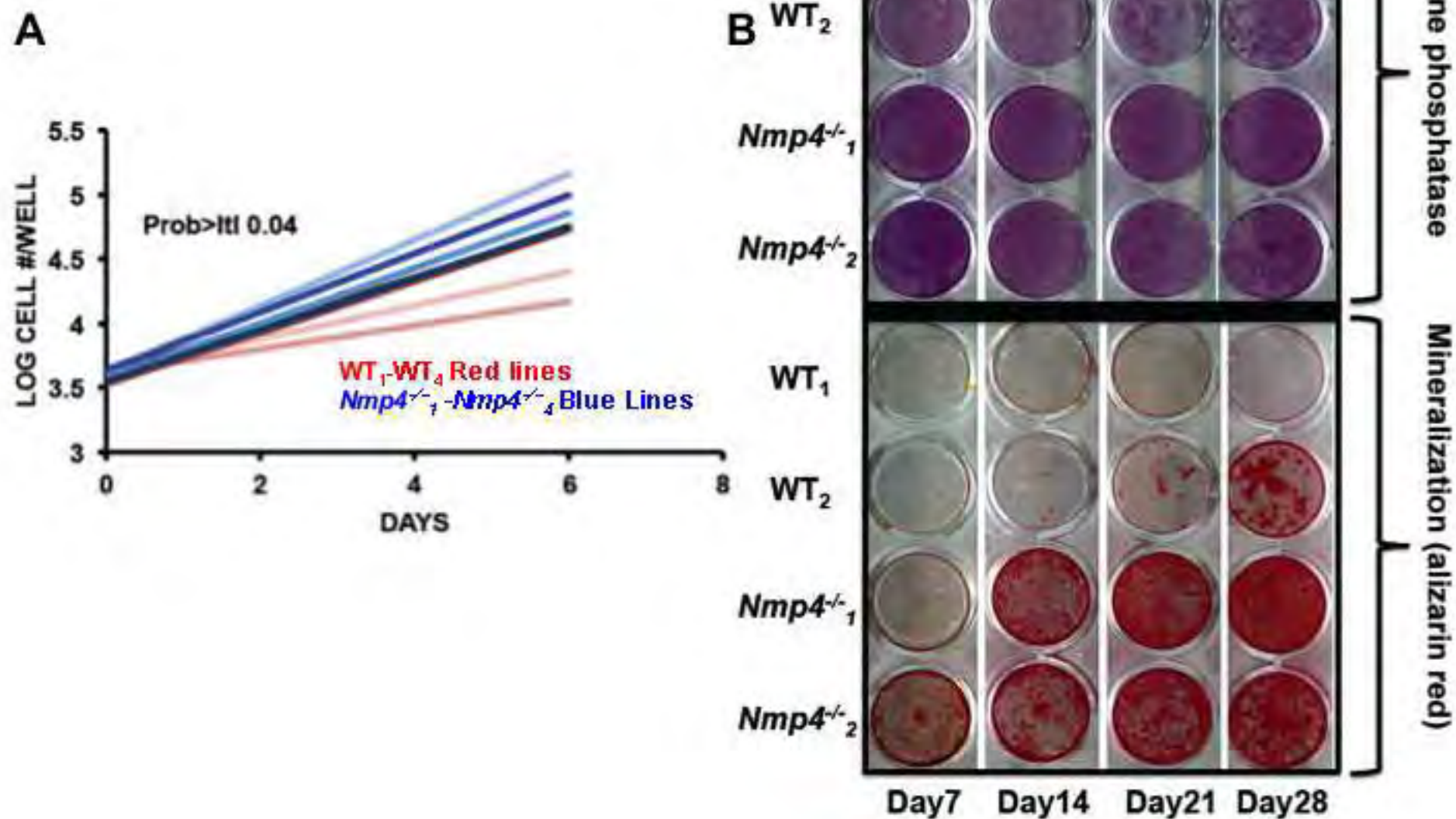


Figure 6  
[Click here to download Figure: FIGURE 6.tif](#)

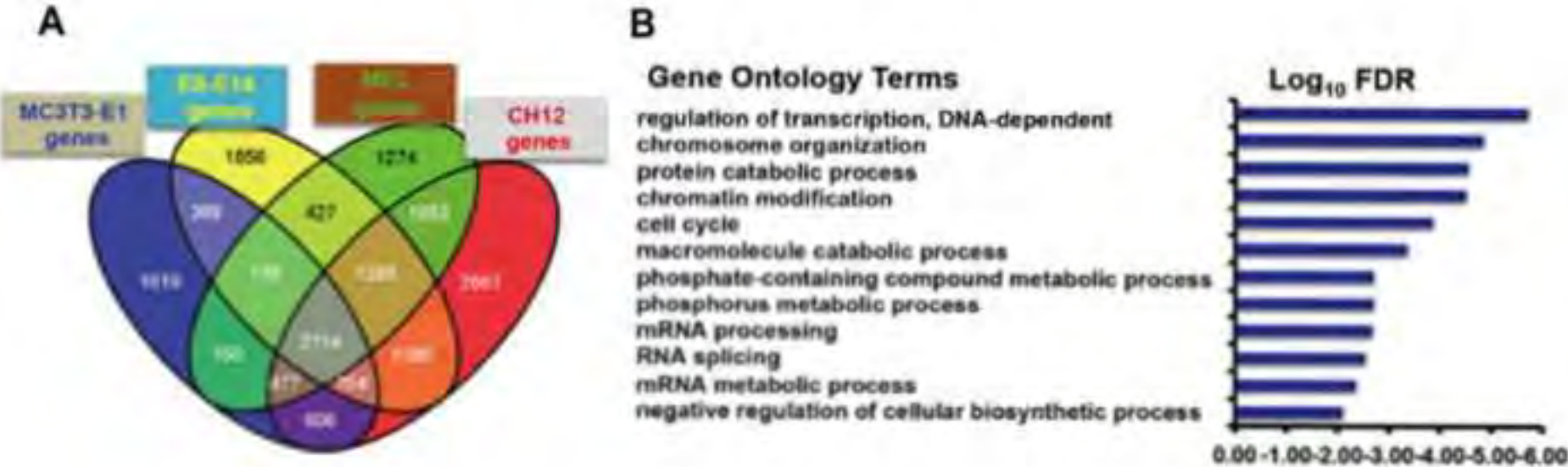
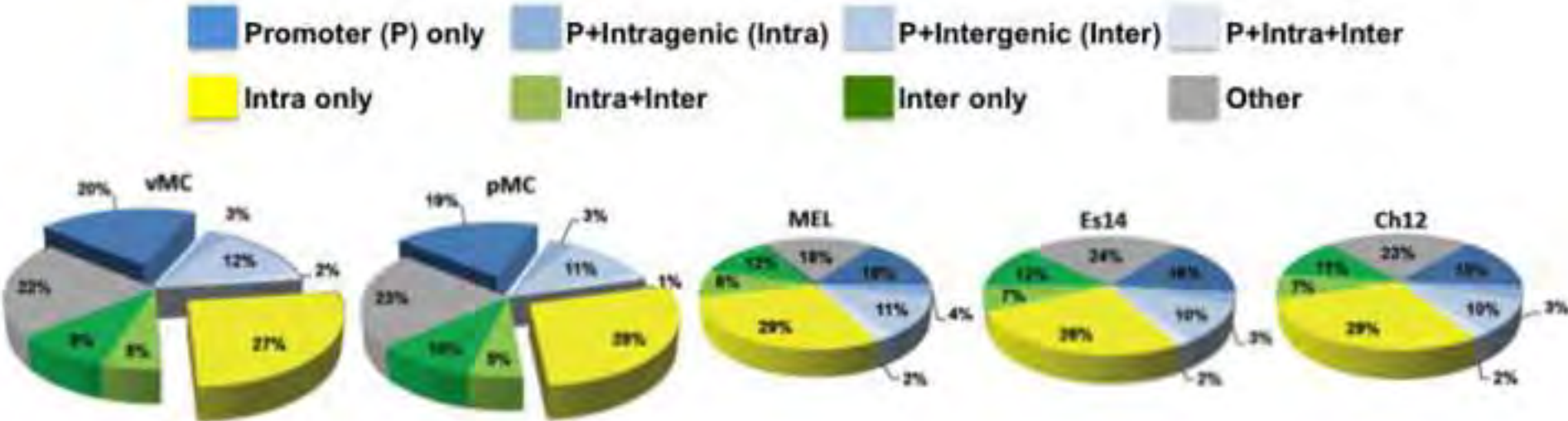




Figure 7  
Click here to download Figure: FIGURE 7.tif

A



B

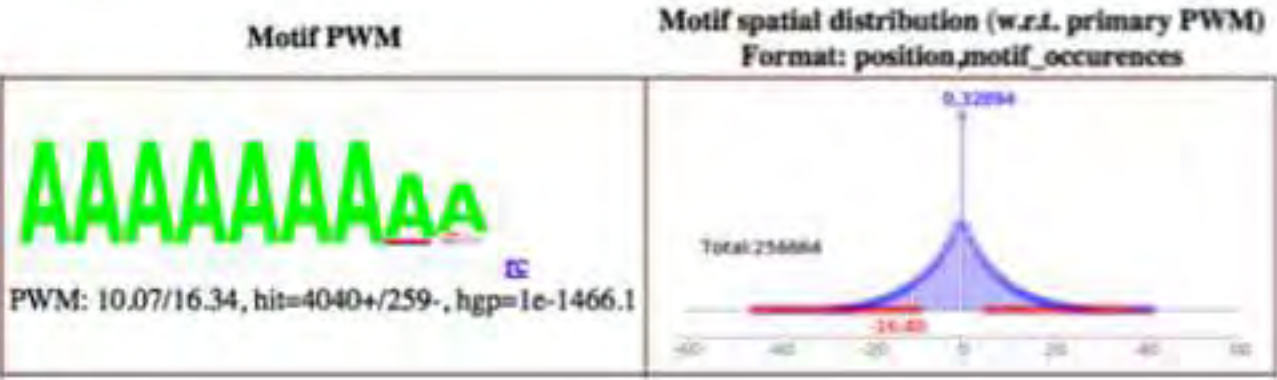


Figure 8  
[Click here to download Figure: FIGURE 8.tif](#)

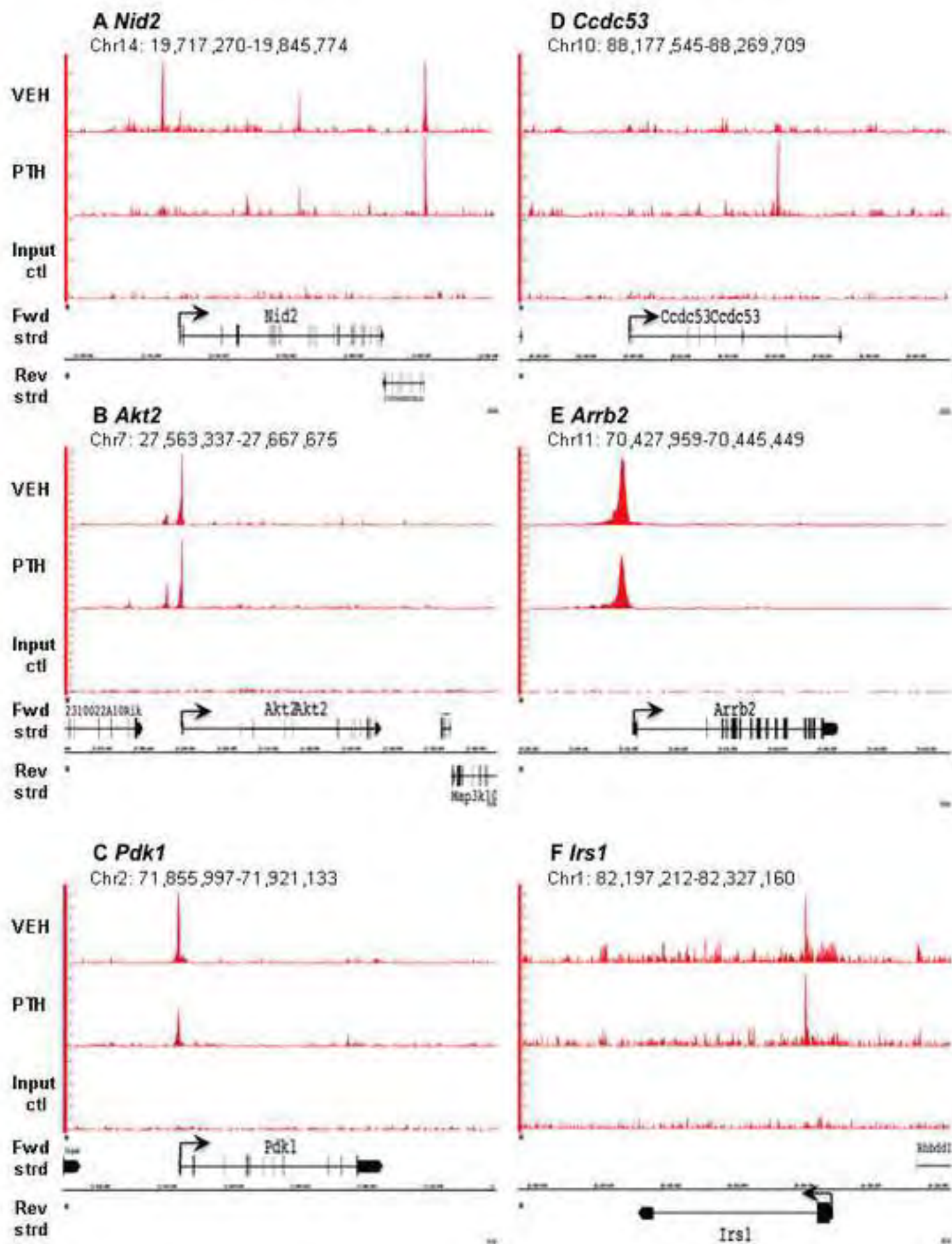


Figure 9

[Click here to download Figure: FIGURE 9.tif](#)

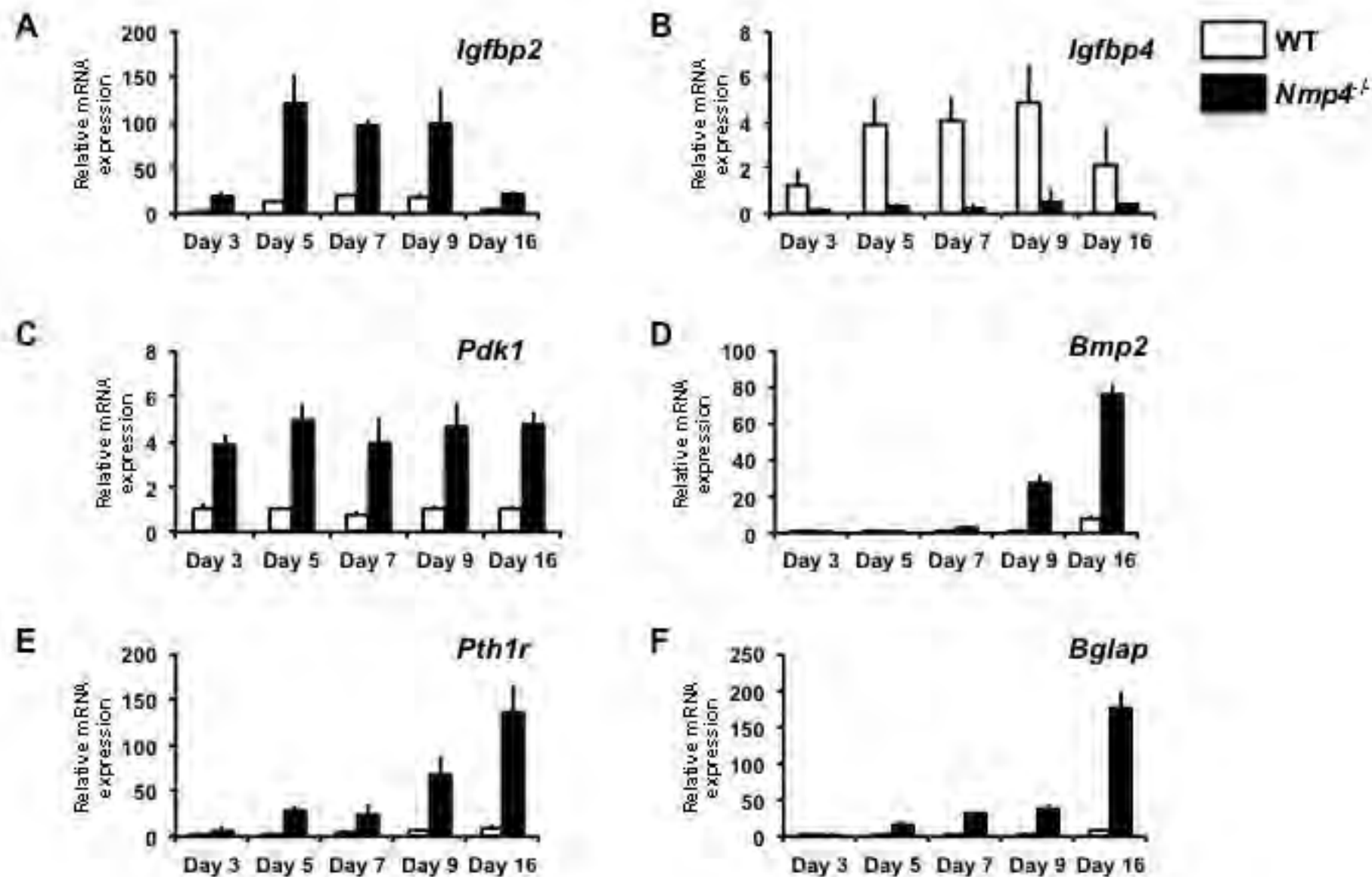
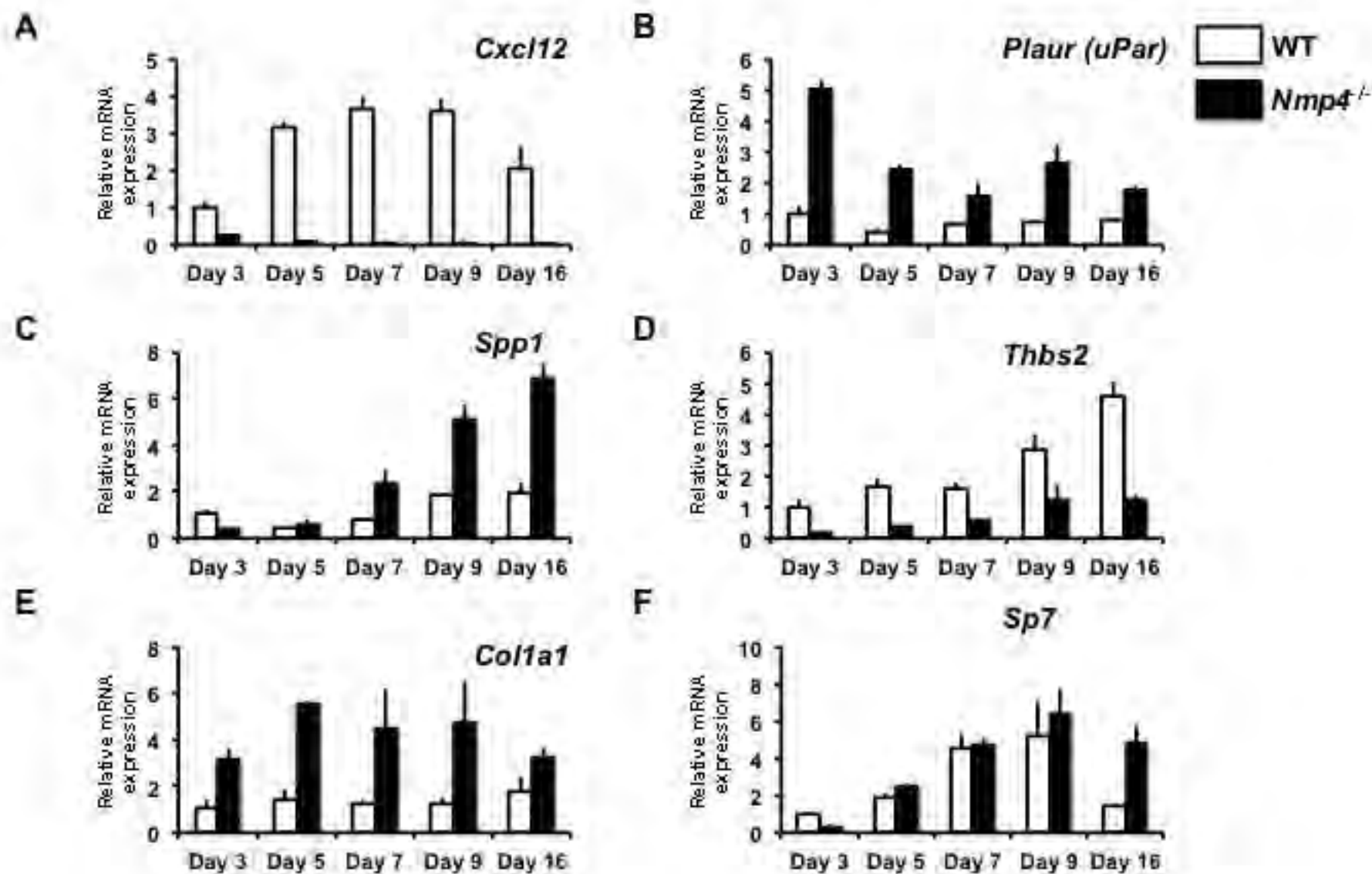
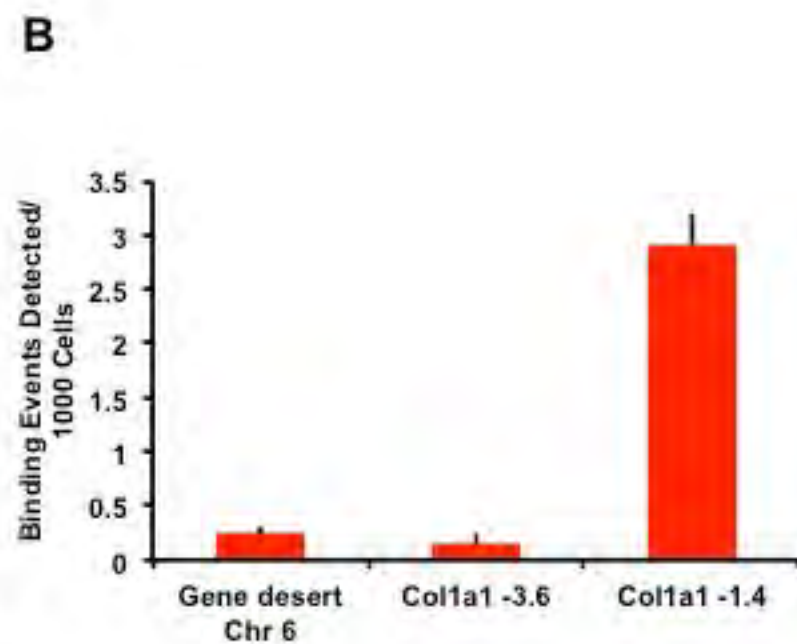
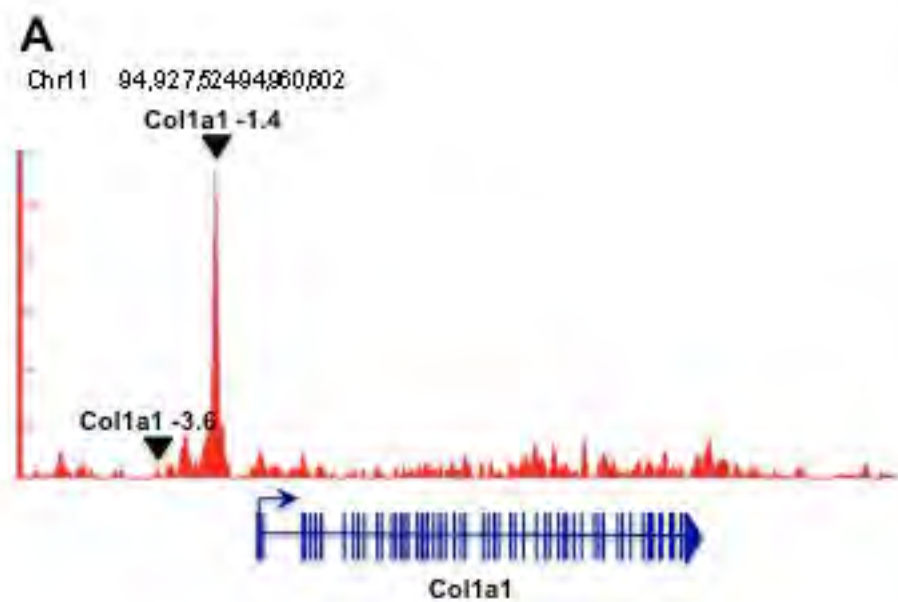


Figure 10  
[Click here to download Figure: FIGURE 10.tif](#)





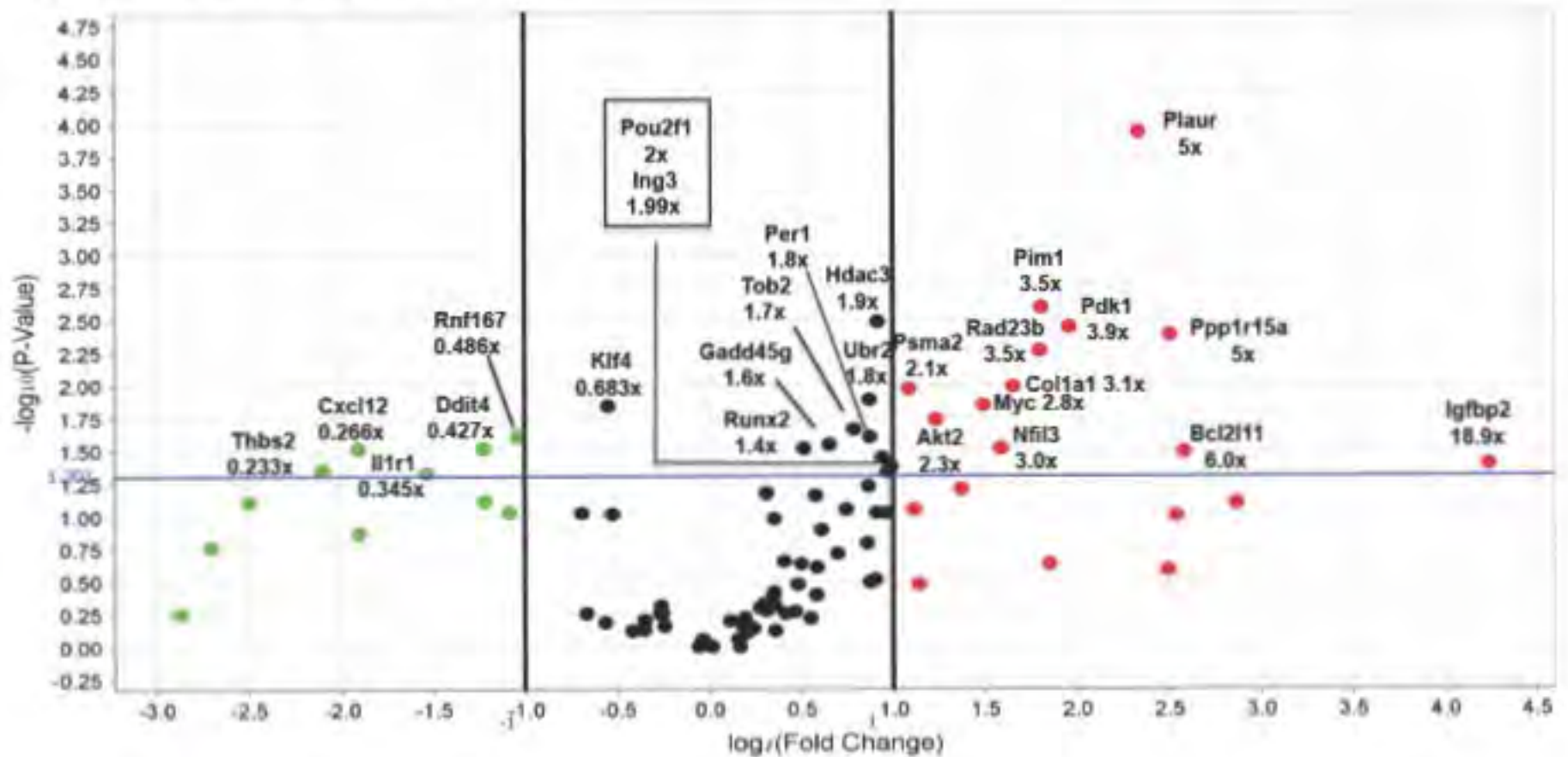


Supplemental Figure 2A

[Click here to download Supplemental Data: SUPPLEMENTAL FIGURE 2A.tif](#)

**Supplemental Figure 2: Volcano Plots (P-Value [Boundary 0.05] vs Fold Change [Boundary 2.0x])**

**A Day 3 *Nmp4*<sup>-/-</sup> vs Day 3 WT**

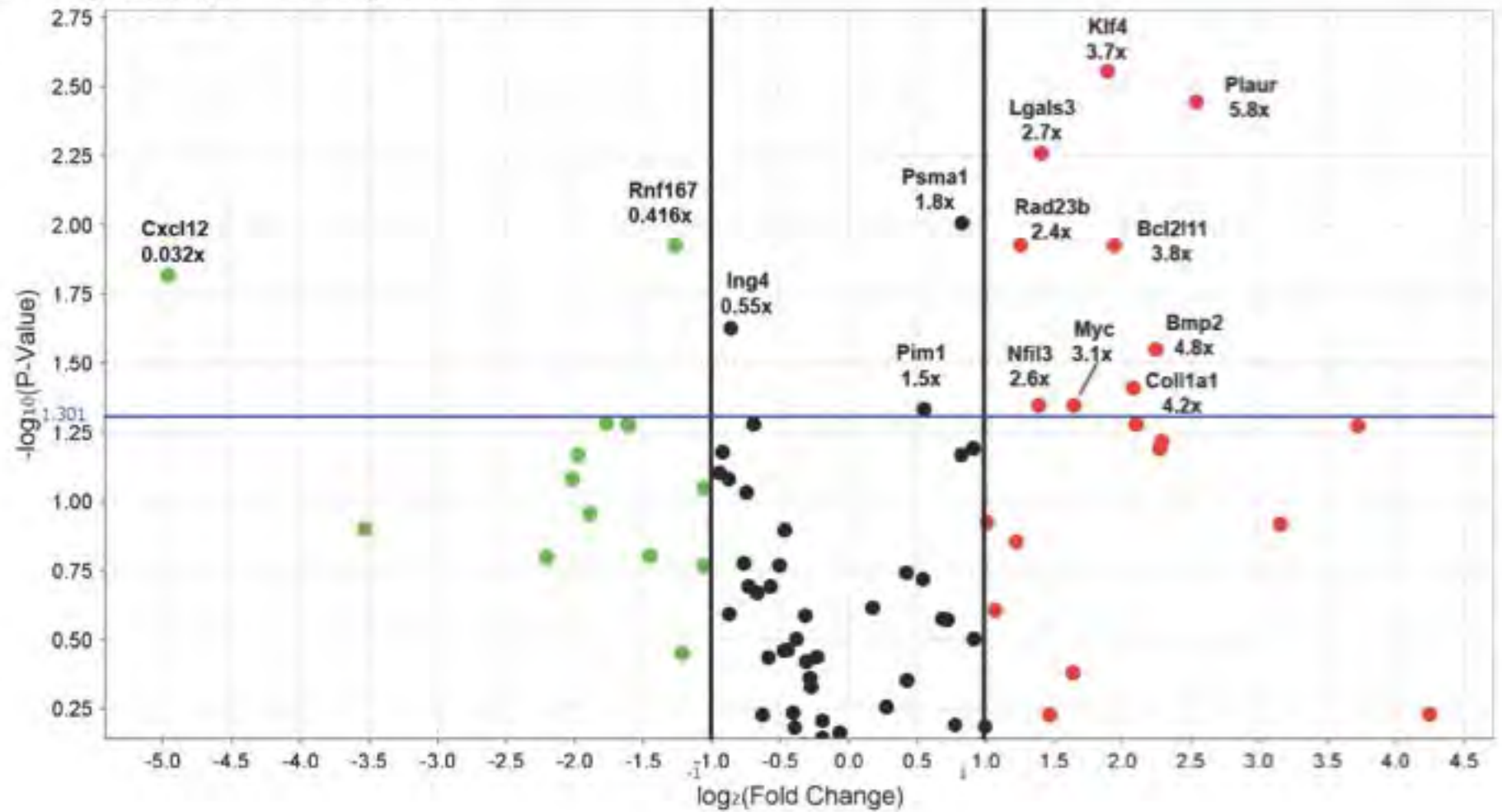


Supplemental Figure 2B

[Click here to download Supplemental Data: SUPPLEMENTAL FIGURE 2B.tif](#)

**Supplemental Figure 2: Volcano Plots (P-Value [Boundary 0.05] vs Fold Change [Boundary 2.0x])**

**B Day 5 *Nmp4*<sup>-/-</sup> vs Day 5 WT**

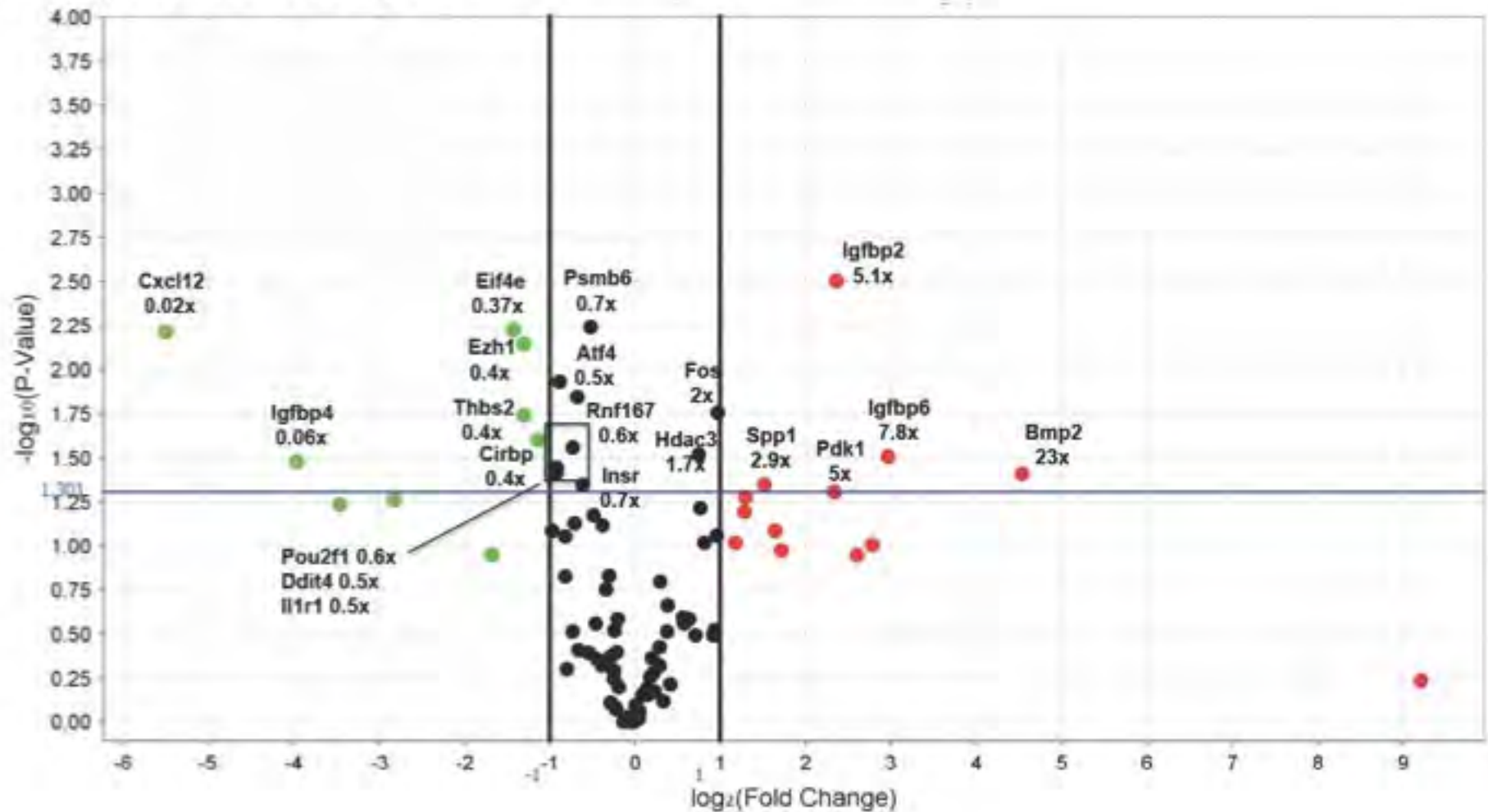


Supplemental Figure 2C

[Click here to download Supplemental Data: SUPPLEMENTAL FIGURE 2C.tif](#)

**Supplemental Figure 2: Volcano Plots (P-Value [Boundary 0.05] vs Fold Change [Boundary 2.0x])**

**C Day 7 *Nmp4*<sup>-/-</sup> vs Day 7 WT**



## Supplemental Figure 2A

[Click here to download Supplemental Data: SUPPLEMENTAL FIGURE 2A.tif](#)

Supplemental Figure 2B

[Click here to download Supplemental Data: SUPPLEMENTAL FIGURE 2B.tif](#)

## Supplemental Figure 2C

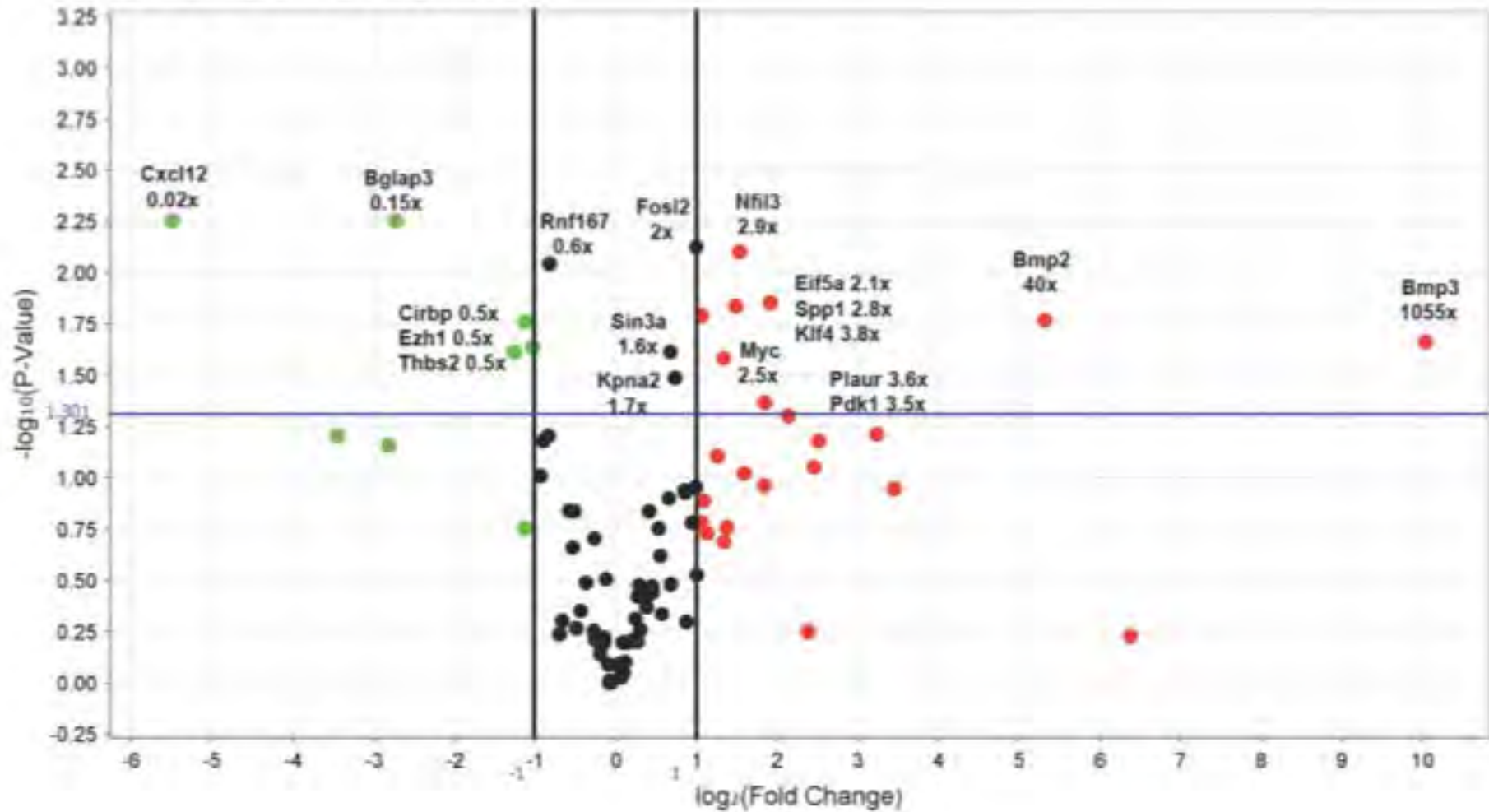
[Click here to download Supplemental Data: SUPPLEMENTAL FIGURE 2C.tif](#)

Supplemental Figure 2D

[Click here to download Supplemental Data: SUPPLEMENTAL FIGURE 2D.tif](#)

## Supplemental Figure 2: Volcano Plots (P-Value [Boundary 0.05] vs Fold Change [Boundary 2.0x])

### D Day 9 *Nmp4*<sup>-/-</sup> vs Day 9 WT





Supplemental Data Legends

[Click here to download Supplemental Data Legends: FIGURE LEGENDS.docx](#)

**FIGURE LEGENDS**

**Figure 1:** Schematic of treatment regimen for WT and *Nmp4*<sup>-/-</sup> mice; Group 1 mice were subjected to ovariectomy (ovx) or sham operation at 12wks of age and evaluated for bone loss 4wks post-op (16wks of age). Group 2 mice were ovx at 12wks of age and began PTH or vehicle therapy at 16wks of age for a duration of 4wks and 8wks. Endpoint analyses included micro-computed tomography  $\mu$ CT, serum analysis for N-terminal propeptide of type 1 procollagen (P1NP) and C-terminal telopeptides (CTX), and dynamic histomorphometry.

**Figure 2:** Disabling *Nmp4* enhances PTH restorative therapy in the distal femur of ovx *Nmp4*<sup>-/-</sup> mice [A] Interaction plots of femoral trabecular bone volume/total volume (BV/TV) of ovx WT and ovx *Nmp4*<sup>-/-</sup> mice as determined by  $\mu$ CT at 4wks of treatment and 8wks of treatment. Data are average  $\pm$  SD, number of mice/experimental group = 8-9). Statistical differences were determined using a 2-way ANOVA and significance was set at  $p \leq 0.05$ . The Tukey's HSD post hoc test was used to determine differences between the treatment groups. There were genotype, treatment and genotype x treatment interaction at both time points. There was no difference between the vehicle-treated WT and *Nmp4*<sup>-/-</sup> mice. [B]  $\mu$ CT images showing PTH-induced improvements in distal femur trabecular architecture in ovx WT and *Nmp4*<sup>-/-</sup> mice after 8 weeks of treatment (12wks post-op, 24wks of age).

**Figure 3:** The exaggerated response to anabolic PTH persists in the L5 vertebra of ovx *Nmp4*<sup>-/-</sup> mice. [A] Interaction plots of L5 vertebra bone volume/total volume (BV/TV) of ovx WT and ovx *Nmp4*<sup>-/-</sup> mice as determined by  $\mu$ CT at 4wks of treatment and 8wks of treatment. Data are average  $\pm$  SD, number of mice/experimental group = 8-9). Statistical differences were determined using a 2-way ANOVA and significance was set at  $p \leq 0.05$ . The LS Means Student t post hoc test was used to determine differences between the treatment groups. There were genotype, treatment effects at both time points and a genotype x treatment interaction at 8wks therapy. There was no difference between the vehicle-treated WT and

*Nmp4*<sup>-/-</sup> mice. [B]  $\mu$ CT images showing PTH-induced improvements in L5 trabecular architecture in ovx WT and *Nmp4*<sup>-/-</sup> mice after 8 weeks of treatment (12wks post-op, 24wks of age).

**Figure 4:** OvX does not abrogate the expanded population of osteoprogenitors and CD8<sup>+</sup> T cells in *Nmp4*<sup>-/-</sup> mice. FACS analysis of BM and PBL osteoprogenitors, CD8<sup>+</sup> T cells, and CD4<sup>+</sup> T cells. [A, D] The frequency of femoral BM and PBL CD45<sup>-</sup>/CD105<sup>+</sup>/CD146<sup>+</sup>/CD105<sup>+</sup>/nestin<sup>+</sup> osteoprogenitor cells in WT and *Nmp4*<sup>-/-</sup> mice at the end of 4wks and 8wks treatment with intermittent PTH or vehicle control; [B, E] the frequency of BM and PBL CD8<sup>+</sup> T cells from the WT and *Nmp4*<sup>-/-</sup> mice; [C, F] the frequency of BM and PBL CD4<sup>+</sup> T cells from the WT and null mice. Data are average  $\pm$  SD, number of mice/experimental group = 8–9; Statistical differences were determined using a 2-way ANOVA and significance was set at  $p \leq 0.05$ .

**Figure 5:** Expanded *Nmp4*<sup>-/-</sup> MSPCs exhibit enhanced proliferation and mineralization in culture. [A] Comparative growth rates of expanded WT and *Nmp4*<sup>-/-</sup> MSPCs. Cell counts/day (n=4 lines per genotype log<sub>10</sub> cells/well, 3 wells/sample, average  $\pm$  SD, t test,  $t < 0.05$ ). Note: each ‘line’ is derived from a single mouse [B] Alkaline phosphatase (alk phos) and alizarin red staining of a WT and *Nmp4*<sup>-/-</sup> MSPC cultures from Day7-Day28. See text for details

**Figure 6:** *Nmp4* associates with core target genes common to multiple cell types and acts as a *negative regulation of cellular biosynthetic processes* [A] Venn diagram illustrating the shared *Nmp4* target genes in the MC3T3-E1 osteoblast-like cells (vehicle-treated), and the three ENCODE cells lines, ES-E14 (embryonic stem cells), MEL, and CH12 cells (B-cell lymphomas). [B] DAVID/REVIGO gene ontology (GO) profile of *Nmp4* core target genes

**Figure 7:** *Nmp4* binds to AT-rich DNA typically proximal to TSS sites or within intragenic regions. [A] Genome-wide mapping of the *Nmp4* binding sites show that most sites are distributed in the TSS and

intragenic regions of the genome. ChIP-seq analysis included vehicle-treated and PTH-treated MC3T3-E1 osteoblast-like cells (vMC and pMC, respectively) and three murine cell lines from the ENCODE Consortium including ES-E14 (Es14), which are E14 undifferentiated mouse embryonic stem cells, and two mouse erythroleukemia cell lines (Ch12 and MEL) derived from B-cell lymphomas. [B] GEM analysis for the Nmp4 consensus sequence derived from MC3T3-E1 cells. A minimal k-mer width of 6 and maximum of 20 were used. The optimal position weight matrix (PWM) score for the MC3T3-E1 data was 10.07. The hypergeometric P-value (hgp) was 1e-1466.1.

**Figure 8:** ChIP-seq reveals Nmp4 binding profiles at specific gene loci. Mouse MC3T3-E1 cells were seeded into twenty-one 150mm plates at an initial density of 50,000 cells/plate (320 cells/cm<sup>2</sup>) and maintained in  $\alpha$ MEM complete medium + ascorbic acid for 14 days. Prior to harvest cells were treated with 25nM hPTH(1-34) or vehicle control for 1hr. Processing for ChIP-seq analysis was performed as described in the Materials and Methods. Sequences (50nt reads, single end) were aligned to the mouse genome (mm10) using the BWA algorithm. Alignments were extended in silico at their 3'-ends to a length of 150bp, which is the average genomic fragment length in the size-selected library, and assigned to 32-nt bins along the genome. Nmp4 (Znf384) peak locations were determined using the MACS algorithm (v1.4.2) with a cutoff of pvalue = 1e-7. The genomic loci including the chromosome number and nucleotide interval are indicated. Read scales are indicated on the Y-axis. An arrow indicates the transcriptional start sites and direction of transcription for each of the genes; vertical boxes within the gene indicate exons. The Nmp4 ChIP-seq gene profiles include (A) *Nid2* (B) *Akt2*, (C) *Pdk1* (D) *ccdc53*, (E) *Arrb2* and (F) *Irs1*. The input DNA profiles were devoid of peaks.

**Figure 9:** Comparison of mRNA expression profiles derived from non-differentiating (Day 3) and osteogenic-differentiating (Days 5-16) WT and *Nmp4*<sup>-/-</sup> cells. All transcript levels are compared to WT Day 3 providing a time course of expression. mRNA profiles [A] *Igf1bp2*; [B] *Igf1bp4*; [C] *Pdk1*; [D] *Bmp2*; [E] *Pth1r* were derived from the TLDA system (Format 96a, Applied Biosystems, Foster City,

CA) performed on a QuantStudio™ 7 Flex Real-Time PCR System and normalized with GusB. Profile [F] *Bglap* mRNA profile qRT-PCR reactions were performed on an Eppendorf Mastercycler® RealPlex<sup>2</sup> using *Rplp2* Mm03059047\_gH) as the normalizer as previously described [Robling et al, 2009]. Comparison of profiles using *GusB* and *Rplp2* as the normalizer showed no differences in the shape of the expression profiles

**Figure 10:** Comparison of mRNA expression profiles derived from non-differentiating (Day 3) and osteogenic-differentiating (Days 5-16) WT and *Nmp4*<sup>-/-</sup> cells. All transcript levels are compared to WT Day 3 providing a time course of expression. mRNA profiles [A] *Cxcl12*; [B] *Plaur*; [C] *Spp1*; [D] *Thbs2*; [E] *Colla1* were derived from the TLDA system (Format 96a, Applied Biosystems, Foster City, CA) performed on a QuantStudio™ 7 Flex Real-Time PCR System and normalized with GusB. Profile [F] *Sp7* mRNA profile qRT-PCR reactions were performed on an Eppendorf Mastercycler® RealPlex<sup>2</sup> using *Rplp2* (Mm03059047\_gH) as the normalizer as previously described [Robling et al., 2009]. The Day 16 WT sample is the average of two replicates. Comparison of profiles using GusB and *Rplp2* as the normalizer showed no differences in the shape of the expression profiles

**Supplemental Figure S1:** qRT-PCR validates the ChIP-seq profiles. [A] The *Nmp4* ChIP-seq profile for the gene *Colla1*. The genomic loci including the chromosome number and nucleotide interval are indicated. Read scale is indicated on the Y-axis. An arrow marks the transcriptional start site and direction of transcription; vertical boxes within the gene identify exons. [B] qRT-PCR was used to authenticate the ChIP-seq peaks as described in the Materials and Methods.

**Supplemental Figure 2:** Volcano plots derived from gene expression profiles of non-differentiating (Day 3) and osteogenic-differentiating (Days 5-16) WT and *Nmp4*<sup>-/-</sup> as described in the Materials and Methods. RNA expression profiling was performed on a QuantStudio™ 7 Flex Real-Time PCR System and data analyzed using the ExpressionSuite v1.0.4™ analysis software (Applied Biosystems) as described in the

Materials and Methods. [A] WT vs *Nmp4*<sup>-/-</sup> cells at Day 3 post-seeding. mRNA transcript expression was compared to WT cells (Day 3). Cells maintained in Mesencult™ Media + Mesencult™ Stimulatory Supplement. [B] WT vs *Nmp4*<sup>-/-</sup> cells at Day 5 post-seeding. mRNA transcript expression was compared to WT cells (Day 5). Cells maintained in differentiation medium for 48hrs [C] WT vs *Nmp4*<sup>-/-</sup> cells at Day 7 post-seeding. mRNA transcript expression was compared to WT cells (Day 7). Cells maintained in differentiation medium for 96hrs [D] WT vs *Nmp4*<sup>-/-</sup> cells at Day 9 post-seeding. mRNA transcript expression was compared to WT cells (Day 9). Cells maintained in differentiation medium for 144hrs [E] WT vs *Nmp4*<sup>-/-</sup> cells at Day 16 post-seeding. mRNA transcript expression was compared to WT cells (Day 16). Cells maintained in differentiation medium for 192hrs. Genes indicated with green dots (left of center) and above the X-axis exhibited a significant downregulation by over 2-fold. Genes indicated with the red dots (right of center) and above the X-axis exhibited a significant upregulation by over 2-fold.

**Supplemental TABLE 1:** 96 *Nmp4* ‘core’ target genes, non-core target genes, and non-target genes including 5 candidate normalizer genes. Individual cDNAs were quantified by qRT-PCR using a custom TLDA system (Format 96a, Applied Biosystems, Foster City, CA) as described in the Materials and Methods on a QuantStudio™ 7 Flex Real-Time PCR System. We used the ExpressionSuite v1.0.4™ analysis software (Applied Biosystems) to analyze these data.

**Supplemental TABLE 2:** 2114 *Nmp4* ‘core’ target genes common to the four cell lines MC3T3-E1 osteoblast-like cells, and three murine cell lines from the ENCODE Consortium including ES-E14 (Es14), which are E14 undifferentiated mouse embryonic stem cells, and two mouse erythroleukemia cell lines (Ch12 and MEL) derived from B-cell lymphomas.

**Supplemental TABLE 3:** IPA analysis of 2114 *Nmp4* ‘core’ target genes common to the four cell lines MC3T3-E1 osteoblast-like cells, and three murine cell lines from the ENCODE Consortium including

130 ES-E14 (Es14), which are E14 undifferentiated mouse embryonic stem cells, and two mouse  
131 erythroleukemia cell lines (Ch12 and MEL) derived from B-cell lymphomas.

132

133

## Supplemental Table 1

Click here to download Supplemental Data: NMP4 MS SUPPLEMENTAL TABLE 1.xlsx

Detector	Reporter	Quencher	Description	Comments Sequence
18S-Hs99999901_s1	FAM	Non Fluorescent	Eukaryotic 18S rRNA	
Akt2-Mm02026778_g1	FAM	Non Fluorescent	thymoma viral proto-oncogene 2	
Alpl-Mm00475834_m1	FAM	Non Fluorescent	alkaline phosphatase, liver/bone/kidney	
Arrb2-Mm00520666_g1	FAM	Non Fluorescent	arrestin, beta 2	
Atf4-Mm00515325_g1	FAM	Non Fluorescent	activating transcription factor 4	
Bcl2l11-Mm00437796_m1	FAM	Non Fluorescent	BCL2-like 11 (apoptosis facilitator)	
Bglap3-Mm00649782_gH	FAM	Non Fluorescent	bone gamma-carboxyglutamate protein 3	
Bmp2-Mm01340178_m1	FAM	Non Fluorescent	bone morphogenetic protein 2	
Bmp3-Mm00557790_m1	FAM	Non Fluorescent	bone morphogenetic protein 3	
Bmp4-Mm00432087_m1	FAM	Non Fluorescent	bone morphogenetic protein 4	
Bmp6-Mm01332882_m1	FAM	Non Fluorescent	bone morphogenetic protein 6	
Bmpr1a-Mm00477650_m1	FAM	Non Fluorescent	bone morphogenetic protein receptor, type 1A	
Cbfb-Mm01251026_g1	FAM	Non Fluorescent	core binding factor beta	
Cbx4-Mm00483089_m1	FAM	Non Fluorescent	chromobox 4	
Cbx7-Mm00520006_m1	FAM	Non Fluorescent	chromobox 7	
Cdc6-Mm03048221_m1	FAM	Non Fluorescent	cell division cycle 6	
Cirbp-Mm00483336_g1	FAM	Non Fluorescent	cold inducible RNA binding protein	
Col1a1-Mm00801666_g1	FAM	Non Fluorescent	collagen, type I, alpha 1	
Crebbp-Mm01342452_m1	FAM	Non Fluorescent	CREB binding protein	
Cxcl12-Mm00445553_m1	FAM	Non Fluorescent	chemokine (C-X-C motif) ligand 12	
Ddit4-Mm00512504_g1	FAM	Non Fluorescent	DNA-damage-inducible transcript 4	
Dnm3os-Mm03455916_s1	FAM	Non Fluorescent	dynamin 3, opposite strand	
Ehmt2-Mm01132261_m1	FAM	Non Fluorescent	euchromatic histone lysine N-methyltransferase 2	
Eif4e-Mm00725633_s1	FAM	Non Fluorescent	eukaryotic translation initiation factor 4E	
Eif5a-Mm01971736_g1	FAM	Non Fluorescent	eukaryotic translation initiation factor 5A	
Ephb4-Mm01201157_m1	FAM	Non Fluorescent	Eph receptor B4	
Ezh1-Mm00468440_m1	FAM	Non Fluorescent	enhancer of zeste homolog 1 (Drosophila)	
Fos-Mm00487425_m1	FAM	Non Fluorescent	FBJ osteosarcoma oncogene	
Fosl2-Mm00484442_m1	FAM	Non Fluorescent	fos-like antigen 2	
Gadd45b-Mm00435121_g1	FAM	Non Fluorescent	growth arrest and DNA-damage-inducible 45 beta	
Gadd45g-Mm01352550_g1	FAM	Non Fluorescent	growth arrest and DNA-damage-inducible 45 gamma	
Gas1-Mm01700206_g1	FAM	Non Fluorescent	growth arrest specific 1	
Hdac3-Mm00515916_m1	FAM	Non Fluorescent	histone deacetylase 3	



Hif1a-Mm00468869_m1	FAM	Non Fluorescent	hypoxia inducible factor 1, alpha subunit
Igf1-Mm00439560_m1	FAM	Non Fluorescent	insulin-like growth factor 1
Igf1r-Mm00802831_m1	FAM	Non Fluorescent	insulin-like growth factor I receptor
Igfbp2-Mm00492632_m1	FAM	Non Fluorescent	insulin-like growth factor binding protein 2
Igfbp4-Mm00494922_m1	FAM	Non Fluorescent	insulin-like growth factor binding protein 4
Igfbp6-Mm00599696_m1	FAM	Non Fluorescent	insulin-like growth factor binding protein 6
Il1r1-Mm00434237_m1	FAM	Non Fluorescent	interleukin 1 receptor, type I
Ing3-Mm00458324_m1	FAM	Non Fluorescent	inhibitor of growth family, member 3
Ing4-Mm00460097_m1	FAM	Non Fluorescent	inhibitor of growth family, member 4
Insr-Mm01211875_m1	FAM	Non Fluorescent	insulin receptor
Irs1-Mm01278327_m1	FAM	Non Fluorescent	insulin receptor substrate 1
Klf4-Mm00516104_m1	FAM	Non Fluorescent	Kruppel-like factor 4 (gut)
Kpna2-Mm00834020_gH	FAM	Non Fluorescent	karyopherin (importin) alpha 2
Lgals3-Mm00802901_m1	FAM	Non Fluorescent	lectin, galactose binding, soluble 3
Lrp1-Mm00464608_m1	FAM	Non Fluorescent	low density lipoprotein receptor-related protein 1
Msx2-Mm00442992_m1	FAM	Non Fluorescent	msh homeobox 2
Myc-Mm00487804_m1	FAM	Non Fluorescent	myelocytomatosis oncogene
Nbr1-Mm01249798_m1	FAM	Non Fluorescent	neighbor of Brca1 gene 1
Ncor1-Mm01333102_m1	FAM	Non Fluorescent	nuclear receptor co-repressor 1
Ncor2-Mm00448796_m1	FAM	Non Fluorescent	nuclear receptor co-repressor 2
Nfil3-Mm00600292_s1	FAM	Non Fluorescent	nuclear factor, interleukin 3, regulated
Nr3c1-Mm00433832_m1	FAM	Non Fluorescent	nuclear receptor subfamily 3, group C, member 1
Pdk1-Mm00554306_m1	FAM	Non Fluorescent	pyruvate dehydrogenase kinase, isoenzyme 1
Per1-Mm00501813_m1	FAM	Non Fluorescent	period circadian clock 1
Phf12-Mm00663497_m1	FAM	Non Fluorescent	PHD finger protein 12
Pim1-Mm00435712_m1	FAM	Non Fluorescent	proviral integration site 1
Plaur-Mm00440911_m1	FAM	Non Fluorescent	plasminogen activator, urokinase receptor
Pou2f1-Mm00448332_m1	FAM	Non Fluorescent	POU domain, class 2, transcription factor 1
Ppp1r15a-Mm01205601_g1	FAM	Non Fluorescent	protein phosphatase 1, regulatory (inhibitor) subunit 15A
Prpf19-Mm00467298_m1	FAM	Non Fluorescent	PRP19/PSO4 pre-mRNA processing factor 19 homolog (S. cerevisiae)
Psma1-Mm00803741_m1	FAM	Non Fluorescent	proteasome (prosome, macropain) subunit, alpha type 1
Psma2-Mm00776364_mH	FAM	Non Fluorescent	proteasome (prosome, macropain) subunit, alpha type 2
Psma3-Mm00834115_g1	FAM	Non Fluorescent	proteasome (prosome, macropain) subunit, alpha type 3
Psmb6-Mm00599713_g1	FAM	Non Fluorescent	proteasome (prosome, macropain) subunit, beta type 6

Pth1r-Mm00441046_m1	FAM	Non Fluorescent	parathyroid hormone 1 receptor
Ptp4a1-Mm00850755_g1	FAM	Non Fluorescent	protein tyrosine phosphatase 4a1
Rad23b-Mm00772280_m1	FAM	Non Fluorescent	RAD23b homolog (S. cerevisiae)
Rffl-Mm00482724_m1	FAM	Non Fluorescent	ring finger and FYVE like domain containing protein
Rnf167-Mm00550967_g1	FAM	Non Fluorescent	ring finger protein 167
Rnf5-Mm01134793_g1	FAM	Non Fluorescent	ring finger protein 5
Rps6kb1-Mm01310033_m1	FAM	Non Fluorescent	ribosomal protein S6 kinase, polypeptide 1
Rptor-Mm00712676_m1	FAM	Non Fluorescent	regulatory associated protein of MTOR, complex 1
Runx2-Mm00501584_m1	FAM	Non Fluorescent	runt related transcription factor 2
Sin3a-Mm00488255_m1	FAM	Non Fluorescent	transcriptional regulator, SIN3A (yeast)
Smad7-Mm00484742_m1	FAM	Non Fluorescent	SMAD family member 7
Sp7-Mm04209856_m1	FAM	Non Fluorescent	Sp7 transcription factor 7
Sparc-Mm00486332_m1	FAM	Non Fluorescent	secreted acidic cysteine rich glycoprotein
Spp1-Mm00436767_m1	FAM	Non Fluorescent	secreted phosphoprotein 1
Suz12-Mm01304145_g1	FAM	Non Fluorescent	suppressor of zeste 12 homolog (Drosophila)
Thbs2-Mm01279240_m1	FAM	Non Fluorescent	thrombospondin 2
Tle3-Mm00437097_m1	FAM	Non Fluorescent	transducin-like enhancer of split 3, homolog of Drosophila E(spl)
Tob2-Mm00451524_s1	FAM	Non Fluorescent	transducer of ERBB2, 2
Ttc3-Mm00493917_m1	FAM	Non Fluorescent	tetratricopeptide repeat domain 3
Ubr2-Mm00524868_m1	FAM	Non Fluorescent	ubiquitin protein ligase E3 component n-recogin 2
Usp15-Mm00452856_m1	FAM	Non Fluorescent	ubiquitin specific peptidase 15
Usp2-Mm00497452_m1	FAM	Non Fluorescent	ubiquitin specific peptidase 2
Xiap-Mm01311594_mH	FAM	Non Fluorescent	X-linked inhibitor of apoptosis
Zbtb7a-Mm00657132_m1	FAM	Non Fluorescent	zinc finger and BTB domain containing 7a
Rplp2-Mm00782638_s1	FAM	Non Fluorescent	ribosomal protein, large P2
Gusb-Mm01197698_m1	FAM	Non Fluorescent	glucuronidase, beta
B2m-Mm00437762_m1	FAM	Non Fluorescent	beta-2 microglobulin
Hprt-Mm01545399_m1	FAM	Non Fluorescent	hypoxanthine guanine phosphoribosyl transferase
Dkk2-Mm01322146_m1	FAM	Non Fluorescent	dickkopf homolog 2 (Xenopus laevis)

Supplemental Table 2

[Click here to download Supplemental Data: NMP4 MS SUPPLEMENTAL TABLE 2.xlsx](#)

Common elements in "vMC3T3", "MEL", "Es14" and "Ch12": **Nmp4 'CORE' genes**

0610031O16Rik  
0610043K17Rik  
1110001J03Rik  
1110002J07Rik  
1110002L01Rik  
1110037F02Rik  
1110038B12Rik  
1110051M20Rik  
1190002F15Rik  
1600002K03Rik  
1600020E01Rik  
1700001G11Rik  
1700007K13Rik  
1700007L15Rik  
1700013F07Rik  
1700016C15Rik  
1700018L02Rik  
1700018M17Rik  
1700021A07Rik  
1700022K14Rik  
1700023H06Rik  
1700030C12Rik  
1700034H15Rik  
1700052N19Rik  
1700063D05Rik  
1700064E03Rik  
1700067K01Rik  
1700095J07Rik

1700101I11Rik  
1700110C19Rik  
1700112E06Rik  
1700120B22Rik  
1810013L24Rik  
1810019N24Rik  
1810059C17Rik  
2010204K13Rik  
2210016F16Rik  
2210408F21Rik  
2210417K05Rik  
2310011J03Rik  
2310034G01Rik  
2310068J16Rik  
2410002F23Rik  
2410022M11Rik  
2500002B13Rik  
2500004C02Rik  
2510009E07Rik  
2610301B20Rik  
2610507B11Rik  
2700029M09Rik  
2700050L05Rik  
2700060E02Rik  
2810403A07Rik  
2810403D21Rik  
2810404F17Rik  
2810408M09Rik  
2810428I15Rik

2810454H06Rik  
3010003L21Rik  
3110009E18Rik  
3110067C02Rik  
3110082J24Rik  
4732471J01Rik  
4921530L18Rik  
4921531C22Rik  
4930402F06Rik  
4930404I05Rik  
4930412O13Rik  
4930432B10Rik  
4930447C04Rik  
4930503L19Rik  
4930509E16Rik  
4930529M08Rik  
4930546H06Rik  
4930552N02Rik  
4931406C07Rik  
4933411K20Rik  
4933433G15Rik  
4933434E20Rik  
5031434O11Rik  
5330430P22Rik  
5530601H04Rik  
5730405O15Rik  
5730420D15Rik  
5730455P16Rik  
5730508B09Rik

9030624J02Rik  
9430008C03Rik  
9430041J12Rik  
9430083A17Rik  
9530026F06Rik  
9530027J09Rik  
9530068E07Rik  
9630014M24Rik  
A330017A19Rik  
A330050B17Rik  
A330069E16Rik  
A430018G15Rik  
A630072M18Rik  
A730036I17Rik  
A830031A19Rik  
A830035A12Rik  
A930001C03Rik  
A930007I19Rik  
AA387883  
AA415398  
AA465934  
Aaas  
Aarsd1  
AB041803  
Abcb6  
Abcc10  
Abcc3  
Abcf3  
Abcg2

Abhd16a  
Abi1  
Abl1  
Ablim1  
Abr  
Acaca  
Acad11  
Acat1  
Acot8  
Acp6  
Acs14  
Actb  
Actr8  
Acyp1  
Adam17  
Adamts1  
Adamts10  
Adamts6  
Adamts14  
Adat1  
Adc  
Adcy3  
Adcy7  
Adk  
Ado  
Adora2b  
Adpgk  
Adrbk1  
Adss

AF357374  
AF357376  
Afap1l1  
Aff1  
Aff4  
Afmid  
Aftph  
Aga  
Agbl5  
Agpat1  
Agt  
Ahcyl2  
Ahsa2  
AI118078  
AI450353  
AI462493  
AI597468  
Aicda  
Aifm1  
AK006189  
AK006245  
AK007083  
AK013187  
AK015545  
AK016837  
AK018891  
AK018967  
AK019250  
AK019365



AK031165  
AK035829  
AK037159  
AK038627  
AK040752  
AK042136  
AK043789  
AK043804  
AK043846  
AK043958  
AK044354  
AK044623  
AK045700  
AK047520  
AK048941  
AK051804  
AK053136  
AK053772  
AK054042  
AK078466  
AK079699  
AK079730  
AK079777  
AK085438  
AK087382  
AK089118  
AK131831  
AK132720  
AK134933

AK140370  
AK141659  
AK142999  
AK154275  
AK155149  
AK155592  
AK156477  
AK158379  
AK162774  
AK163160  
AK164218  
AK165329  
AK166079  
AK167137  
AK172386  
AK188991  
AK204212  
AK212603  
AK212710  
Ak3  
Akap1  
Akap13  
Akirin1  
Akirin2  
Akt2  
Aldoa  
Alg5  
Alkbh5  
Aloxe3

Ambra1  
Ammecr1  
Anapc1  
Anapc5  
Ang  
Ank3  
Ankrd24  
Ankrd40  
Ankrd52  
Ankrd54  
Antxr1  
Anxa2  
Anxa7  
Ap1g1  
Ap1s2  
Ap3m1  
Ap4s1  
Aph1c  
Appl1  
Arf3  
Arfgap1  
Arhgap12  
Arhgap18  
Arhgap21  
Arhgap26  
Arhgap4  
Arhgef10l  
Arhgef25  
Arhgef7

Arid1b  
Arl15  
Arl2bp  
Arl3  
Arl5a  
Arl6ip5  
Arpc3  
Arrb2  
Arrdc3  
Arvcf  
Asap1  
Asb4  
Ash2l  
Asl  
Asun  
Asxl1  
Asxl2  
Atad2  
Atat1  
Atf7ip  
Atg16l1  
Atg16l2  
Atg2a  
Atg2b  
Atl3  
Atp13a1  
Atp1b2  
Atp2b1  
Atp5a1

Atp5b  
Atp6v0a1  
Atp6v1a  
Atp6v1b2  
Atp6v1e1  
Atpaf2  
Atpif1  
Atraid  
Atrnl1  
Atxn2  
Atxn3  
Atxn7l1  
Atxn7l3  
Avl9  
AW209491  
AW495222  
B230217C12Rik  
B230325K18Rik  
B330016D10Rik  
B3gnt2  
B930003M22Rik  
B930082K07Rik  
Bach2  
Banf1  
Baz2b  
BB019430  
Bbc3  
BC004004  
BC024582

BC025920  
BC030867  
BC055111  
BC055823  
BC065397  
BC099561  
BC126883  
Bcar1  
Bcas2  
Bcas3  
Bcl11a  
Bcl2l1  
Bcl7a  
Bdp1  
Bend3  
Bgn  
Birc6  
Blcap  
Blmh  
Bloc1s4  
Bola2  
Bptf  
Brat1  
Brca1  
Brd3  
Brf1  
Bri3  
Brwd3  
Bscl2

Btaf1  
Btd  
Btf3l4  
C030013C21Rik  
C030034L19Rik  
C030037D09Rik  
C1ra  
C1rb  
C1rl  
C2  
C2cd2l  
C2cd5  
C330006A16Rik  
C330007P06Rik  
Cabin1  
Cacna1f  
Cad  
Cage1  
Calm2  
Camk2d  
Capn8  
Capn9  
Capns1  
Car12  
Carhsp1  
Cask  
Caskin2  
Casp8  
Cat

Catsper2  
Catsperg1  
Cbfb  
Cbr1  
Cbx4  
Cbx7  
Ccdc116  
Ccdc136  
Ccdc14  
Ccdc146  
Ccdc176  
Ccdc22  
Ccdc65  
Ccdc77  
Ccdc84  
Ccdc92  
Ccdc93  
Ccnd2  
Ccnh  
Ccnk  
Ccser2  
Cct6a  
Cd164  
Cd164l2  
Cd247  
Cd276  
Cd2ap  
Cd300lh  
Cdc14b



Cdc25a  
Cdc26  
Cdc6  
Cdc73  
Cdca5  
Cdh12  
Cdh16  
Cdk11b  
Cdk17  
Cdk2ap1  
Cdk5rap3  
Cdkal1  
Cdkl3  
Cdkl5  
Cdkn1b  
Cdkn2c  
Cdv3  
Celf1  
Cep128  
Cfdp1  
Cfi  
Cflar  
Chd2  
Chd3  
Chek1  
Chfr  
Chrac1  
Chrna1  
Chrn4

Chst11  
Chst3  
Chsy1  
Cic  
Cirbp  
Cisd3  
Ciz1  
Ckap5  
Clasp1  
Clca1  
Clcf1  
Clcn2  
Clcn5  
Cldn14  
Clic4  
Clint1  
Clip1  
Clk3  
Clptm1  
Clspn  
Clta  
Cltc  
Cmah  
Cmip  
Cnn2  
Cnot3  
Cnot6  
Cnot6l  
Cnppd1

Cnpy3  
Cnpy4  
Cog4  
Col8a2  
Commd1  
Commd7  
Commd8  
Comt  
Cops7a  
Cops8  
Copz2  
Coq10a  
Coq5  
Cox7b  
Cpeb3  
Cpm  
Cpt1c  
Cradd  
Creb3  
Crebbp  
Crebl2  
Creld1  
Crem  
Crk  
Crif3  
Crnkl1  
Crocc  
Cryl1  
Cryzl1

Cse1l  
Csgalnact2  
Csnk1a1  
Csnk1g3  
Cspp1  
Csrnp1  
Ctnna3  
Ctnnd1  
Ctsa  
Ctse  
Ctsl  
Cttb  
Cuedc1  
Cux1  
Cwc15  
Cyb5  
Cyb5d1  
Cyb5r1  
Cyp2t4  
Cyth1  
D030025P21Rik  
D030028A08Rik  
D14Abb1e  
D17Wsu104e  
D630003M21Rik  
D6Wsu163e  
D830025C05Rik  
Dapk2  
Dbi

Dbp  
Dbr1  
Dcaf17  
Dcakd  
Dck  
Ddb2  
Ddit4  
Ddx20  
Deb1  
Def8  
Dennd1b  
Des  
Desi1  
Dgat1  
Dgcr14  
Dgka  
Dhodh  
Dhrs3  
Dhx38  
Dhx57  
Dhx58  
Dhx8  
Dlat  
Dleu2  
Dmtf1  
Dmtn  
Dnajb14  
Dnajc25  
Dnajc3

Dnajc8  
Dnm1  
Dnmt1  
Dnttip2  
Dopey2  
Dpagt1  
Dpcd  
Dpep1  
Dpep2  
Dph3  
Dpy30  
Dpysl2  
Dpysl5  
DQ544183  
DQ548101  
DQ552992  
DQ553098  
DQ565977  
DQ566768  
DQ692659  
DQ694768  
DQ695092  
DQ695356  
DQ703023  
DQ704415  
DQ704975  
DQ705542  
DQ712916  
DQ713407

DQ716966  
DQ725849  
Dr1  
Drg1  
Drg2  
Drp2  
Dscr3  
Dtd2  
Dtnb  
Dtx3  
Dus1l  
Dus2l  
Dus3l  
Dusp13  
Dusp16  
Dynll1  
Dynll2  
Dyrk1a  
Dzip3  
E030042O20Rik  
E130102H24Rik  
E130304I02Rik  
E2f2  
E530001K10Rik  
Eapp  
Ebf1  
Ece1  
Ech1  
Ecsit

Edem1  
Eed  
Eef1b2  
Eef2k  
Efcab2  
Ehbp1  
Ehmt2  
Eid1  
Eif1ad  
Eif3c  
Eif3d  
Eif3k  
Eif3l  
Eif4e  
Eif4ebp2  
Eif4g3  
Eif4h  
Eif5a  
Eif5b  
Elk3  
Elk4  
Ell  
Elmsan1  
Emp1  
Entpd5  
Epb4.1  
Epb4.1l1  
Epc1  
Ephb4



Epo  
ErbB2  
Ercc6l  
Ergic1  
Erln2  
Ern1  
Esys2  
Ets2  
Etv5  
Evi5  
Ewsr1  
Exd2  
Exosc8  
Extl2  
Eya3  
F420014N23Rik  
Fam111a  
Fam117a  
Fam129b  
Fam131a  
Fam134a  
Fam136a  
Fam185a  
Fam188a  
Fam19a2  
Fam214b  
Fam216a  
Fam35a  
Fam49b

Fam57b  
Fam63b  
Fam73b  
Fam98a  
Fanca  
Fancc  
Fance  
Fancg  
Fars2  
Fbxl16  
Fbxl20  
Fbxo30  
Fbxo36  
Fbxo42  
Fbxo47  
Fbxo9  
Fchsd2  
Fdps  
Fes  
Fgd2  
Fgfr1op2  
Fhl3  
Fhl4  
Fig4  
Figf  
Figl1  
Fis1  
Fkbp10  
Fkbp14

Fkbp1a  
Fkbp5  
Fkbp7  
Fkbp8  
Flna  
Fmnl2  
Fnbp1  
Fndc3a  
Fndc7  
Fnip1  
Fosl2  
Foxh1  
Foxj3  
Foxn2  
Foxn3  
Foxo1  
Foxp1  
Frat1  
Frat2  
Frg1  
Frmd4a  
Frs2  
Fry  
Fstl1  
Fus  
Fut8  
Fxr2  
Fyttd1  
Fzd7

G730013B05Rik

Gabarapl1

Gabarapl2

Gabpb1

Gabpb2

Gadd45b

Gadd45g

Gadd45gip1

Gak

Gapdh

Gapvd1

Gareml

Gast

Gata3

Gatad2a

Gatc

Gbas

Gbp3

Gcc2

Gclc

Gdf9

Gdi2

Gemin2

Gemin6

Gfpt2

Gga2

Ggnbp2

Ggt5

Gimap8

Gins1  
Git2  
Glg1  
Glipr1  
Glo1  
Glud1  
Gm10433  
Gm10463  
Gm10610  
Gm10642  
Gm10653  
Gm10655  
Gm10657  
Gm10658  
Gm10762  
Gm10837  
Gm11184  
Gm11206  
Gm11292  
Gm11335  
Gm11336  
Gm11437  
Gm11453  
Gm11464  
Gm11474  
Gm11491  
Gm11521  
Gm11602  
Gm11612

Gm11619  
Gm11627  
Gm11630  
Gm11680  
Gm11696  
Gm11715  
Gm11827  
Gm12035  
Gm12054  
Gm12057  
Gm12060  
Gm12063  
Gm12245  
Gm12257  
Gm12279  
Gm12308  
Gm12309  
Gm12314  
Gm12358  
Gm12396  
Gm12795  
Gm12951  
Gm12974  
Gm12981  
Gm13054  
Gm13182  
Gm13201  
Gm13256  
Gm13297

Gm13334  
Gm13363  
Gm13375  
Gm13398  
Gm13447  
Gm13548  
Gm13559  
Gm13564  
Gm13626  
Gm13630  
Gm13657  
Gm13705  
Gm13770  
Gm13830  
Gm13836  
Gm13855  
Gm13936  
Gm14005  
Gm14167  
Gm14216  
Gm14455  
Gm14634  
Gm15411  
Gm15420  
Gm15454  
Gm15688  
Gm15747  
Gm15760  
Gm15787

Gm15831  
Gm15860  
Gm15892  
Gm15903  
Gm15927  
Gm15962  
Gm16023  
Gm16185  
Gm16196  
Gm16197  
Gm16230  
Gm16274  
Gm16540  
Gm16557  
Gm16580  
Gm16740  
Gm16880  
Gm17077  
Gm17098  
Gm17112  
Gm17138  
Gm17157  
Gm17300  
Gm17617  
Gm17661  
Gm17705  
Gm19705  
Gm20257  
Gm20748



Gm4221  
Gm4673  
Gm4978  
Gm5069  
Gm5134  
Gm5258  
Gm5428  
Gm5432  
Gm5464  
Gm5512  
Gm608  
Gm6225  
Gm6297  
Gm6444  
Gm6471  
Gm6525  
Gm7598  
Gm9812  
Gm9850  
Gm9900  
Gm9959  
Gm9985  
Gna13  
Gnb2  
Gnb2l1  
Gnl3  
Golga3  
Got2  
Gpbar1

Gpn3  
Gpr19  
Gpr35  
Gpr82  
Gpr85  
Gramd1a  
Grb2  
Grcc10  
Grik4  
Gse1  
Gskip  
Gstt3  
Gtf2h2  
Gtf2i  
Gtf2ird2  
Gyk  
Gypc  
Gys1  
Gzmm  
H1f0  
H2afz  
H2-D1  
H2-DMb1  
H2-DMb2  
H2-L  
Hac1  
Hbp1  
Hdac7  
Hdgfrp2

Heatr5a  
Helb  
Helz  
Herc4  
Hes1  
Hes7  
Hexim2  
Hic1  
Hic2  
Hif1a  
Hint2  
Hip1r  
Hira  
Hirip3  
Hist1h2ac  
Hist1h2af  
Hist1h2bb  
Hist1h2bc  
Hist1h3c  
Hivep1  
Hlcs  
Hlx  
Hmbs  
Hmg20b  
Hmox2  
Hnrnpf  
Hnrnph1  
Hnrnph3  
Hnrnpk

Hnrnpl  
Hnrnpu  
Hnrnpul1  
Hnrnpul2  
Homer1  
Hoxb6  
Hoxb8  
Hoxc5  
Hoxd10  
Hoxd3  
Hps3  
Hsd17b12  
Hsp90ab1  
Hspa13  
Hspa4  
Hspb9  
I830077J02Rik  
Ica1  
Icam1  
Id3  
Ifi35  
Ift80  
Igf1r  
Igfbp6  
Ik  
Il1rap  
Il3ra  
Ilf2  
Ilf3

Ilk  
Immt  
Impdh1  
Ing1  
Ing3  
Ing4  
Inip  
Ino80  
Ino80d  
Ino80e  
Inpp5b  
Ints8  
Ipo11  
Iqce  
Iqcg  
Irf2bp2  
Irf2bpl  
Irs3  
Itfg2  
Itgb2  
Itgb5  
Itm2b  
Itpkb  
Izumo4  
Jarid2  
Kalrn  
Kansl1  
Kars  
Kat2a

Kat2b  
Kbtbd7  
Kcnh3  
Kctd19  
Kctd20  
Kdm3a  
Kdm4d  
Kdm5a  
Kif11  
Kif23  
Kif24  
Kif5b  
Klc1  
Klhdc10  
Klhl11  
Klhl18  
Kmt2d  
Kntc1  
Kpna2  
Kpnb1  
Krt222  
L3mbtl2  
L3mbtl3  
Lamp2  
Lamtor3  
Larp4  
Lars2  
Las1l  
Lck

Lctl  
Ldb1  
Leo1  
Leprel4  
Leprotl1  
Letm2  
Lhb  
Lias  
Lipe  
Lmf2  
Lmna  
Lmo2  
Lmo4  
Lmtk2  
Lnx2  
LOC100504608  
LOC100504703  
Loxl3  
Lpar5  
Lphn1  
Lpin2  
Lpxn  
Lrch1  
Lrg1  
Lrig2  
Lrp2bp  
Lrrc1  
Lrrc16a  
Lrrc16b

Lrrc46  
Lrrc49  
Lrrc58  
Lrrk1  
Lrsam1  
Lsmd1  
Luc7l  
Luc7l2  
Luc7l3  
Luzp1  
Ly6g6f  
Lym4  
Lym7  
Lysmd3  
Lyzl6  
Mad2l1  
Mad2l1bp  
Madd  
Maea  
Magt1  
Malat1  
Maml2  
Manea  
Map2k6  
Map2k7  
Map3k12  
Map3k3  
Map4k1  
Map4k2



Map4k3  
Mapk6  
Mapkbp1  
Mapt  
March5  
March6  
March7  
March8  
Mark2  
Marveld1  
Mast4  
Mbnl2  
Mbnl3  
Mbtps2  
Mccc1  
Mcm3  
Mcm3ap  
Mcm9  
Mcts1  
Mdp1  
Med13  
Med14  
Med18  
Med6  
Melk  
Memo1  
Mettl1  
Mettl14  
Mettl17

Mettl8  
Mga  
Mical3  
Midn  
Mif4gd  
Mir125a  
Mir132  
Mir152  
Mir15b  
Mir17  
Mir17hg  
Mir18  
Mir1931  
Mir1956  
Mir199b  
Mir19a  
Mir19b-1  
Mir20a  
Mir212  
Mir3058  
Mir3109  
Mir5122  
Mir5135  
Mir615  
Mir670  
Mir677  
Mir702  
Mir92-1  
Mir99b

Mirlet7e  
Mitd1  
Mkks  
Mlec  
Mlf2  
Mlt10  
Mlxip  
Mmp25  
Mms19  
Mob1a  
Mob3a  
Morc3  
Morf4l1  
Morf4l2  
Morn1  
Morn2  
Morn3  
Mpnd  
Mpp6  
Mpv17  
Mrc2  
Mrfap1  
Mrpl10  
Mrpl14  
Mrpl30  
Mrpl32  
Mrpl40  
Mrpl45  
Mrpl48

Mrpl52  
Mrpl9  
Mrps2  
Mrps36  
Mrps6  
Mrs2  
Ms4a10  
Msh5  
Msl1  
Msrb3  
Mtf2  
Mtif3  
Mtmr3  
Muc6  
Mxi1  
Mxra7  
Myadm  
Myc  
Myg1  
Myh9  
Myl12b  
Mylpf  
Myo1g  
Myo1h  
Myo9a  
Mzf1  
N4bp2  
N4bp2l2  
Naa16

Naa20  
Naa25  
Naa50  
Nadk  
Nagk  
Nap1l1  
Napa  
Nasp  
Nat10  
Nat2  
Nbeal1  
Nbeal2  
Nbr1  
Ncaph2  
Nck1  
Ncoa3  
Ncoa4  
Ncor1  
Ncor2  
Ncrna00085  
Ndfip2  
Ndr4  
Nduf4  
Ndufs7  
Necap1  
Nedd4  
Nek10  
Nek8  
Nek9

Neu1  
Neur12  
Nf2  
Nfat5  
Nfic  
Nfil3  
Nfix  
Nfkbia  
Nfx1  
Nfxl1  
Nhirc2  
Nhp2  
Nipbl  
Nkrf  
Nktr  
Nlk  
Nol7  
Nono  
Nop58  
Notch3  
Npepps  
Nphp1  
Nploc4  
Nppa  
Nptn  
Nqo2  
Nr2f6  
Nr3c1  
Nr4a2

n-R5s79

Nrf1

Nrg4

Nt5c2

Ntf5

Nub1

Nubp2

Nufip2

Numa1

Nup133

Nup153

Nup205

Nup98

Nyx

Oas1b

Oas1c

Oas2

Ocr1

Ogt

Olfr1414

Oma1

Opn1sw

Orai2

Orc1

Orc2

Osbp13

Osbp17

Osbp18

Otub1

Otud4  
Ovol1  
Oxnad1  
Oxsr1  
P2rx4  
P4ha1  
Pacsin2  
Palld  
Pan3  
Papd4  
Papss1  
Papss2  
Paqr8  
Parl  
Patz1  
Pax2  
Pax6  
Pbld2  
Pbrm1  
Pcbd2  
Pcbp1  
Pcbp2  
Pcca  
Pccb  
Pcgf2  
Pcm1  
Pcnxl2  
Pcsk4  
Pde4d



Pdia3  
Pdia6  
Pdk1  
Pdpk1  
Pdxdc1  
Peg13  
Peli1  
Pes1  
Pex19  
Pfkf  
Pfn2  
Pgam1  
Pgap2  
Pgd  
Phactr4  
Phc1  
Phc3  
Phf12  
Phf15  
Phf20  
Phf21a  
Phf6  
Phf8  
Phgdh  
Phip  
Phospho1  
Phyhd1  
Pias4  
Picalm

Pif1  
Pigl  
Pigp  
Pigv  
Pik3c3  
Pik3ca  
Pik3cb  
Pik3cd  
Pik3r1  
Pik3r3  
Pim1  
Pisd  
Pisd-ps1  
Pisd-ps2  
Pitpnc1  
Pitpnm2  
Pja1  
Pkd2l1  
Pkig  
Pkn3  
Pknox1  
Pla2g6  
Plbd2  
Plcg1  
Plcl2  
Plekha3  
Plekha4  
Plekha8  
Plekhf2

Plekhg2  
Plekhg3  
Plin3  
Plk1s1  
Plod3  
Plxna2  
Plxnd1  
Pml  
Pmm2  
Pnpla8  
Poc1a  
Poldip2  
Pole2  
Polg  
Polg2  
Poll  
Polr2h  
Polr2i  
Polr3c  
Polrmt  
Pop4  
Pou2f1  
Pou4f3  
Pou6f1  
Ppard  
Ppcdc  
Ppfia3  
Ppil1  
Ppm1b

Ppm1h  
Ppm1k  
Ppp1r12a  
Ppp1r15a  
Ppp1r16a  
Ppp1r3f  
Ppp1r8  
Ppp2cb  
Ppp2r5c  
Ppp6r2  
Prdm1  
Prex1  
Prickle1  
Prkaa1  
Prkag1  
Prkag2  
Prkar1a  
Prkcg  
Prkrip1  
Prpf19  
Prpf3  
Prpf38a  
Prpf38b  
Prpf39  
Prpf4  
Prpf4b  
Prpsap1  
Prpsap2  
Prr12

Prr13  
Prr14l  
Prrc2a  
Prrg2  
Psap  
Psma1  
Psma2  
Psma3  
Psemb3  
Psemb6  
Psmc1  
Psmc14  
Psmc7  
Pspc1  
Pspk  
Ptbp3  
Ptch1  
Ptp4a1  
Ptp4a2  
Ptplad2  
Ptpmt1  
Ptpn11  
Ptpn6  
Ptpnj  
Ptrh2  
Pttg1  
Pum1  
Pycard  
Pycr2

Pygl  
Qk  
Qrich1  
Qsox2  
R3hdm2  
Rab1  
Rab21  
Rab28  
Rab3gap2  
Rab42  
Rab5b  
Rab6a  
Rab7  
Rad51ap1  
Rad51c  
Rad9b  
Ralbp1  
Ralgapa1  
Ralgps1  
Rap1b  
Rap2a  
Rapgef6  
Rarg  
Rasal2  
Rasd1  
Rb1  
Rbbp5  
Rbbp6  
Rbck1

Rbm12b2  
Rbm27  
Rbms1  
Rcc1  
Rcc2  
Rccd1  
Rcor1  
Rdh10  
Rdm1  
Rel1  
Reps2  
Rere  
Rexo2  
Rffl  
Rft1  
Rftn2  
Rfwd3  
Rfx2  
Rfx3  
Rhbdd2  
Rhbg  
Rhob  
Rhobtb2  
Rhot1  
Rilp12  
Riok1  
Rlim  
Rmi1  
Rmnd1

Rnase4  
Rnf10  
Rnf121  
Rnf13  
Rnf146  
Rnf157  
Rnf167  
Rnf2  
Rnf34  
Rnf5  
Rnft1  
Rp9  
Rpa1  
Rpa2  
Rpl10  
Rpl10-ps2  
Rpl12  
Rpl24  
Rpl27  
Rpl30-ps5  
Rpl35a  
Rpl35a-ps2  
Rpl38  
Rpl41  
Rpl5  
Rpl6  
Rpl7  
Rpl9  
Rpp21



Rprd2  
Rps10  
Rps15a  
Rps26  
Rps6ka1  
Rps6kb1  
Rps8  
Rptor  
Rreb1  
Rrm1  
Rrm2b  
Rrp8  
Rsbn1l  
Rsrc2  
Rtfdc1  
Rtn4rl2  
Rufy3  
Rundc3a  
Runx1  
Rybp  
S100pbp  
Sacm1l  
Sae1  
Samd1  
Samd8  
Samd9l  
Samhd1  
Sap30  
Sapcd2

Sarm1  
Sbds  
Sbf1  
Sbno2  
Scamp3  
Scara5  
Scarb1  
Scgb1a1  
Schip1  
Scmh1  
Scn1a  
Scn3a  
Scpep1  
Sec14l1  
Sec22c  
Sec23a  
Sec24b  
Sec24c  
Sec31a  
Sec31b  
Sec61a1  
Seh1l  
Selt  
Sema3c  
Seph1  
Sept5  
Sept8  
Serf1  
Serp1b9

Sertad1  
Sertad2  
Sesn2  
Setd2  
Setd3  
Setd4  
Setd5  
Setd7  
Setd8  
Sfmbt1  
Sfpq  
Sfxn2  
Sgk1  
Sgk2  
Sgk3  
Sgms2  
Sh2b3  
Sh3bgrl  
Sh3bp5l  
Sh3glb2  
Sh3kbp1  
Shc4  
Shisa5  
Shmt1  
Shroom3  
Siae  
Sigmar1  
Sin3a  
Sirt1

Sit1  
Six6  
Skil  
Slain2  
Slc16a1  
Slc18a1  
Slc23a2  
Slc25a11  
Slc25a14  
Slc25a3  
Slc25a35  
Slc25a36  
Slc25a38  
Slc25a39  
Slc25a43  
Slc25a51  
Slc26a10  
Slc30a1  
Slc30a7  
Slc31a2  
Slc32a1  
Slc35b1  
Slc35b4  
Slc38a10  
Slc38a2  
Slc39a2  
Slc3a2  
Slc43a2  
Slc5a3

Slc5a6  
Slc7a7  
Slc9a1  
Slc9a8  
Slu7  
Slx1b  
Slx4ip  
Smad6  
Smad7  
Smad1  
Smarca2  
Smarcc2  
Smarcd2  
Smc4  
Smg7  
Smim13  
Smndc1  
Smpd1  
Smyd4  
Snai1  
Snf8  
Snhg1  
Snhg12  
Snhg5  
Snora16a  
Snora44  
Snora61  
Snora70  
Snord19

Snord21  
Snord38a  
Snord52  
Snord55  
Snord7  
Snord88a  
Snord88c  
Snord96a  
Snord99  
Snrnp35  
Snrnp70  
Sntb2  
Snupn  
Snx10  
Snx27  
Snx29  
Snx30  
Soat1  
Socs1  
Socs2  
Socs3  
Socs7  
Sod1  
Sorbs1  
Sos2  
Sp1  
Sp3  
Spa17  
Spag8

Specc1  
Spg11  
Spin1  
Spp1  
Sppl2a  
Spred1  
Spred2  
Spry4  
Spryd3  
Spryd4  
Spsb3  
Sptan1  
Sptlc2  
Sqrdl  
Srek1  
Srgap3  
Srrm1  
Srrm2  
Srsf1  
Srsf3  
Ssb  
Ssbp3  
Ssbp4  
Ssh2  
St13  
St6galnac2  
Stac2  
Stag2  
Stam

Stam2  
Stard6  
Stard9  
Stat2  
Stim2  
Stip1  
Stk25  
Stk30  
Stk38  
Stk38l  
Stoml1  
Strada  
Strn3  
Stx11  
Stx16  
Styk1  
Suco  
Sumo1  
Sun1  
Suz12  
Swsap1  
Syne1  
Syngr1  
Syngr3  
Syngr4  
Synj1  
Synj2  
Tacc1  
Tacc2



Taco1  
Taf1  
Taf1c  
Taf1d  
Taf3  
Taf4a  
Taf6  
Tagln2  
Tango2  
Tango6  
Taok2  
Taok3  
Tarbp2  
Tatdn2  
Tbc1d1  
Tbc1d10a  
Tbc1d10b  
Tbcb  
Tbcc  
Tb11xr1  
Tbx15  
Tcam1  
Tceanc2  
Tcf12  
Tcf4  
Tcf7l2  
Tcof1  
TCR-alpha chain  
Tctn1

Tdrd3  
Tead2  
Tecr  
Terf2  
Terf2ip  
Tet2  
Tex14  
Tex30  
Tfap4  
Tfdp2  
Tfg  
Tfrc  
Tgif1  
Thrap3  
Tia1  
Tial1  
Ticam1  
Timm13  
Timm8a2  
Timm9  
Timmdc1  
Tipin  
Tjap1  
Tjp3  
Tle2  
Tle3  
Tle6  
Tlk2  
Tln1

Tm2d2  
Tm9sf4  
Tmbim1  
Tmcc2  
Tmem100  
Tmem106a  
Tmem120b  
Tmem143  
Tmem156  
Tmem164  
Tmem18  
Tmem180  
Tmem186  
Tmem192  
Tmem194  
Tmem199  
Tmem231  
Tmem242  
Tmem259  
Tmem29  
Tmem33  
Tmem5  
Tmem59  
Tmem67  
Tmem82  
Tmem88  
Tmpo  
Tnfaip8  
Tnfrsf9

Tnk2  
Tnp2  
Tnp2  
Tnp2  
Tnp3  
Tnrc18  
Tnrc6a  
Tob1  
Tob2  
Tom1l1  
Top1  
Top2a  
Tor1aip1  
Tor1aip2  
Tpm1  
Tprgl  
Tpt1  
Tpx2  
Tra2b  
Traf6  
Trafd1  
Traj58  
Traj59  
Tram1  
Trap1  
Trdv5  
Trerf1  
Triap1  
Trib1  
Trib2

Trim35  
Trim37  
Trim59  
Trim7  
Trim8  
Triobp  
Trip12  
Trmt12  
Trpc2  
Trpv2  
Trpv4  
Trub2  
Tsc22d3  
Tsen54  
Tspan10  
Tspan14  
Tspan17  
Tspan31  
Ttc17  
Ttc19  
Ttc28  
Ttc3  
Ttc7  
Ttc9c  
Tuba1a  
Tuba1c  
Tubb5  
Tubd1  
Tulp1

Tulp3  
Txlna  
Txn2  
Txndc12  
Txndc9  
Txnl4b  
Txnrd1  
Txnrd2  
Tyw1  
U05342  
U3  
U7  
Uba1  
Uba5  
Uba52  
Ubald1  
Ubap2l  
Ubb  
Ubc  
Ube2b  
Ube2e3  
Ube2f  
Ube2h  
Ube2v1  
Ublcp1  
Ubn2  
Ubr2  
Ubtcd2  
Ubtg

Ubxn1  
Ubxn4  
Ubxn7  
Uchl4  
Ulk2  
Umodl1  
Unc119  
Uqcrq  
Urgcp  
Urm1  
Usb1  
Usf2  
Usp1  
Usp10  
Usp15  
Usp2  
Usp20  
Usp28  
Usp3  
Usp32  
Usp34  
Usp45  
Usp48  
Usp49  
Utp14a  
Vac14  
Vcp  
Vdac1  
Vezf1

Vezt  
Vgll4  
Vhl  
Vmp1  
Vprbp  
Vps13d  
Vps29  
Vps37b  
Vps53  
Vps54  
Vtn  
Wbscr16  
Wdfy2  
Wdpcp  
Wdr1  
Wdr34  
Wdr37  
Wdr47  
Wdr5  
Wdr6  
Wdr63  
Wdr75  
Wee1  
Whsc1  
Whsc1l1  
Wibg  
Wipf1  
Wrnip1  
Wtap



Wwp1  
Wwp2  
Xbp1  
Xiap  
Xpnpep3  
Xpot  
Yars  
Ybey  
Ydjc  
Yipf2  
Yipf4  
Ypel2  
Ywhag  
Yy2  
Zan  
Zbtb1  
Zbtb24  
Zbtb25  
Zbtb38  
Zbtb45  
Zbtb7a  
Zc3h10  
Zc3h6  
Zc3hav1  
Zc3hc1  
Zcchc8  
Zdhhc17  
Zdhhc5  
Zer1

Zfand3  
Zfat  
Zfp1  
Zfp101  
Zfp106  
Zfp182  
Zfp184  
Zfp207  
Zfp217  
Zfp251  
Zfp27  
Zfp280b  
Zfp319  
Zfp324  
Zfp36l1  
Zfp383  
Zfp384  
Zfp39  
Zfp395  
Zfp40  
Zfp428  
Zfp438  
Zfp507  
Zfp512  
Zfp52  
Zfp553  
Zfp592  
Zfp606  
Zfp607

Zfp608  
Zfp64  
Zfp646  
Zfp664  
Zfp668  
Zfp672  
Zfp703  
Zfp719  
Zfp809  
Zfp866  
Zfp91  
Zfp948  
Zfpl1  
Zfx  
Zkscan17  
Zkscan3  
Zmat1  
Zmiz2  
Zmym5  
Zmynd11  
Zmynd8  
Znhit1  
Znhit3  
Zscan25  
Zswim7  
Zufsp  
Zw10